Master's Thesis

École Polytechnique Fédérale de Lausanne

Institute of Physics

and

Université de Genève

Department of Theoretical Physics

Implications of Primordial Black Holes physics at high redshifts

Author:
Giona Sala

Supervisors:
Prof. Antonio Riotto
Prof. Victor Gorbenko

2023/03/03

Acknowledgements

This Master's thesis was an exciting introduction to the research world of physics for me. For this reason, I am deeply thankful to my primary supervisor Prof. Antonio Riotto for making this project possible, and above all, for being an excellent mentor and working with me regularly.

Secondly, I am also grateful to my supervisor at EPFL Prof. Victor Gorbenko for the availability to oversee, read and evaluate my thesis, as well as for managing its administration.

As this work represents an important milestone in the course of my studies, I would like to take this opportunity to also thank all the people who majorly contributed to it. First and foremost my parents, Marco and Paola, gave me the possibility to embark on this path in the first place.

In addition to that, I would like to extend my gratitude to all the people I encountered during my academic route to date, who shared my interests and inspired me. A particular thank you goes to Prof. Lesya Shchutska and Prof. Mikhail Shaposhnikov for transmitting to me their passion for their respective areas of expertise.

Last but not least, I am very grateful to everyone who surrounded me and supported me over these five years: my family, my friends and especially Lisa, who has always been there for me.

Abstract

Primordial black holes are a hypothetical type of black holes that formed in the very early universe, typically before the matter dominated epoch. These objects are supposed to make up a fraction of dark matter, however, their observation has never been confirmed. In the last year, James Webb space telescope discovered very massive galaxies $\sim 10^{10} M_{\odot}$ in the early universe $z \sim 10$, which cannot be explained with the cosmological standard model. These measurements raised many questions, and many different approaches have been explored to explain them. One possibility to solve this mystery lies in primordial black holes, as their presence could have boosted galaxy formation.

In this report, the presence of primordial black holes is hypothesised and the conditions for which they could have led the observed galaxies to form so early are investigated. In particular, the case in which primordial black holes are initially randomly distributed throughout the universe is studied with two main approaches. The first analysis consists in finding the stellar mass density that explains James Webb space telescope observations in a scenario where primordial black holes are Poisson distributed. The second study is based on situations where primordial black holes evolve in clusters, dominating the formation of galaxies. While the first investigation reveals that the observed galaxies could have formed only for extremely massive primordial black holes, the second analysis can relax these conditions. However, the new parameters suffer some constraints dictated by observation, which should be reevaluated with the consideration of the clustering effect.

Contents

1 Introduction

One of the biggest open questions in modern physics is understanding the composition of the universe, in particular, the large share of non-relativistic matter that is expected to exist but has not been observed yet: dark matter (DM). Many are the possibilities being studied at the moment and it is most likely that there is not only one answer but that this unknown constituent of the universe is composed of different elements. One possibility that is being explored and has gained much interest in the last decade with the detection of gravitational waves, is the existence of *primordial black holes* (PBH) [1]. In this report, these objects are further examined, as their theorised presence could be of interest to explain the unforeseen observation made by *James Webb space telescope* (JWST) in the last year, making a step forward to prove their contribution to DM.

It is believed that there are two types of black holes (BH): the astrophysical ones and the PBHs. The first kind of BH existence is confirmed and its name comes from its formation process. They originate from the gravitational collapse of astrophysical objects, stars, thus they can be produced in the present universe. On the other hand, PBHs are hypothetical BHs since they have been theorised, but their existence has yet to be proven. The most popular possibility for their formation is also due to gravitational collapse, but in the primordial universe [2]. While in the late universe, densities large enough to form a BH are only found in stars, the primordial universe was much more packed, hence smaller overdensities could have caused a collapse. With this formation process, their origin is traced back to the radiation dominated (RD) universe. Specifically, the gravitational collapse into a PBH is expected to take place when an isocurvature perturbation of cold dark matter (CDM) reenters the Hubble horizon (see section C.4). Consequently, while astrophysical BHs must have masses on the order of the stellar ones, PBHs are more flexible to have much smaller masses.

On Christmas 2021 JWST was launched into orbit to open a new era of space observations based on electromagnetic waves. In the last year, besides several other tasks, it was able to look for galaxies far away as never before. Specifically, it discovered a population of massive galaxies $M_* \gtrsim 10^{10} M_\odot$ in the early universe, at high redshift $7 \lesssim z \lesssim 11$ [3] [4] [5]. These observations were particularly surprising as the cosmological standard model, Lambda cold dark matter (ΛCDM) model, does not allow the formation of galaxies so massive and so early in time [6] [7] [8]. This observation opened therefore the question of whether the standard model is incorrect or if there are missing elements that need to be taken into account. In this report, the possibility that these latter missing elements are PBHs is of interest.

The challenge of proving PBH existence is dictated on one side by the observational constraints on their population, while on the other by the difficulty of finding proof of their presence. JWST measurements could represent a consequence of their existence, hence one of the first detected proofs. Thus the objective of this thesis is to explore the possibility that the presence of randomly distributed PBHs

in the primordial universe has boosted galaxy formation at early times, explaining how JWST observations could represent proof of PBH existence. An article that chased this goal has already been written [9]. Consequently, this paper is taken as inspiration. At first, it is replicated for educational purposes and to understand some properties required for the existence of PBHs to have led to JWST galaxies detection. In particular, two variables related to PBHs are investigated: the first is the fraction of DM that PBH could fill $f_{PBH} = \frac{\Omega_{PBH}}{\Omega_{DM}} \leq 1$ and the second is their mass m_{PBH}[1]. In addition to that, some novelty is added to these results, by considering the *clustering effect* of PBHs. As it will be discussed, this phenomenon could further boost halo formation, expanding the possibilities of PBH existence.

As both PBH and halos, which in turn generate galaxies, are based on *matter overdensities*[2], this quantity is of main importance for this report. These density contrasts are due to the matter density perturbations and can be written in the following way.

$$\delta(\mathbf{x}) = \frac{\rho_m(\mathbf{x}) - \overline{\rho}_m}{\overline{\rho}_m} = \frac{\delta\rho_m}{\overline{\rho}_m} \tag{1.1}$$

where $\overline{\rho}_m$ represents the mean comoving value of matter energy density in the universe or background matter energy density, while $\rho_m(\mathbf{x})$ is the local energy density in $\mathbf{x}$. For actual overdensities $\delta(\mathbf{x}) > 0$, while the local energy density is equal to average $\delta(\mathbf{x}) = 0$. Underdensities have $\delta(\mathbf{x}) < 0$, however, they are not of high relevance throughout this work. Their Fourier transform is also extensively used during this report.

$$\delta(\mathbf{k}) = \int d^3\mathbf{x}\delta(\mathbf{x})e^{i\mathbf{kx}} \tag{1.2}$$

This quantity also defines the *power spectrum*, another fundamental property used in this project. A brief summary of its derivation and utilisation can be found in Appendix D.

In addition to that, Appendix C provides a review of important cosmological properties used in the report, as well as a clarification of the notation.

This report is composed of three main chapters. After this introduction, chapter 2 discusses the *spherical model*, which represents a very successful method to study perturbation evolution, very useful throughout the report. In particular, it is helpful to study collapses and the isocurvature perturbation introduced by the presence of PBHs. However, it has the flaw of assuming that fluctuations have spherical symmetry. In chapter 3, article [9] is studied, replicated and its limits are discussed. The analysis included in this segment is based on the power spectrum recovered from observations, together with the one coming from the addition of PBHs in the picture. In chapter 4 the evolution of clusters from initially Poisson

[1] It must be noted that for simplicity all analysis are performed considering PBHs' mass function to be monochromatic. An extended PBH mass function could be considered to further improve the results [10].

[2] This includes non-relativistic matter's energy, due to both baryons and dark matter (DM). Often matter energy density will be called simply energy density, implying the reference to non-relativistic matter (see section C.3).

distributed PBHs is discussed. Firstly the correctness of the previous chapter's analysis is questioned, based on the absence of clusters. Secondly, the scenario in which PBH clusters push massive halo formations is studied, considering accretion and evaporation. The report ends with chapter 5, where conclusions are drawn and the results obtained in relation to the constraints coming from observations [2] are discussed.

Furthermore, the possibility that PBHs formed in the RD universe with an initially non-Poisson distribution, hence with a clustering component, is superficially treated in Appendix E. A general overview of the consequences of this addition is presented.

2 Spherical model

Energy density perturbations are one of the main subjects of this project. However, it can be very difficult to deal with them. In order to do this, the spherical model is used, as it is an approximated model which makes it more feasible to face particularly complex fluctuations. As it is given away by its name, the spherical model is based on the supposition that perturbations have spherical symmetry. In this chapter, an introduction to this model and more generally on perturbations is provided, as these topics will be recurrent in the report.

Fluctuations can be of two types: *adiabatic* or *isocurvature*. While adiabatic fluctuations are perturbations of the energy density, isocurvature ones have constant energy density but their perturbations are due to the different species, hence not perturbing the curvature directly. This definition is however very strict. In fact, isocurvature perturbation can be the result of energy density fluctuations, which yet do not alter the curvature on large scale. For example, DM (matter) energy density contrasts in the RD universe, which also lead to PBHs formation, are isocurvature perturbations, as they do not influence the general curvature since it is dictated by radiation. Large scale fluctuations can be well described by the observation of the cosmic microwave background (CMB). On the other hand, small scale fluctuations are difficult to be detected and could have large amplitudes. In addition to that, small amplitude fluctuations respect linear theory and do not grow in the RD universe but only in the matter dominated (MD) universe, as will be discussed in subsection 2.1.2. However large amplitude fluctuations, which are non-linear and small in scale, can reenter Hubble horizon in RD universe and already collapse.

Therefore this section starts by focusing on small scale perturbations, but with large amplitudes, which are non-linear. In particular, this model is useful to better understand collapse and fluctuations in RD, such as isocurvature perturbations, and their evolution. In fact, PBHs are expected to collapse in the very early universe, when radiation dominates, due to isocurvature fluctuations of CDM. For this reason, the non-linear spherical model is important to better understand this process as well as the consequences. The results will then be relevant for the whole report. The subjects treated in this section are mostly taken from [11], [12][1] and [13].

In the first part, in section 2.1, the spherical model is introduced and a few useful approximations are highlighted, such as the linear limit. In section 2.2, the specific case of PBH is discussed, considering isocurvature fluctuations and their evolution. To conclude the chapter, section 2.3 discusses the critical energy density for a perturbation to collapse with the spherical model, which is a quantity useful for the whole report.

[1] In particular chapter 15 of [12].

2.1 Perturbations in the spherical model

The spherical collapse analysis starts with the equation of motion around a massive object of proper radius $\tilde{R}$, which experiences the effect of pressure due to radiation[2], and the gravitational field due to its own mass.

$$\ddot{\tilde{R}} = -\frac{8\pi G}{3}\tilde{R}\tilde{\tilde{\rho}}_r - \frac{GM_{tot}}{\tilde{R}^2} \tag{2.1}$$

where $\tilde{\tilde{\rho}}_r$ is the proper mean energy density of relativistic matter (which pressure is $\tilde{p}_r = \frac{\tilde{\tilde{\rho}}_r}{3}$) and M_{tot} is the total mass of non-relativistic matter included in the sphere of radius $\tilde{R}$. For gravity to be relevant, the sphere is supposed to be in casual contact, hence within Hubble horizon. Thus a transformation to comoving coordinates and conformal time η can be applied (see section C.1).

$$\tilde{R}(\eta) = a(\eta)\zeta(\eta)R \tag{2.2}$$

$$\eta = \int_0^t \frac{dt'}{a(t)} \qquad \text{or} \qquad d\eta = \frac{dt}{a(t)} \tag{2.3}$$

where R is the comoving radius of the shell at the start, which is fixed, while $\zeta(\eta)$ represents the deviation from the standard universe expansion, which is not strictly followed by the non-linear clump of interest.

In the next step, Friedmann equations need to be recalled (see section C.2).

$$\frac{\dot{a}^2}{a^2} + \frac{K}{a^2} - \frac{\Lambda}{3} = \frac{8\pi G}{3}\tilde{\rho} \qquad \text{and} \qquad 2\frac{\ddot{a}}{a} + \frac{\dot{a}^2}{a^2} + \frac{K}{a^2} - \Lambda = -8\pi G\tilde{p} \tag{2.4}$$

where $\tilde{\rho}$ is the energy density, $\tilde{p}$ is the pressure, Λ is the cosmological constant and K is the curvature factor. Considering a flat universe with no cosmological constant (universe dominated by relativistic and non-relativistic matter) it is possible to rewrite these equations using the conformal time derivative[3].

$$a'^2 = \frac{8\pi G}{3}(\tilde{\tilde{\rho}}_m + \tilde{\tilde{\rho}}_r)a^4 \qquad \text{and} \qquad a'' = \frac{4\pi G}{3}\tilde{\tilde{\rho}}_m a^3 \tag{2.5}$$

Putting them back into (2.1), the solution is found in terms of conformal time.

$$a\zeta'' + a'\zeta' + \left(\frac{GM_{tot}}{R^3\zeta^2} - \frac{4\pi G}{3}a^3\tilde{\tilde{\rho}}_m\zeta\right) = 0 \tag{2.6}$$

$$a(\eta) = a_{eq}\left[2\frac{\eta}{\eta_*} + \frac{\eta^2}{\eta_*^2}\right] \qquad \text{where} \qquad \eta_*^{-2} = \frac{2\pi G\tilde{\tilde{\rho}}_{eq}a_{eq}^3}{3} \tag{2.7}$$

where a_{eq} and $\tilde{\tilde{\rho}}_{eq}$ are respectively the scale factor and the energy density at the time when radiation and matter components have the same energy densities ($\tilde{\tilde{\rho}}_{eq} = \tilde{\tilde{\rho}}_r(\eta_{eq}) = \tilde{\tilde{\rho}}_m(\eta_{eq})$). The energy densities of the two components can then be

[2]It can be checked with (C.11) that in a RD universe $\ddot{a} = -\frac{8\pi G}{3}a\tilde{\tilde{\rho}}_r$, which applied to proper distances leads to the first term of the equation of motion.

[3]See section C.1 for the notation.

found at any time using their scaling relations (C.15) and (C.26), which can also be derived from Friedmann equations (see section C.1).

$$\tilde{\bar{\rho}}_r \propto \frac{1}{a^4} \qquad \Rightarrow \qquad \tilde{\bar{\rho}}_r = \tilde{\bar{\rho}}_{eq} \frac{a_{eq}^4}{a^4} \tag{2.8}$$

$$\tilde{\bar{\rho}}_m \propto \frac{1}{a^3} \qquad \Rightarrow \qquad \tilde{\bar{\rho}}_m = \tilde{\bar{\rho}}_{eq} \frac{a_{eq}^3}{a^3} \tag{2.9}$$

The matter perturbation is $\Phi = \frac{\delta\tilde{\bar{\rho}}_m}{\tilde{\bar{\rho}}_m} = \frac{\delta\rho_m}{\bar{\rho}_m} = \delta$ (1.1) and the mass can be written as follows.

$$M_{tot} = \frac{4\pi}{3} \tilde{\bar{\rho}}_{eq} a_{eq}^3 \left(1 + \Phi\right) R^3 \tag{2.10}$$

It must be noted that this mass comes from all matter within the initial sphere, when no deviation from the background was present $\zeta = 1$. Consequently ζ component is absent from its formula.

A further substitution can be performed by using (2.7) and replacing η with $\frac{a}{a_{eq}}$.

$$\eta = \eta_* \left(\pm \sqrt{1 - \frac{a}{a_{eq}}} - 1 \right) \tag{2.11}$$

which can get further simplified by knowing that both η and a must be positive.

$$\eta = \eta_* \left(\sqrt{1 - s} - 1 \right), \qquad s = \frac{a}{a_{eq}} \tag{2.12}$$

With this substitution also the derivative over the conformal time must be modified.

$$\frac{d}{d\eta} = 2 \frac{\sqrt{1+s}}{\eta_*} \frac{d}{ds} \tag{2.13}$$

Once this substitution is applied to (2.6) together with the mass formula (2.10) and η_* (2.7), it gives the general perturbation evolution of the spherical model.

$$\boxed{s(1+s)\frac{d^2\zeta}{ds^2} + \left(1 + \frac{3}{2}s\right)\frac{d\zeta}{ds} + \frac{1}{2}\left(\frac{1+\Phi}{\zeta^2} - \zeta\right) = 0} \tag{2.14}$$

where $\Phi = \delta$.

2.1.1 Early times

If a moment really early in the universe is considered $s \to s_0 \approx 0$. At that time it can be expected that no collapse has started yet $\zeta(s_0) = 1$. From these assumptions, it is possible to find a solution of (2.14) at $s \ll 1$, by neglecting the second derivative term $\frac{d^2\zeta}{ds^2}$, due to its small contribution from s. The numerical solution is the following [11].

$$\zeta \approx (1 - \frac{3}{2}\Phi s)^{\frac{1}{3}} \approx 1 - \frac{\Phi s}{2} + \mathcal{O}(s^2) \tag{2.15}$$

which holds only for small s. Its validity can be checked by putting it back into (2.14) for s_0. From this approximation, the initial conditions of a perturbation can be calculated.

$$\zeta(s_0 \approx 0) = 1 \qquad \text{and} \qquad \frac{d\zeta}{ds}(s_0 \approx 0) \approx -\frac{\Phi}{2} \tag{2.16}$$

2.1.2 Maszaros equation

From (2.14) also the *Maszaros equation* can be extracted. This equation is particularly important for small perturbations as it shows that in a RD universe these kinds of fluctuations do not grow. In fact, for an arbitrary small perturbation $\delta \ll 1$ the deviation from the background is small $\zeta \approx 1 - \delta$ as well as the amplitude of the overdensity $\Phi \approx 0$. Maszaros equation can be found by applying these approximations to (2.14), and looking at the linear terms only. In fact for small perturbations $\mathcal{O}(\delta^2)$ terms can be neglected.

$$s(1+s)\frac{d^2\delta}{ds^2} + \left(1 + \frac{3}{2}s\right)\frac{d\delta}{ds} - \frac{3}{2}\delta = 0 \tag{2.17}$$

This equation can be solved analytically and the highest growing solution is $\delta = \delta_0\left(1 + \frac{3}{2}s\right)$ [11], which shows that for a small initial amplitude, the perturbation will not grow substantially for $s \lesssim 1$. This translates to small amplitude fluctuations not growing in the RD universe ($a \lesssim a_{eq} \Rightarrow s \lesssim 1$), but only in a MD universe ($a \gtrsim a_{eq} \Rightarrow s \gtrsim 1$).

2.1.3 Turnaround

One goal of the spherical model is also to shed light on the collapse of overdense regions. In order to do that, the radius and density of fluctuations are studied. Since perturbations collapse only after a first expansion phase, the maximum size of a clump is found at *turnaround*, where this process is inverted $\dot{\tilde{R}} = 0$. For this reason, the radius and density of perturbations at turnaround are studied, as they provide important information on the fluctuations. In comoving coordinates, this translates to

$$\zeta + s\frac{d\zeta}{ds} = 0 \tag{2.18}$$

If the perturbation reaches turnaround in the early universe ($s_{ta} \ll 1$), the approximation of early times (2.15), up to order $\mathcal{O}(s^2)$, can be applied, giving the time and deviation from the background at turnaround.

$$s_{ta} = \frac{const}{\Phi} \qquad \Rightarrow \qquad \zeta_{ta} = const \tag{2.19}$$

Regarding the density of perturbations in the spherical model, the clumps are spherically symmetric, meaning that despite inner regions can be more or less dense than outer ones, each shell will have a constant surface density. This density difference between the shells can be represented by $\frac{dM}{d\tilde{R}}$. Matter energy density can then be found by dividing this derivative by the shell's surface.

$$\tilde{\rho}_m = \frac{1}{4\pi\tilde{R}^2}\frac{dM}{d\tilde{R}} \tag{2.20}$$

Consequently, in comoving coordinates, the parameters at turnaround are the following [11].

$$s_{ta} = \frac{C_s}{\Phi}, \qquad \tilde{\rho}_{ta} = C_{\tilde{\rho}}\tilde{\rho}_{eq}\frac{\Phi^3}{3R^2}\frac{d}{dR}\left(1+\Phi\right)R^3 \tag{2.21}$$

where (2.10) was used, while C_s and $C_{\tilde{\rho}}$ are values that can be found numerically and have a weak dependence on the parameter Φ. These latter two values are numerical result, and for practical applications with $\Phi \ll 1$ and $\Phi \gg 1$ can be considered constants [11].

2.2 PBH perturbations

Regarding PBHs there is no knowledge about the composition of the non-relativistic matter that leads to their collapse. Even if PBH were made out of baryons, which is most likely not the case, as their collapse is expected to take place in the RD universe, their components would not be considered in the known baryon abundance Ω_b. For this reason, the matter that collapses into PBH, and consequently the PBHs themselves, is cold dark matter (DM)[4]. The baryonic component of non-relativistic matter does not contribute to the spherical collapse that leads to PBH, thus only DM perturbations are involved.

It follows that the collapsing object mass (2.10), together with the equation of motion in conformal time (2.6), must be written differently for PBHs, considering DM only[5].

$$a\zeta'' + a'\zeta' + \left(\frac{GM_{tot}}{R^3\zeta^2} - \frac{4\pi G}{3}a^3\tilde{\bar{\rho}}_{DM}\zeta\right) = 0 \tag{2.22}$$

$$M_{tot} = \frac{4\pi}{3}\left[\tilde{\bar{\rho}}_{DM}\left(1+\Psi\right)\right]a^3R^3 \tag{2.23}$$

where the ensemble of dark matter and baryons make up the entire non-relativistic matter $\tilde{\bar{\rho}}_m = \tilde{\bar{\rho}}_{DM} + \tilde{\bar{\rho}}_b$. It must be noted that the perturbation Ψ is different from the one used in the previous section. In fact, while $\Phi = \frac{\delta\rho_m}{\bar{\rho}_m}$, the new perturbation is $\Psi = \frac{\delta\rho_{DM}}{\bar{\rho}_{DM}}$. This shift to DM fluctuations can also be written as

$$a\zeta'' + a'\zeta' + \gamma\left(\frac{GM_{tot}}{R^3\zeta^2} - \frac{4\pi G}{3}a^3\bar{\rho}_m\zeta\right) = 0 \qquad \text{with} \qquad \gamma = \frac{\Omega_c}{\Omega_m} = \frac{\Omega_m - \Omega_b}{\Omega_m} \tag{2.24}$$

where Ω_c is the non-relativistic matter abundance (see section C.3) that clusters and could form PBHs, or DM. From this point, perturbations can be developed as previously done in (2.14).

$$s(1+s)\frac{d^2\zeta}{ds^2} + \left(1+\frac{3}{2}s\right)\frac{d\zeta}{ds} + \frac{1}{2}\gamma\left(\frac{1+\Psi}{\zeta^2} - \zeta\right) = 0 \tag{2.25}$$

Maszaros equation (2.17) for DM then reads

$$\boxed{s(1+s)\frac{d^2\delta_{DM}}{ds^2} + \left(1+\frac{3}{2}s\right)\frac{d\delta_{DM}}{ds} - \frac{3}{2}\gamma\delta_{DM} = 0} \tag{2.26}$$

This equation is often recalled throughout the paper. The fact that DM overdensities, instead of matter, are used in this last equation is not a problem, as they will be used to study DM perturbations only.

[4] It is implicit here that cold dark matter is discussed since the ΛCDM model is being studied.

[5] The baryonic component is excluded because not perturbed, therefore in a confined region $M_b = \frac{4\pi}{3}r^3\tilde{\bar{\rho}}_b = \frac{4\pi}{3}a^3\zeta^3R^3\tilde{\bar{\rho}}_b$.

2.2.1 Early times

Recalling subsection 2.1.1, the study of early times for DM perturbations will lead to the same solution, but with the inclusion of the γ factor.

$$\zeta \approx (1 - \frac{3}{2}\gamma\Psi s)^{\frac{1}{3}} \approx 1 - \gamma\frac{\Psi s}{2} + \mathcal{O}(s^2) \tag{2.27}$$

Analogously to the previous section, this equation only holds for small s and the initial conditions are the following.

$$\zeta(s_0 \approx 0) = 1 \qquad \text{and} \qquad \frac{d\zeta}{ds}(s_0 \approx 0) \approx -\gamma\frac{\Psi}{2} \tag{2.28}$$

2.2.2 Perturbations evolution

The presence of PBHs generates isocurvature fluctuations, as they from DM overdensities in the RD universe. An important step for this report is to find the perturbation evolution of these objects. This result can be achieved by solving the evolution equation given above (2.25). However, on large scales, the linear solution provides sufficient information for this study, therefore Maszaros equation for DM (2.26) can be used to find the fluctuations evolution of PBHs.

Resolutions of (2.26) are discussed in [14], where Maszaros equation for DM leads to two independent solutions. It must be mentioned, that although PBHs generate isocurvature perturbations, they are not expected to explain all DM. The remaining component can still be considered to form adiabatic perturbations. Thus the two solutions can be combined into these two types of fluctuations evolution: $D_{ad}(a)$ represents the adiabatic perturbations component and $D_{iso}(a)$ the isocurvature ones. The adiabatic part is well known, and its evolution will be discussed in section 3.1 [15]. On the other hand, isocurvature perturbations property of remaining constant through horizon crossing and RD universe can be used to find asymptotic solutions [14] [16] [17].

$$D_{iso}(s) \approx 1 + \frac{3\gamma}{2}s \qquad \text{for} \qquad s \ll 1 \tag{2.29}$$

$$D_{iso}(s) \propto s^{a_-} \qquad \text{for} \qquad s \gg 1 \tag{2.30}$$

However, a good fit for matching these asymptotic limits and describing the evolution of isocurvature perturbations at all s is given by [14].

$$\boxed{D_{iso}(s) \approx \left(1 + \frac{3\gamma}{2a_-}s\right)^{a_-}, \qquad a_- = \frac{1}{4}\left(\sqrt{1+24\gamma} - 1\right)} \tag{2.31}$$

where a precision of 1.5% for $0.5 \leq \gamma \leq 1$ is claimed [14]. This constraint on γ is expected to be true by observations (see Appendix A).

2.3 Critical overdensity

A fundamental element for the calculations of this project is the *critical overdensity*. This value represents the matter energy density contrast required for a perturbation to collapse and it can be computed using the spherical model. The standard value for this missing element in a MD universe, which highlights the overdensity required for matter to collapse or virialise, is the following.

$$\boxed{\delta_c = 1.686} \tag{2.32}$$

In this section the analytical derivation of this variable is computed, firstly only for the case of interest, therefore in a flat MD universe, in subsection 2.3.1. Although this first explanation is sufficient for the computations of this report, a general derivation of the critical overdensity, which is valid at any time, is also carried out in subsection 2.3.2.

2.3.1 Matter dominated universe derivation

It is possible to derive the critical overdensity from analytical calculations for the scenario of interest, a MD universe ($z \gg z_{eq}$), following article [13]. In order to do that, the properties of a flat MD universe and its linear perturbations should be recalled from subsection C.2.1. More specifically, the background matter energy density (C.15) and the linear matter overdensity dependence on time (C.22).

$$\tilde{\bar{\rho}}_m = \frac{1}{6\pi G}\frac{1}{t^2} \propto \frac{1}{a^3} \tag{2.33}$$

and

$$\delta_L \propto a \propto t^{\frac{2}{3}} \tag{2.34}$$

The critical overdensity determines the barrier required for a perturbation to collapse. To calculate this value the spherical model is used by looking at the equation of motion dictated by gravity (2.1), where no radiation is involved, because of matter domination.

$$\ddot{\tilde{R}} = -\frac{GM_{tot}}{\tilde{R}^2} \tag{2.35}$$

This equation can be integrated, leading to

$$\frac{1}{2}\dot{\tilde{R}}^2 - \frac{GM}{\tilde{R}} = E \tag{2.36}$$

where E is the conserved specific energy on a spherical shell of radius $\tilde{R}$, the first term on the left correspond to the kinetic term dictated by the expansion of the universe $\dot{\tilde{R}} = H\tilde{R}$ and the mass M can be rewritten in terms of the overdensity of the region of interest.

$$M = \frac{4}{3}\pi\tilde{R}^3\tilde{\bar{\rho}}_m\left[1 + \delta_{sp}\right] \tag{2.37}$$

where δ_{sp} is the spherical overdensity. Using the background energy density (2.33), the energy conservation (2.36) can also be written as follows[6].

$$E = \frac{1}{2}\dot{\tilde{R}}^2 - \frac{GM}{\tilde{R}} = -\delta_{sp}\frac{1}{2}H^2\tilde{R}^2 \tag{2.38}$$

For a collapsing object, the specific energy must be negative $E < 0$, so that gravitational forces prevail, hence $\delta_{sp} > 0$. As a consequence, (2.36) has the following solution [13].

$$\tilde{R} = A(1-\cos(\theta)) \qquad t = B(\theta - \sin(\theta)) \tag{2.39}$$

$$A^3 = GMB^2 \qquad E = -\frac{1}{2}\frac{A^2}{B^2} < 0 \tag{2.40}$$

where θ, A and B are new variables and t is the time. This result can be correlated to physical situations considering different values of θ.

$\theta = 0$: radius is $\tilde{R} = 0$ and time $t = 0$, the mass shell starts expanding from a point mass.

$\theta = \pi$: the radius of the mass shell $\tilde{R} = \tilde{R}_{ta}$ is maximum and time $t = t_{ta}$. This situation is called turnaround and represents the moment when the mass shell reaches its maximum extension and starts to recollapse (see subsection 2.1.3). In fact it can be checked that $\dot{\tilde{R}}|_{t_{ta}} = 0$. From this, variables A and B can be computed at this moment.

$$A = \frac{\tilde{R}_{ta}}{2}, \qquad B = \frac{t_{ta}}{\pi} \tag{2.41}$$

$\theta = 2\pi$: once again $\tilde{R} = 0$, but the time $t = t_{vir} \approx 2t_{ta}$, the mass shell has collapsed. This situation is also called virialization. In fact, not all physical objects can collapse to a singularity, but because of non-homogeneous densities and differences from a perfect sphere, they find their equilibrium in a non-singular collapsed object called virialized ($\tilde{R}_{vir} \approx \frac{1}{2}\tilde{R}_{ta}$).

Knowing the time dependent formula of the background density (2.33), the overdensity can be written in terms of θ.

$$\tilde{\rho}_m = \frac{3M}{4\pi\tilde{R}^3} = \frac{3M}{4\pi A^3(1-\cos(\theta))^3}, \qquad \tilde{\bar{\rho}}_m = \frac{1}{6\pi G t^2} = \frac{1}{6\pi G B^2(\theta-\sin(\theta))^2} \tag{2.42}$$

$$\Rightarrow \delta_{sp} = \frac{\tilde{\rho}_m}{\tilde{\bar{\rho}}_m} - 1 = \frac{9}{2}\frac{(\theta-\sin(\theta))^2}{(1-\cos(\theta))^3} - 1 \tag{2.43}$$

Now consider an initially small perturbation $\delta_{sp}(t_i) = \delta_i \ll 1$, which allows the application of the linear regime. Since an object that undergoes a collapse,

[6] This result is given by the fact that in a MD universe equation (C.34) reads $H^2 = H_0^2\Omega_m\left(\frac{1}{a}\right)^3$ or in proper coordinates $H^2 = H_0^2\tilde{\Omega}_m$. Consequently, using abundances (see section C.3), the mass (2.37) reads $M = \frac{4}{3}\pi\tilde{R}^3\rho_{cr}\tilde{\Omega}_m\left[1+\delta_{sp}\right]$ and the kinetic term $\frac{1}{2}\dot{\tilde{R}}^2 = \frac{1}{2}H^2\tilde{R}^2 = \frac{1}{2}H_0^2\tilde{\Omega}_m\tilde{R}^2$.

firstly goes through an expansion, until the turnaround, and only then collapses, continuously increasing its overdensity, a perturbation before initial expansion $t_i = t(\theta \ll 1)$ is considered here. Consequently, both t and δ_{sp} can be Taylor expanded around 0 for $\theta \ll 1$[7].

$$t_i = B\frac{\theta^3}{6} + \mathcal{O}(\theta^5) \tag{2.44}$$

$$\delta_i = \frac{9}{2}\frac{\frac{\theta^6}{36}\left(1-\frac{\theta^2}{10}\right)+\mathcal{O}(\theta^{10})}{\frac{\theta^6}{8}\left(1-\frac{\theta^2}{4}\right)+\mathcal{O}(\theta^{10})} - 1 \approx \left[\left(1-\frac{\theta^2}{10}\right)\left(1+\frac{\theta^2}{4}\right)+\mathcal{O}(\theta^{10})\right] - 1 \tag{2.45}$$

$$\approx \frac{3\theta^2}{20} + \mathcal{O}(\theta^4) \tag{2.46}$$

$$\Rightarrow \qquad \delta_i = \frac{3}{20}(6\pi)^{\frac{2}{3}}\left(\frac{t_i}{t_{ta}}\right)^{\frac{2}{3}} \tag{2.47}$$

where the relations (2.41) were used in the last passage. Since δ_i is considered to be small, it can be evolved using linear perturbation theory (2.34) instead of the spherical model, to understand its limits in this regime.

$$\delta_L \propto t^{\frac{2}{3}} \qquad \Rightarrow \qquad \delta_L(t) = \delta_i\left(\frac{t}{t_i}\right)^{\frac{2}{3}} = \frac{3}{20}(6\pi)^{\frac{2}{3}}\left(\frac{t}{t_{ta}}\right)^{\frac{2}{3}} \tag{2.48}$$

It follows that both the spherical model and linear theory overdensities can be evolved from the initial δ_i to turnaround t_{ad} and virialization time $t_{vir} = 2t_{ta}$.

	δ_{sp}	δ_L
t_i and θ_i	$\frac{9}{2}\frac{(\theta_i-\sin(\theta_i))^2}{(1-\cos(\theta_i))^3} - 1$	$\frac{3}{20}(6\pi)^{\frac{2}{3}}\left(\frac{t_i}{t_{ta}}\right)^{\frac{2}{3}}$
t_{ta} and $\theta = \pi$	$\frac{9}{16}\pi^2 - 1 = 4.55$	$\frac{3}{20}(6\pi)^{\frac{2}{3}} = 1.062$
$t_{vir} = 2t_{ta}$ and $\theta = 2\pi$	∞	$\frac{3}{20}(12\pi)^{\frac{2}{3}} = 1.686$

While the spherical model collapse ends at infinity overdensity, meaning it reaches a singularity, the linear model gives a finite value. Combining the two models, this result means that if the linear perturbation is used, an overdensity $\delta_L = 1.686$ would highlight the presence of a collapsed or virialized object, as described by the more reliable spherical model. For this reason, this value is called critical overdensity and gives the threshold for collapse, matching the value mentioned above (2.32).

$$\delta_c = 1.686 \tag{2.49}$$

2.3.2 General derivation

A general derivation of the critical overdensity, which is not restricted to a MD universe can be performed starting from the evolution of perturbation, studied

[7] Expanding $(\theta - \sin(\theta))^2$ and $(1-\cos(\theta))^3$ gives respectively $\frac{\theta^6}{36}\left(1-\frac{\theta^2}{10}\right)+\mathcal{O}(\theta^{10})$ and $\frac{\theta^6}{8}\left(1-\frac{\theta^2}{4}\right)+\mathcal{O}(\theta^{10})$.

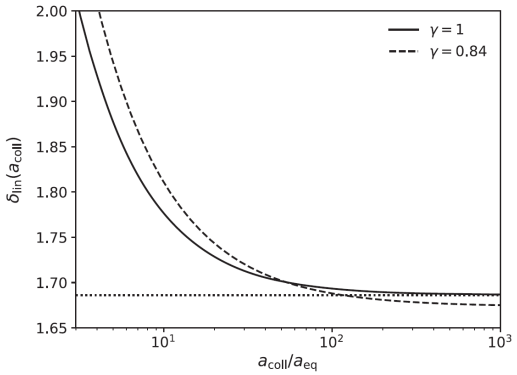

Figure 2.1: Evolution of the critical overdensity after radiation-matter equality epoch. This image is taken from [14], and the critical overdensity $\delta_{lin}(a_{coll})$ must be interpreted as $\delta_c(z_{obs})$ (2.53), hence a perturbation must have collapsed by a_{coll} or z_{obs}.

in the spherical model (2.14). Or even better considering only the matter that undergoes clustering (2.25). What needs to be found is the linear evolution of the initial critical density required for collapse, so that it can be observed. However, it is also required that virialization had happened at the time of observation. In terms of parameter ζ, which is the deviation from the standard universe expansion of the perturbation, this means finding a minimal initial DM overdensity $\delta_i = \Psi = \frac{\delta\rho_{DM}}{\bar{\rho}_{DM}}$, which leads to collapse, or $\zeta = 0$, at the time of the observed object. For the purpose of this paper, the observation time can vary approximately from $z = 0$ until $z = 20$. The next derivation takes inspiration from both [14] and [18].

The analytical objective is to find δ_i in (2.25) with initial conditions given by (2.28), so that at the redshift of interest the object has collapsed, or ζ has value 0.

$$s(1+s)\frac{d^2\zeta}{ds^2} + \left(1 + \frac{3}{2}s\right)\frac{d\zeta}{ds} + \frac{1}{2}\gamma\left(\frac{1+\delta_i}{\zeta^2} - \zeta\right) = 0 \tag{2.50}$$

$$\zeta(s_0 \approx 0) = 1, \qquad \frac{d\zeta}{ds}(s_0 \approx 0) \approx -\gamma\frac{\delta_i}{2}, \qquad \zeta(z_{obs}) \approx 0 \tag{2.51}$$

where once again $s = \frac{a}{a_{eq}}$. Solving this equation leads to finding the critical initial DM overdensity required for an object to collapse within z_{obs}: $\delta_i(z_{obs})$. It must be noted that depending on z_{obs} this value can change. In addition to that, only the initial critical overdensity δ_i is searched, while the form of $\zeta(s)$ is not required. This, together with the approximations of the constraints suggests looking for a numerical solution to the problem.

Once the value of $\delta_i(z_{obs})$ has been computed, the linear evolution of this overdensity can be calculated. This means that $\delta_i(z_{obs})$ can be evolved from early times until z_{obs} with linear theory, hence using Maszaros equation (2.26) for small perturbations. The resolution of this equation has already been done in subsection 2.2.2 and leads to the evolution factor (2.31).

$$D_{iso}(a) \approx \left(1 + \frac{3\gamma}{2a_-}\frac{a}{a_{eq}}\right)^{a_-}, \qquad a_- = \frac{1}{4}\left(\sqrt{1+24\gamma} - 1\right) \tag{2.52}$$

This is used to linearly evolve the critical overdensity until z_{obs} [14].

$$\delta_c(z_{obs}) = D_{iso}(z_{obs})\delta_i(z_{obs}) \tag{2.53}$$

More concretely the critical overdensity $\delta_c(z_{obs})$ represents the overdensity threshold at z_{obs} over which a perturbation must have collapsed or virialized. Thus every observed density contrast, which is equal to or higher than $\delta_c(z_{obs})$ at z_{obs}, indicates a collapsed object. The value $\delta_c = 1.686$ can be derived considering all matter as clustering ($\gamma = 1$) and setting $z_{obs} = 0$. However, it is also possible to find the critical overdensities for many different and high redshifts.

On the other hand, solving (2.50) is not straightforward and could require complex numerical methods. In Figure 2.1 a plot of critical overdensities over a large span of redshifts is reported, taken from [14]. This shows that the value $\delta_c = 1.686$ is in fact a very good approximation for the MD universe, especially for $z \lesssim 100$. For this reason, the result (2.32) is used throughout this report.

3 Galaxy formation with Poisson distributed PBHs

The article "Accelerating early massive galaxy formation with primordial black holes" [9] tries to give an explanation of how an initial Poisson distribution of PBHs in the universe could have led to boost galaxy formations, to match with JWST observations. In this chapter, a similar analysis of that study is reported. The objective of this task is both educational, to better understand the concepts behind this work, by having the possibility to compare the results, and for research purposes. In fact, this chapter represents the first part of this study. In the next chapter, the limits of this analysis will be studied, together with possible improvements.

PBHs are still surrounded by mystery since their existence has not been proven yet nor their variables have been fixed. The goal of this study is to determine the *stellar mass density*, for different PBH parameters. Specifically, the fraction of DM occupied by PBHs f_{PBH} and their mass m_{PBH}, considering them to be monochromatic[1]. Finding the stellar mass density for different variables will highlight if and which possible combination could have enhanced galaxy formation so that JWST observations had been possible.

This chapter's analysis proceeds as follows: in section 3.1 the power spectrum is discussed, at first the adiabatic component only, recalling its general derivation, then the isocurvature power spectrum, coming from the addition of PBHs to the universe. In section 3.2 the *Press-Schechter* (PS) formalism is introduced, as this is the model used to compute the *halo mass function* (HMF). In section 3.3, the previous findings are put together to calculate the resulting stellar mass density. In addition to the analytical results, this section also includes the numerical ones. Lastly, section 3.4 concludes this chapter with a discussion of the results obtained and a small comparison with the conclusions of article [9].

[1]The assumption that PBHs are monochromatic is clearly a simplification, which should however describe relatively well a distribution of masses around the chosen one.

3.1 Power spectrum

The first step in this study is to understand and derive the matter power spectrum of the ΛCDM standard model before, and with the addition of PBHs after. The power spectrum is a powerful tool in cosmology which is used to describe different overdensities of the universe depending on the scale. Mathematically is defined as the Fourier transform of the matter correlation function. In Appendix D an introduction about the properties and usage of the power spectrum is reported.

In this section, the standard model adiabatic power spectrum and the isocurvature one coming from a Poisson distribution of PBHs are computed and shown.

3.1.1 Adiabatic power spectrum

The derivation of the adiabatic power spectrum is complex and related to observations. In this first part, a brief introduction of its origin, in terms of two main components, *transfer function* and *growth factor*, is proposed, following the references [19], [20] and [21][2].

One way to calculate the power spectrum is to consider the universe as a fluid and start from the Poisson equation to find a relation between energy overdensities of non-relativistic matter perturbations (baryons and dark matter). In particular in the matter domination, after radiation-matter equality z_{eq}[3], the universe can be considered as composed of a single fluid, since radiation do not play a significant role anymore. The linearized Poisson equation then reads as follows [20] [21].

$$\nabla^2 \delta\varphi(\tilde{\mathbf{x}}, a) = 4\pi G \delta_m \tilde{\rho}_m(\tilde{\mathbf{x}}, a) = 4\pi G \tilde{\bar{\rho}}_m(a) \delta_m(\tilde{\mathbf{x}}, a) \tag{3.1}$$

where $\delta_m = \frac{\delta\tilde{\rho}_m}{\tilde{\bar{\rho}}_m} = \frac{\delta\rho_m}{\bar{\rho}_m}$ as defined in (1.1), with $\tilde{\bar{\rho}}_m$ being the proper mean matter energy density, thus only depending on the scale factor a. The term $\delta\varphi$ represents the fluctuation of the gravitational potential used in perturbation theory. In Fourier space (3.1) transforms to the equation shown below.

$$k^2 \delta\varphi(\mathbf{k}, a) = 4\pi G \frac{\bar{\rho}_m}{a} \delta_m(\mathbf{k}, a) \tag{3.2}$$

where the additional a comes from the fact that a transformation to comoving coordinates is applied (see subsection C.1.1). For clarity, the proper variables are written here extensively.

$$\tilde{k} = \frac{k}{a}, \qquad \tilde{\bar{\rho}}_m = \frac{\bar{\rho}_m}{a^3} = \frac{\Omega_m \rho_{cr}}{a^3}, \qquad \rho_{cr} = \frac{3H_0^2}{8\pi G} \tag{3.3}$$

where ρ_{cr} is the so called critical density (see section C.3). This leads to find the matter overdensity explicitly.

$$\delta_m(\mathbf{k}, a) = \frac{2k^2 a}{3\Omega_m H_0^2} \delta\varphi(\mathbf{k}, a) \tag{3.4}$$

[2] In particular chapter 8 of [20] and chapter 19 of [21].
[3] For the precise value of z_{eq} see Appendix A.

This equation is valid within the Hubble horizon (see section C.4), hence for $k < aH$, meaning for perturbations which re-entered the Hubble horizon ($l_H = \frac{1}{aH}$)[4].

On the other hand, the gravitational field perturbation $\delta\varphi$ can be written in terms of transfer function $T(k)$, growth factor $D(a)$ and an additional term coming from its initial conditions $\Phi(\mathbf{k})$ [20] [21].

$$\delta\varphi(\mathbf{k}, a) = T(k)D(a)\Phi(\mathbf{k}) \tag{3.5}$$

Details on these three components are found below.

3.1.1.1 Initial curvature perturbation

The term $\Phi(\mathbf{k})$ represents the curvature perturbations generated during inflation. Without going into too many details, the derivation of $\Phi(\mathbf{k})$ for a MD universe comes from perturbed Einstein equations [21].

$$\delta G^{\mu}_{\nu} = 8\pi G \delta T^{\mu}_{\nu} \tag{3.6}$$

where G^{μ}_{ν} is the so called *Einstein tensor* and T^{μ}_{ν} is the *energy-momentum tensor*. These last equations are the linearization of the more general energy-momentum conservation.

$$\nabla_{\mu} T^{\mu}_{\nu} = 0 \tag{3.7}$$

The Poisson equation mentioned above (3.1), comes in fact from the $(0,0)$ component of Einstein equation (3.6) with the approximations that a single-component fluid (MD universe) is considered, within the Hubble horizon $k \ll aH$.

In order to find the value of the initial curvature perturbation a complex analysis is required. Specifics of this derivations are beyond the scope of this study, however a brief summary is reported here[5]. The initial perturbations are based on adiabatic conditions for all relevant modes. To find their values, the introduction of two new variables ζ and $\mathcal{R}$ for the adiabatic modes is required. These new variables can be used to find the following equalities. For the RD universe

$$\mathcal{R} = \frac{3}{2}\Phi_{RD} \tag{3.8}$$

where Φ_{RD} is constant over $\mathbf{k}$ and represents the perturbation conditions deep in the RD universe. For the RD-MD transition

$$\zeta = \frac{3}{2}\Phi_{RD} = \frac{5}{3}\Phi_{MD} \qquad \Rightarrow \qquad \Phi_{MD} = \frac{9}{10}\Phi_{RD} \tag{3.9}$$

where Φ_{MD} is also constant and represents the perturbation conditions deep in the MD universe. This leads to finding two different relations between the new cosmological variable $\mathcal{R}$ and the perturbation conditions for RD and MD universe.

$$\mathcal{R} = \frac{3}{2}\Phi_{RD} \qquad \text{and} \qquad \mathcal{R} = \frac{5}{3}\Phi_{MD} \tag{3.10}$$

[4]The normalization here and throughout the report is $k = \frac{1}{L}$ instead of $k = \frac{2\pi}{L}$, where L is the characteristic length of the perturbation. See Appendix D.

[5]An extensive explanation can be found in sections 19.2-3 of [21].

These relations are important because, while the value of $\mathcal{R}$ cannot be measured, its autocorrelation function can.

$$\langle|\mathcal{R}(k)|^2\rangle = P_{\mathcal{R}}(k) = 2\pi^2 \mathcal{A}_{\mathcal{R}} k^{-3} \left(\frac{k}{k_p}\right)^{n_s-1} \tag{3.11}$$

where $\mathcal{A}_{\mathcal{R}}$ is also called the primordial power spectrum amplitude at *pivot scale* k_p and n_s is the scalar spectral index. This power spectrum is evaluated with a power law solution around a reference value, the pivot scale k_p, which normally has a defined value of $k_p = 0.05\,\mathrm{Mpc}^{-1}$. The value of $\mathcal{A}_{\mathcal{R}}$ can be calculated from observations, but also depends on the chosen cosmological models. The best fit for $\mathcal{A}_{\mathcal{R}}$ so far, considering an ΛCDM model, is evaluated in [22] and its value is listed in Appendix A, as well as the one for n_s. As a consequence of (3.10) the initial condition of the power spectra in RD and MD are written below.

$$P_{RD}(k) = \frac{4}{9} P_{\mathcal{R}}(k) = \frac{8}{9}\pi^2 \mathcal{A}_{\mathcal{R}} k^{-3} \left(\frac{k}{k_p}\right)^{n_s-1} \tag{3.12}$$

$$\langle|\Phi(\mathbf{k})|^2\rangle = P_{MD}(k) = \frac{9}{25} P_{\mathcal{R}}(k) = \frac{18}{25}\pi^2 \mathcal{A}_{\mathcal{R}} k^{-3} \left(\frac{k}{k_p}\right)^{n_s-1} \tag{3.13}$$

where the MD primordial power spectrum is the autocorrelation function of the initial conditions of the perturbation from (3.5).

3.1.1.2 Transfer function

Secondly, the transfer function $T(k)$ is defined as follows [20].

$$T(k) = \frac{\delta\varphi(k,a)}{\delta\varphi_{large-scale}(k,a)} \tag{3.14}$$

It describes the evolution of perturbations through the epochs of horizon crossing. Once again, without going into the complexity of its derivation, the transfer function can be approximated with observations. A useful explicit fitted solution, known as BBKS[6] transfer function, is written below [21].

$$\boxed{T(k) = \frac{\ln(1+0.171\kappa)}{0.171\kappa}\left[1+0.284\kappa+(1.18\kappa)^2+(0.399\kappa)^3+(0.490\kappa)^4\right]^{-\frac{1}{4}}} \tag{3.15}$$

where $\kappa = \frac{k}{k_{eq}}$ and k_{eq} is the inverse comoving horizon at RD-MD equality.

3.1.1.3 Growth factor

Lastly, the growth factor $D(a)$ is defined as the wavelength-independent growth of the perturbations due to gravity and the expansion of the universe [20].

$$D(a) = \frac{D_+(a)}{a} = \frac{\delta\varphi(k,a)}{\delta\varphi(k,a')}, \qquad a > a' \tag{3.16}$$

[6] BBKS approximation comes from the physicists who found this fit: Bardeen, Bond, Kaiser and Szalay [23].

The explicit formula that describes this parameter can be found analytically [21].

$$\boxed{D_+(a) = \frac{5\Omega_m}{2} h(a) \int_0^a \frac{da'}{(a'h(a'))^3}} \tag{3.17}$$

where $h(a) = \Omega_m^{\frac{1}{2}} a^{-\frac{3}{2}}$ is the dimensionless Hubble parameter in a MD universe, with time dependence on the scale factor. For a MD universe with $\Omega_m = 1$ $D_+(a_0) = a_0$ and consequently $D(a_0) = 1$. As was the case for the transfer function, it is possible to approximate the growth factor and write it in terms of abundances instead of scale factor [24].

$$D(a) = D(\Omega_m, \Omega_\Lambda) \approx \frac{5\Omega_m}{2\left[\Omega_m^{\frac{4}{7}} - \Omega_\Lambda + \left(1 + \frac{\Omega_m}{2}\right)\left(1 + \frac{\Omega_\Lambda}{70}\right)\right]} \tag{3.18}$$

Nevertheless, in this report (3.17) is used.

3.1.1.4 Final adiabatic power spectrum

Now that all the elements composing the perturbation (3.5) have been defined, the adiabatic power spectrum can be computed. It must be noted that both transfer function and growth factor may vary depending on the model and convention used. In this case, the model for fitting is the ΛCDM standard model.

The power spectrum can be found by applying the autocorrelation function to the matter overdensity (3.4) and plugging in the gravitational field perturbation found before (3.5) together with the initial curvature fluctuations (3.13).

$$\boxed{P(k,a) = \frac{18\pi^2}{25} \mathcal{A}_\mathcal{R} \left(\frac{D_+(a)T(k)}{H_0^2 \Omega_m}\right)^2 \frac{k^{n_s}}{k_p^{n_s - 1}}} \tag{3.19}$$

where the explicit transfer function is (3.15) while the growth factor used in this report is given by (3.16) .

Finding an approximated explicit formula for the power spectrum is also possible by substituting the elements discussed above in this result.

$$P(k,a) = \frac{9\pi^2 \mathcal{A}_\mathcal{R} k^{n_s}}{2H_0^4 k_p^{n_s-1}} h^2(a) \left(\int_0^a \frac{da'}{(a'h(a'))^3}\right)^2 \frac{\ln(1 + 0.171\kappa)^2}{(0.171\kappa)^2 \sqrt{1 + 0.284\kappa + (1.18\kappa)^2 + (0.399\kappa)^3 + (0.490\kappa)^4}} \tag{3.20}$$

where $\kappa = \frac{k}{k_{eq}}$ and there are many constants that need to be evaluated: $\mathcal{A}_\mathcal{R}$ primordial power spectrum amplitude at pivot scale k_p, scalar spectral index n_s, and Hubble parameter at present time H_0. Their measured values, coming from observations [22], can be found in Appendix A and once applied to the formula (3.20) lead to finding the adiabatic power spectrum, shown in Figure 3.1.

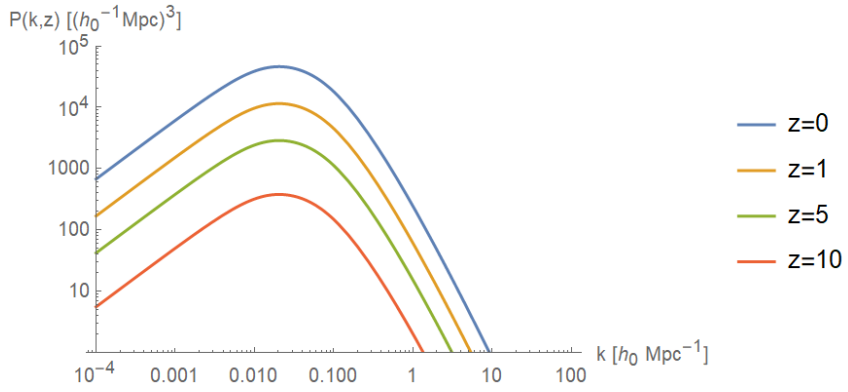

Figure 3.1: Standard ΛCDM adiabatic power spectrum evaluated with formula (3.20), over different redshifts. The peak shows the turnover of power spectrum at equality between MD and RD, since the standard ΛCMD suppresses perturbations that reenter the Hubble horizon in RD. The values used for the calculation of the power spectrum are found in Appendix A.

3.1.2 Isocurvature power spectrum

In order to finalise the power spectrum, with the inclusion of PBHs, the addition of a component due to the isocurvature perturbations is needed. In fact, as mentioned before, PBHs are expected to be the only component to initially generate isocurvature perturbation, since they form from isothermal overdensities of DM in a RD universe (see section 2.2). Therefore achieving the objective of completing the power spectrum with PBHs requires turning the attention to DM. The steps to do that are described below and follow the articles [14] and [25].

3.1.2.1 Dark matter perturbations

The assumption made by asserting the existence of PBHs is that they make up a fraction of DM: f_{PBH}, not all of it. The remaining DM can be considered to be composed of other weakly interacting massive particles: particle dark matter (PDM). In terms of perturbations, these two components have different properties. While PBHs generate isocurvature perturbation, the rest of DM is considered to be part of the ΛCDM model, hence has adiabatic fluctuations.

$$\delta_{DM}(a) = D_{ad}(a)\delta^0_{ad} + D_{iso}(a) f_{PBH}\delta^0_{iso} = (1 - f_{PBH})\delta_{PDM}(a) + f_{PBH}\delta_{PBH}(a) \quad (3.21)$$

where $D_{ad}(a)$ and $D_{iso}(a)$ play a role similar to the growth factor, but not exactly, respectively for the adiabatic and isocurvature perturbations. For this reason, these functions are called *evolution functions* in this report. The superscript 0 indicates a time prior to the entry in the Hubble horizon, hence these terms are considered the initial overdensities.

Despite PBHs being the only objects that initially produce isocurvature perturbation, this does not exclude that they can also influence adiabatic fluctuations. In addition to that, PDM can acquire an isocurvature perturbation component due to interaction with PBHs. In any case, it is assumed that all adiabatic perturbations, due to PDM, PBH or baryons, are the same before entering the horizon. All the

elements together are expected to produce one set of adiabatic fluctuations. Consequently, also their primordial relative velocity is considered to be the same. It follows that their adiabatic overdensities behave in the same way, since they are independent of their separate energy density magnitude. Even if $\rho_b \neq \rho_{PDM} \neq \rho_{PBH}$, the equalities of their adiabatic overdensities components $\delta^0_{ad} = \delta^0_b = \delta^0_{PDM} = \delta^{ad\,0}_{PBH}$ and $\dot{\delta}^0_{ad} = \dot{\delta}^0_{PDM} = \dot{\delta}^{ad\,0}_{PBH}$ are valid. On the other hand, PBHs are the only entities generating isocurvature perturbations, which are considered to remain still, even after crossing the horizon [14]. Thus they have a negligible initial relative velocity $\dot{\delta}^0_{iso} \approx 0$.

As a consequence of what was mentioned above, adiabatic perturbations have the property that their different components move together and maintain the same ratios. These perturbations modify the total energy density spatially. For $\rho_1, ..., \rho_n$ components with adiabatic perturbations, their relative variations should be the same.

$$\frac{\delta_1}{\dot{\delta}_1} = \frac{\delta_2}{\dot{\delta}_2} = ... = \frac{\delta_n}{\dot{\delta}_n} \tag{3.22}$$

On the other hand, isocurvature perturbations do not need to respect this property having different components composition.

$$S_{ij} = \frac{\delta_i}{\dot{\delta}_i} - \frac{\delta_j}{\dot{\delta}_j} \neq 0 \tag{3.23}$$

However for this second type of fluctuation, the total energy density stays the same on large scales.

Some considerations on the initial overdensities, hence before entering Hubble horizon, can be made. From what was said above, the adiabatic component of perturbations coming from PBH and PDM should be the same.

$$\delta^0_{PBH} = \delta^0_{ad} + \delta^0_{iso}, \qquad \delta^0_{PDM} = \delta^0_{ad} \tag{3.24}$$

$$\Rightarrow \delta^0_{PBH} - \delta^0_{PDM} = \delta^0_{iso} \tag{3.25}$$

Additionally, since initial isocurvature perturbations are assumed to be still, this difference should be constant through time.

$$\delta_{PBH}(a) - \delta_{PDM}(a) = \delta^0_{iso} \tag{3.26}$$

Despite the initial PDM fluctuations being purely adiabatic, the evolution of PDM cannot be set equal to the only adiabatic overdensity discussed in subsection 3.1.1. The reason for this is that PBH can influence the adiabatic overdensities and the other way around. The explicit formula for PDM and PBH overdensities is thus the following.

$$\delta_{PDM}(a) = D_{ad}(a)\delta^0_{ad} + (D_{iso}(a) - 1) f_{PBH}\delta^0_{iso} \tag{3.27}$$

$$\delta_{PBH}(a) = \delta^0_{iso} + \delta_{PDM}(a) \tag{3.28}$$

An additional approximation that can be performed is to set the initial PBHs perturbation to be only isocurvature ones $\delta^0_{iso} \approx \delta^0_{PBH}$ [14]. In fact, the origin of perturbations due to PBH is completely different from the adiabatic one. For this reason, the properties of the two perturbations are so different that it can be expected that PBHs only generate isocurvature perturbations.

3.1.2.2 Isocurvature perturbations

While for the adiabatic perturbations, which are similar for each component, the evolution function is well known, and can be extracted from subsection 3.1.1, for isocurvature fluctuations it still needs to be defined. In fact, both evolution factor $D_{iso}(a)$ and initial perturbation δ^0_{iso} for this latter type of perturbation are still to determine.

Regarding the first missing piece, subsection 2.2.2 can be recalled, where this topic was already discussed and solved. That analysis led to the result that for the studied scenarios (where $0.5 \leq \gamma \leq 1$) a good fit for the evolution factor is the following (2.31).

$$D_{iso}(s) \approx \left(1 + \frac{3\gamma}{2a_-}s\right)^{a_-}, \qquad a_- = \frac{1}{4}\left(\sqrt{1+24\gamma} - 1\right) \tag{3.29}$$

where once again $s = \frac{a}{a_{eq}}$ and $\gamma = \frac{\Omega_c}{\Omega_m} = \frac{\Omega_m - \Omega_b}{\Omega_m}$ is the non-relativistic fraction of matter that clusters, hence DM.

Secondly, the initial isocurvature overdensity is required δ^0_{iso}. However, from the previous subsubsection the usage of the approximation $\delta^0_{iso} \approx \delta^0_{PBH}$ is justified. Since the PBHs are discrete and randomly distributed objects, their initial power spectrum, hence autocorrelation function (see D.9), instead of their overdensity can be found. Knowing these properties, the PBHs' Poisson distribution can be used to find their primordial power spectrum, which must be given by a *shot noise* (or *Poisson noise*)[7] [9].

$$P^0_{PBH}(k) = \frac{1}{\overline{n}_{PBH}} \tag{3.30}$$

where $\overline{n}_{PBH}$ is the comoving number density of PBHs. This last value can be written explicitly for a monochromatic mass function of PBH with mass m_{PBH}, which is the case studied.

$$\overline{n}_{PBH} = \frac{\rho_{cr} f_{PBH} \Omega_{DM}}{m_{PBH}} = f_{PBH} \frac{3H_0^2}{8\pi G} \frac{\Omega_m - \Omega_b}{m_{PBH}} \tag{3.31}$$

With these elements, the isocurvature power spectrum can be computed following (3.21) and (D.9).

$$\begin{aligned} P_{iso}(k,a) &\approx \frac{D^2_{iso}(a) f^2_{PBH}}{V} \left\langle |\delta^0_{iso}|^2 \right\rangle \approx D^2_{iso}(s) f^2_{PBH} \frac{1}{V} \left\langle |\delta^0_{PBH}|^2 \right\rangle \\ &= D^2_{iso}(s) f^2_{PBH} P^0_{PBH} = \frac{D^2_{iso}(s) f^2_{PBH}}{\overline{n}_{PBH}} \end{aligned} \tag{3.32}$$

where $s = \frac{a}{a_{eq}}$, $D_{iso}(s)$ is given by (3.29) and $\overline{n}_{PBH}$ by (3.31).

3.1.3 Total power spectrum

The total power spectrum must be a combination of adiabatic and isocurvature spectra, which were find respectively in subsection 3.1.1 and 3.1.2.

[7] A derivation of this property is carried out later in subsection 4.2.1.

Before computing the final result, it is necessary to look back at the DM component only. In fact, from (3.21) the power spectrum for the total DM overdensity can be calculated to be the following.

$$P_{DM}(k,a) = D_{ad}^2(a)P_{ad}^0(k) + D_{iso}^2(a)f_{PBH}^2 P_{iso}^0(k) + P_{mix}(k,a) \tag{3.33}$$

where P_{ad}^0 and P_{iso}^0 are respectively the primordial power spectrum of the adiabatic and isocurvature perturbations. The term P_{mix} is the mixing power spectrum given by the interference of the two modes, in particular, the influence of the isocurvature perturbations on adiabatic ones[8].

Besides, it is also interesting to look at PDM and PBH power spectra separately. Their formulas can be calculated by applying the autocorrelation to their overdensities (3.27) and (3.28).

$$P_{PDM}(k,a) = D_{ad}^2(a)P_{ad}^0(k) + (D_{iso}(a)-1)^2 f_{PBH}^2 P_{iso}^0(k) + P_{PDM}^{mix}(k,a) \tag{3.34}$$

$$P_{PBH}(k,a) = D_{ad}^2(a)P_{ad}^0(k) + \left[1 + (D_{iso}(a)-1)f_{PBH}\right]^2 P_{iso}^0(k) + P_{PBH}^{mix}(k,a) \tag{3.35}$$

where P_{ad}^0 and P_{iso}^0 are respectively the primordial power spectrum of the adiabatic and isocurvature perturbation, while P_{PDM}^{mix} and P_{PBH}^{mix} are the power spectra that describe the mixing of the two modes for PDM and PBH.

Nonetheless, the mixing term can be neglected due to the weak correlation between adiabatic and isocurvature perturbations. In fact, this event is not expected to play any relevant role, as its value is small [9] [14].

Finally, all the steps done before can be put together. Clearly the total perturbation is given by the addition of the adiabatic power spectrum of subsection 3.1.1 to the isocurvature one of subsection 3.1.2, similarly to (3.33). The adiabatic component of (3.33) does not add up, as it is expected to be the same as the one found before, following the discussion in subsubsection 3.1.2.1. Therefore, while (3.19) provides the formula for the adiabatic part, (3.32) does the same for the isocurvature perturbations. The result is summarised below [9] [25] [26].

$$\boxed{P(k,a) = P_{ad}(k,a) + P_{iso}(k,a), \qquad P_{iso}(k,a) \approx \frac{\left[f_{PBH}D_{iso}(a)\right]^2}{\overline{n}_{PBH}}} \tag{3.36}$$

with values

$$D_{iso}(s) \approx \left(1 + \frac{3\gamma}{2a_-}s\right)^{a_-}, \qquad s = \frac{a}{a_{eq}} \tag{3.37}$$

$$\gamma = \frac{\Omega_m - \Omega_b}{\Omega_m}, \qquad a_- = \frac{1}{4}\left(\sqrt{1+24\gamma} - 1\right) \tag{3.38}$$

$$\overline{n}_{PBH} = f_{PBH}\frac{3H_0^2}{8\pi G}\frac{\Omega_m - \Omega_b}{m_{PBH}} \tag{3.39}$$

[8] This means that adiabatic perturbations can influence the isocurvature themselves and vice versa. This is different from saying that adiabatic/isocurvature fluctuations perturb PBHs/PDM. In fact, this latter behaviour is already included in (3.27) and (3.28) by having adiabatic/isocurvature components in their overdensities.

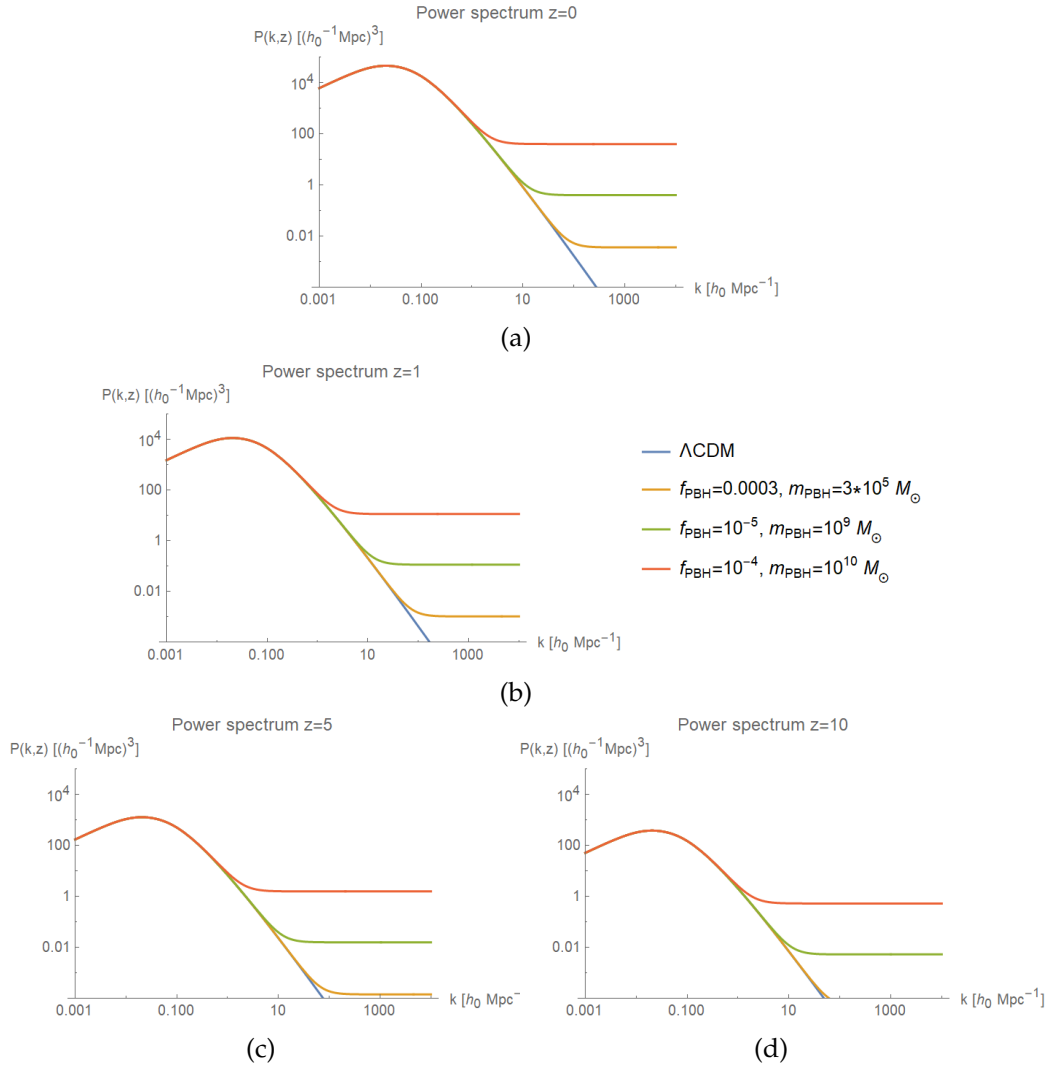

Figure 3.2: Total power spectrum at different redshifts and for different PBH variables, analogously to [9]. The power spectrum comes from formula (3.36) and is evaluated with quantities from Appendix A.

where f_{PBH} is the fraction of dark matter in form of PBHs and m_{PBH} is the monochromatic mass of PBHs.

Figure 3.2 shows the numerical results of the total power spectrum (3.36) once the observed values from Appendix A are inserted.

3.2 Press-Schechter

In this section, an important model to predict the HMF is introduced, which is called by the name of its inventors: Press-Schechter formalism [27]. This is a statistical model used to estimate the number density of virialized objects, hence the HMF. It is based on the assumption that a critical overdensity of a smoothed density contrast, for which clumps collapse, can be identified, and the volume of the perturbation that reaches that threshold is related to the mass of the halo formed. This means that large amplitude perturbations, which are found at small scales and have non-linearities, do not play an important role on a wider scale, since their mass is found to be related to the volume of a specific smoothed threshold, the critical overdensity. Although PS formalism is not as rigorous as other models, it is able to well describe the formation of non-linear structures, and their masses, by using linear theory and critical overdensity.

The critical overdensity, which is covered in detail in section 2.3, represents the linear evolution of energy contrast required for a collapse to have taken place in the past.

In this section, the PS formalism is discussed by first introducing smoothed overdensities with the *window functions*, in subsection 3.2.1. A brief part on fluctuations distribution will follow in subsection 3.2.2, while the actual PS formalism will be applied only in the last part, subsection 3.2.3, leading to the HMF. The study found below regarding the PS model, follows the steps of the article [28]. In conclusion, as the analysis is done using the spherical model, in subsection 3.2.4 the ellipsoidal correction is discussed and an adjusted HMF is computed [29].

3.2.1 Window function

In order to make it easier to deal with functions with high peaks or irregularities a window function (or *filter*) can be introduced. In this scenario, the window function is used to smooth large overdensities. Its application can be done as follows.

$$\delta(\mathbf{x}, R_W) = \int d^3\mathbf{x}' W(|\mathbf{x}' - \mathbf{x}|, R_W)\delta(\mathbf{x}') \tag{3.40}$$

where $W(|\mathbf{x}' - \mathbf{x}|, R_W)$ represents the window function that weights and smooths the function of interest, while R_W is the scale of interest that needs to be smoothed. In Fourier space, this translates to

$$\delta(\mathbf{k}, R_W) = W(\mathbf{k}, R_W)\delta(\mathbf{k}) \tag{3.41}$$

where the Fourier transforms of each component are used.

Window functions can have different forms and characteristics, one of them is their volume of influence, which is calculated in real space.

$$V_W = \int d^3\mathbf{x} W'(x, R_W) \tag{3.42}$$

and is called *window volume*. W' is the normalized dimensionless window function $W = \frac{W'}{V_W}$. This volume is related to the smoothing scale $V_W \sim R_W^3$. The three most common window functions are the following.

- *Real-space tophat window*:

$$W(x, R_W) = \begin{cases} \frac{3}{4\pi R_W^3} & x \leq R_W \\ 0 & x > R_W \end{cases} \tag{3.43}$$

$$W(k, R_W) = \frac{3\left[\sin(kR_W) - kR_W\cos(kR_W)\right]}{(kR_W)^3} \tag{3.44}$$

and has window volume $V_W = \frac{4\pi R_W^3}{3}$.

- *Fourier-space tophat window*:

$$W(k, R_W) = \begin{cases} 1 & k \leq R_W^{-1} \\ 0 & k > R_W^{-1} \end{cases} \tag{3.45}$$

$$W(x, R_W) = \frac{1}{2\pi^2 R_W^3} \frac{\left[\sin(xR_W^{-1}) - xR_W^{-1}\cos(xR_W^{-1})\right]}{(xR_W^{-1})^3} \tag{3.46}$$

The window volume is not well defined.

- *Gaussian window*:

$$W(x, R_W) = \frac{e^{-\frac{x^2}{2R_W^2}}}{(\sqrt{2\pi}R_W)^3} \tag{3.47}$$

$$W(k, R_W) = e^{-\frac{k^2}{2R_W^{-2}}} \tag{3.48}$$

and has window volume $V_W = (2\pi)^{\frac{3}{2}} R_W^3$.

3.2.2 Density fluctuations

The overdensity field is expected to be present in the universe with a random probability, hence dictated by a Gaussian field. This property can be applied to the case of smoothed functions at scale R. Therefore for each smoothing scale, the variance of the searched Gaussian random field can be found by applying the normal method.

$$\sigma^2(R) = \langle \delta^2(\mathbf{x}, R) \rangle = \int d\ln(k) \Delta^2(k, a) |W(k, R)|^2 \tag{3.49}$$

The Gaussian distribution for smoothed overdensities at scale R can then be written in its classic form.

$$p_G(\delta, R) d\delta = \frac{1}{\sqrt{2\pi\sigma^2(R)}} e^{-\frac{\delta^2}{2\sigma^2(R)}} d\delta \tag{3.50}$$

Since a hierarchical density field model is assumed, structures at all scales should exist, but as the scale gets very small, they fade away leaving room for single components that do not really have neither structures nor overdensities.

$$R \to 0 \quad \Rightarrow \quad \sigma^2(R) \to \infty \quad \Rightarrow \quad G(\delta, R) \to 0 \tag{3.51}$$

3.2.3 Halo mass function

The PS model can now be applied to the smoothed perturbation distribution, considering that overdensities higher than the critical one δ_c lead to a collapse or virialization. This overdensity threshold is therefore a key ingredient for PS formalism, in addition to primordial density fluctuations (power spectrum) and evolution (growth factor) characterizations. The value of this critical overdensity has been found using the non-linear spherical collapse and is discussed in detail in section 2.3. Following PS theory, the regions with smoothed overdensity higher than the threshold δ_c will then have mass proportional to the window volume for which the barrier is crossed. This proportionality is applied by multiplying this window volume by the background energy density. Thus for matter overdensities, the virialized object masses can be approximated with the formula written below.

$$M(R) = V_W(R)\overline{\rho}_m \tag{3.52}$$

Finding the halo mass function requires an additional reasoning step coming from PS formalism. In order to do this, it must be noted that for every region of scale R with smoothed overdensity higher than the threshold $\delta(\mathbf{x}, R) > \delta_c$, there is a larger scale $R' > R$ for which the same region exactly meets the critical value $\delta(\mathbf{x}, R') = \delta_c$. From this concept, it follows that the probability of finding a region of scale R with overdensity above the threshold is equal to the fraction given by the volume occupied by virialized objects with a window scale larger than R. In fact for the above reasoning, a region larger than the scale that virializes $R' > R$ should be composed of many smaller regions of scale R which exceed the threshold. This probability or volume fraction $F(M)$ can be calculated by using the Gaussian probability (3.50). Since the interest is focused on the mass of virialized objects, instead of their window volume, the mass can be kept as the variable by using the equation shown above (3.52).

$$F(M) = \int_{\delta_c}^{\infty} p_G(\delta, R(M))d\delta = \frac{1}{2}\,\mathrm{erfc}\left(\frac{\nu(M)}{\sqrt{2}}\right) \tag{3.53}$$

where $\nu(M) = \frac{\delta_c}{\sigma(M)}$ and erfc is the complementary Gauss error function[9].

The limit for small scale $R \to 0$ should give the fraction of all virialized masses. Nevertheless, it leads to the result $F(M) = \frac{1}{2}$, while the value 1 is expected because on that scale every object can be considered as collapsed on itself. The proposal from PS is that this problem arises because underdense regions are not taken into account. They should in fact collapse onto overdense regions through accretion and double their volume. For this reason the result (3.53) needs to be multiplied by a factor of two[10].

$$F'(M) = 2F(M) = \mathrm{erfc}\left(\frac{\nu(M)}{\sqrt{2}}\right) \tag{3.54}$$

[9]The (Gauss) error function is used to describe the integration of a normal distribution in a simpler way and can be written explicitly as $\mathrm{erf}(z) = \frac{2}{\sqrt{\pi}}\int_0^z dt e^{-t^2}$. Its complementary function used here is $\mathrm{erfc}(z) = 1 - \mathrm{erf}(z)$.

[10]This is one of the flaws of PS formalism, which applies a factor of 2 without a proper justification. Nonetheless, the success of the model seems to excuse this correction.

The final step to reach HMF consists in calculating the number of virialized objects with mass between M and $M + dM$.

$$\boxed{\frac{dn}{dM}dM = \frac{\overline{\rho}_m}{M}\left|\frac{dF'(M)}{dM}\right|dM = \sqrt{\frac{2}{\pi}}\frac{\overline{\rho}_m}{M^2}\nu\frac{d\ln(\nu)}{d\ln(M)}e^{-\frac{\nu^2}{2}}dM} \tag{3.55}$$

where $\nu = \frac{\delta_c}{\sigma}$ as before.

This is the result of PS formalism, which has multiple applications, however when applied to the formation of halos and their virialization it can be called halo mass function. In fact, it describes the number of non-relativistic matter halos (both baryonic and dark matter) with a mass between M and $M + dM$, which can lead to galaxy formation.

3.2.4 Ellipsoidal correction

Although the formula (3.55) already provides a good approximation of the HMF, an additional correction can be applied to this result. This adjustment comes from the assumption that the collapse of objects is more likely to have an ellipsoidal shape rather than a perfect spherical one. This problem is discussed in detail in [29] and [30], while here only a brief summary of the results is reported.

Equation (3.55) has two main dependencies on cosmological properties both included in the term $\nu(M) = \frac{\delta_c}{\sigma(M)}$. While the variance $\sigma(M)$ depends on the shape of the power spectrum, the critical overdensity δ_c is based on the underlying dynamics of the non-linear collapse of objects. The value of this latter element is based on the spherical collapse, as discussed in section 2.3 and is therefore the one that should be modified to incorporate the ellipsoidal corrections. As explained in [29] the ellipsoidal collapse has three additional parameters: initial ellipticity e, prolateness p, and density contrast δ_{ec}. A reasonable approximated relation between ellipsoidal and spherical critical overdensity is the following [29].

$$\frac{\delta_{ec}(e,p)}{\delta_c} = 1 + \beta\left[5(e^2 \pm p^2)\frac{\delta_{ec}^2(e,p)}{\delta_c^2}\right]^\lambda \tag{3.56}$$

where $\beta = 0.47$ and $\lambda = 0.615$, while the plus (minus) is used for p positive (negative).

Including the new variables e and p leads to the problem of evaluating them. In fact, the range of these values can differ depending on the dimension R and mass M of the collapsing object. It is possible to average $\delta_{ec}(e,p)$ over the distribution of e, p and $\frac{\delta_c}{\sigma(M)}$ suitably. Considering a Gaussian field as usual, this leads to prolateness $p = 0$ and typical initial ellipticity $e = \frac{\sigma(M)}{\sqrt{5}\delta_c}$ [29]. A simplified solution for the ellipsoidal critical density contrast can then be written [29].

$$\delta_{ec}(e,p) = \delta_c\left[1 + \beta\left(\frac{\sigma^2(M)}{\delta_c^2}\right)^\lambda\right] \tag{3.57}$$

With this result, it can be seen that for more massive objects (which means smaller variance $\sigma(M)$), the collapse is well described by the spherical solution. For the

collapse of smaller objects, the importance of external tides, hence their ellipsoidal shape, becomes more relevant instead.

Without going into details, article [29] applies the ellipsoidal correction (3.57) and provides the results of numerical simulations, trying different approaches. The result consists of the best fit for the HMF, instead of (3.55), considering these adjustments and is reported below [29].

$$\boxed{\frac{dn}{dM}dM = \sqrt{\frac{2}{\pi}}A\left(1+\frac{1}{\nu'^{2q}}\right)\frac{\bar{\rho}_m}{M^2}\nu'\frac{d\ln(\nu)}{d\ln(M)}e^{-\frac{\nu'^2}{2}}dM} \tag{3.58}$$

where $\nu' = \sqrt{a}\nu$ with $a = 0.707$, $q = 0.3$ and $A \approx 0.322$ [29].

3.3 Stellar mass density

In order to conclude the analysis of how PBHs could have influenced galaxy formation, the stellar mass density must be calculated, as it represents the possible observable quantity. In order to do that, PS formalism application is performed following the process done in [9].

With all the tools studied in the previous sections, it is now possible to calculate the *comoving cumulative stellar mass density*, hence the density of galaxies with stellar mass M_* or higher. This result is achieved by putting together the halo mass function (3.55) found with PS formalism, or (3.58) with ellipsoidal correction, and the *star formation efficiency* (SFE) $\varepsilon = \frac{M_*}{f_b M_{halo}}$, where $f_b = \frac{\Omega_b}{\Omega_m}$ and M_{halo} is the minimum halo mass of the galaxies of interest. The SFE is a fundamental parameter for the computation of stellar mass from DM halos, which however has not been measured yet. Thus SFE is a free parameter. Consequently, the total stellar mass density of galaxies, formed from DM halos, with a mass larger than M_* is found below [6] [9].

$$\boxed{\rho_*(>M_*) = \varepsilon f_b \rho(>M_{halo}) = \varepsilon f_b \int_{M_{halo}}^{\infty} M \frac{dn}{dM} dM} \tag{3.59}$$

3.3.1 Plots and results

In this subsection, the different graphs, replicating [9], but also additional ones, are shown and their numerical calculation is discussed. The way the stellar mass density is plotted is pretty straightforward and involved the utilisation of the software *Mathematica*. The results of the power spectrum from section 3.1 (equation (3.19) complemented by (3.15) and (3.17) for the adiabatic power spectrum and (3.36-3.39) for the PBH component) are used to compute the variance (3.49) applying a Gaussian window (3.48). In addition to that, the Gaussian window volume was used to shift variables, from size to mass, using (3.52). Unfortunately, the variance resulting from the adiabatic power cannot be computed by *Mathematica* directly, as it involves operations that cannot be carried out analytically. Consequently, a power law logarithmic fit was performed on it $\sigma^2_{ad} \approx c_1 M^{-c_2}$, for the range of masses of interest, which is approximately $10^4 - 10^{14} M_\odot$ from [9].

Afterwards, the HMF, for both the pure PS model (3.55) and the one with ellipsoidal correction (3.58) are computed, using the critical density $\delta_c = 1.686$ (2.32). For the final step, these two HMFs are inserted in (3.59) to output the searched stellar mass densities. The numerical results are computed by applying measured values, mostly given by Plank Collaboration [22]. The constants used are listed in Appendix A.

As mentioned above, both scenarios, with and without ellipsoidal correction, are studied for different PBH variables, which are reported in Table 3.1. It must be noted that PBH fraction of DM f_{PBH} and monochromatic mass m_{PBH} always come together in the stellar mass density function (3.59). For this reason, the last column of Table 3.1 is particularly interesting, as it represents one single PBH variable that could vary the cumulative stellar mass density.

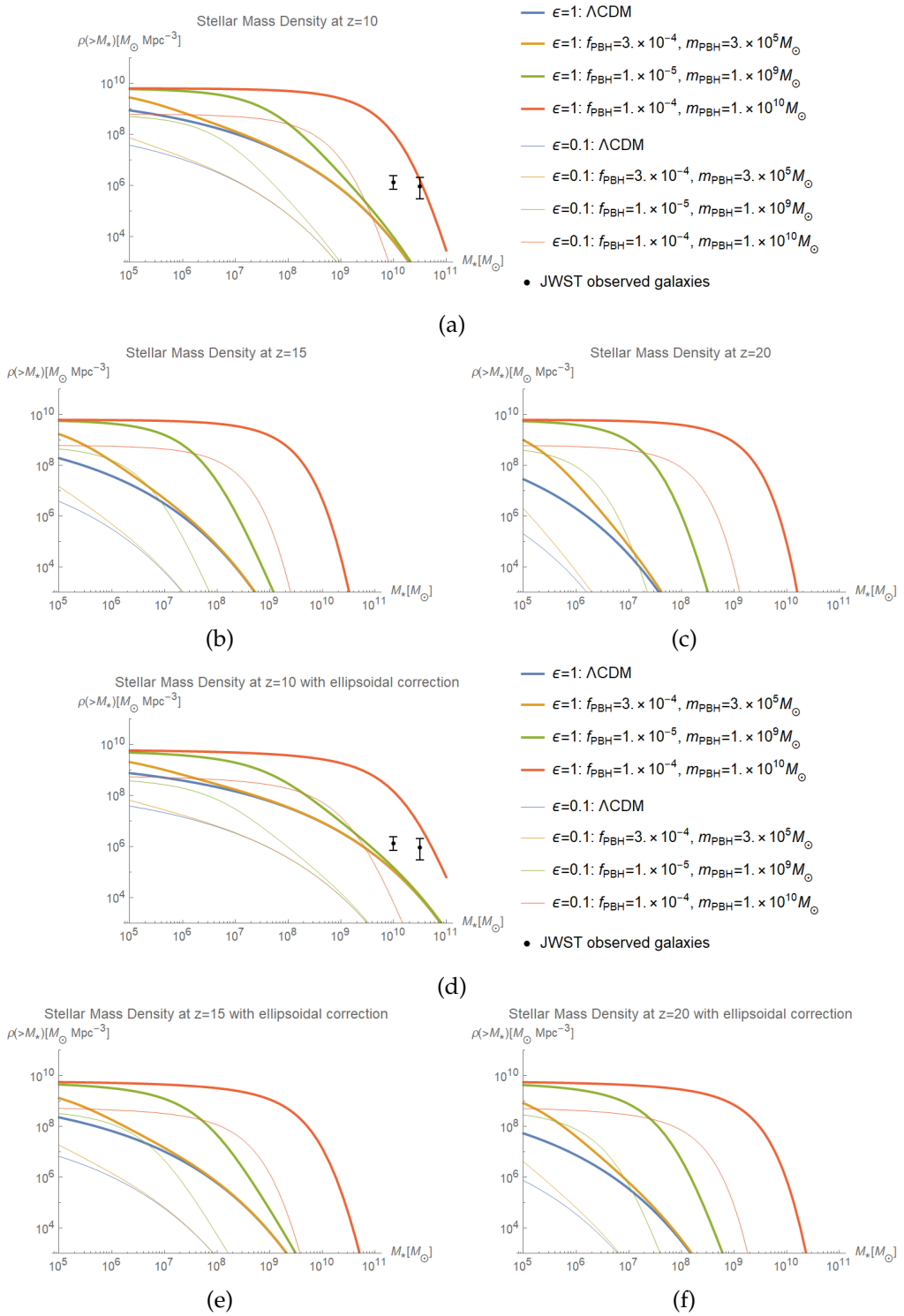

Figure 3.3: Comoving cumulative stellar mass density (3.59) for Press-Schechter model in Figure 3.3a, 3.3b and 3.3c and with ellipsoidal corrections in Figure 3.3d, 3.3e and 3.3f. These results come from the explanations above and are calculated for different parameters reported in Table 3.1. The numerical evaluation is performed using quantities from Appendix A. In addition to that, two galaxy populations observed by JWST at redshift $z \sim 10$ and reported in (3.60) are plotted in Figure 3.3a and 3.3d [5].

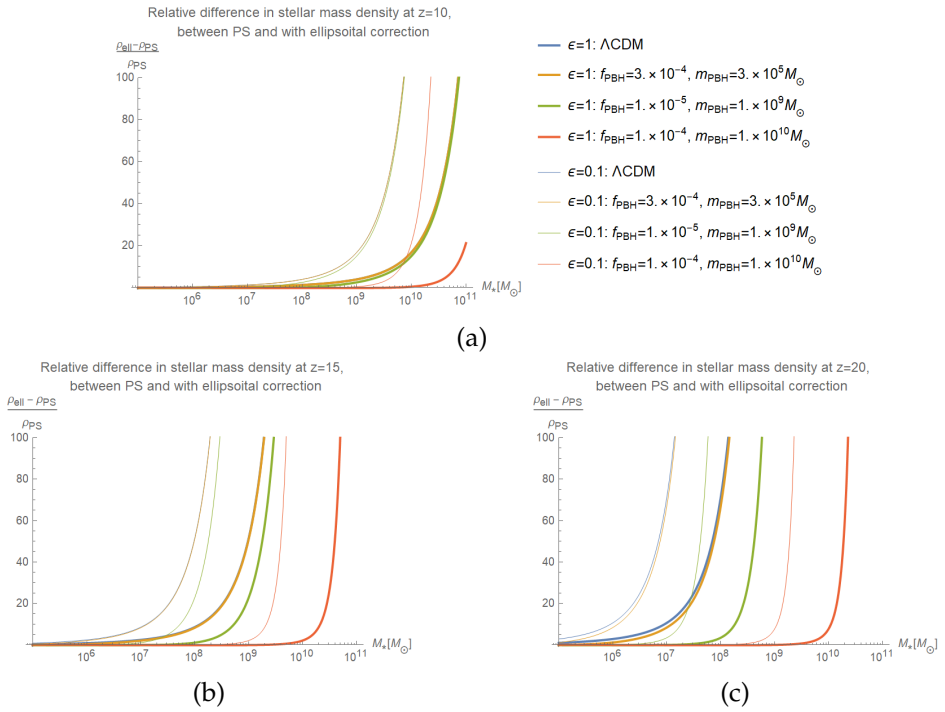

Figure 3.4: Since Figure 3.3 displays the stellar mass density with two different approaches (3.55) and (3.58), these graphs highlight the relative difference between the two cases.

	f_{PBH}	m_{PBH}	$f_{PBH}m_{PBH}$
1	$3 \cdot 10^{-4}$	$3 \cdot 10^5 M_\odot$	$90 M_\odot$
2	10^{-5}	$10^9 M_\odot$	$10^4 M_\odot$
3	10^{-4}	$10^{10} M_\odot$	$10^6 M_\odot$

Table 3.1: PBH variables in Figure 3.3.

Figure 3.3 shows the cumulative stellar mass density at redshift 10, 15 and 20, for two different SFEs and compares the cases including PBHs with the ΛCDM model scenario, similarly to [9]. The results are reported twice, whereas the second time ellipsoidal corrections are included. On the other hand, Figure 3.4, shows the relative error between the two previous models, for each time reference. It is clear that the ellipsoidal correction is able to increase the stellar mass density as the mass increases. It is therefore important to take this adjustment into consideration.

In Figure 3.3a and 3.3d, in addition to the stellar mass densities, two values of reference at $z = 10$ are highlighted. Analogously to [9], these values represent the estimated cumulative stellar mass densities for $M_* \gtrsim 10^{10} M_\odot$ and $M_* \gtrsim 10^{10.5} M_\odot$. As mentioned before, in the last year, JWST opened the possibility of observing the universe at very high redshifts. In article [5], more than a dozen observations of very massive galaxies $M_* \gtrsim 10^{10} M_\odot$ are reported, which were used to calculate

the values displayed in [9].

$$\rho_*(\gtrsim 10^{10}\,\mathrm{M}_\odot) \approx 1.3^{+1.1}_{-0.6}\cdot 10^6\,\mathrm{M}_\odot\mathrm{Mpc}^{-3} \qquad (3.60)$$
$$\rho_*(\gtrsim 10^{10.5}\,\mathrm{M}_\odot) \approx 9^{+11}_{-6}\cdot 10^5\,\mathrm{M}_\odot\ \mathrm{Mpc}^{-3}$$

It must be noted, that the exact shape of the curves of Figure 3.3 is dependent on the fit of the adiabatic component of the variance, especially moving to higher masses. Despite the general shape of Figure 3.3 matches with article [9] results, the exact shape does not, as it can vary through this process. In fact, these plots are very rough, since they are the results of many approximations and estimations. Nevertheless, the general outcome of [9] and these figures can be considered as analogous.

3.4 Discussion for Poisson distributed PBHs

In order to close this chapter, a few words must be spent on the results obtained in the previous section. The main conclusions are clearly the same as in [9], as this part of the study is analogue to this article.

From Figure 3.3 it can be understood that only for very high values of $f_{PBH}m_{PBH}$ the observations of JWST at $z \sim 10$ can be reached. In fact, the only line that passes them is given by $f_{PBH}m_{PBH} = 10^6 M_\odot$ with the highest SFE considered. Therefore it can be expected that $f_{PBH}m_{PBH}$ would be even higher with a lower SFE. From [9] the limits are approximately $f_{PBH}m_{PBH} \gtrsim 2 \cdot 10^5 M_\odot$ for $\varepsilon = 1$ and $f_{PBH}m_{PBH} \gtrsim 6 \cdot 10^6 M_\odot$ for $\varepsilon = 0.1$. This means that the mass is expected to be at least $10^5 M_\odot$ as f_{PBH} can have a maximum value equal to 1. However, this last quantity is further restricted by observation of BHs accretion effects for the previously mentioned masses [31] [32], and by dynamical friction for higher ones [33], as shown in Figure 3.5 [2]. These constraints limit the possible combinations that produce $f_{PBH}m_{PBH} \gtrsim 2 \cdot 10^5 M_\odot$ to very massive PBH, roughly speaking $m_{PBH} \gtrsim 10^9 M_\odot$. There are also boundaries on mass from above, as almost none black hole having mass $\gtrsim 10^{11} M_\odot$ have been observed [34].

For these reasons, the possibility that Poisson distributed PBHs dominate the formation of massive galaxies at $z \sim 10$ is weak. In fact, this prospect has many limits: the unknown SFE must be high and in addition to that, PBHs have to be extremely massive $m_{PBH} \approx 10^9 - 10^{10} M_\odot$, which is unlikely, given the few observations of BHs with such masses.

Nonetheless, there are two more possibilities, yet to explore, that could justify the formation of galaxies at high redshift with the presence of less massive PBHs. The first one would be to lift the constraints on high f_{PBH} for the combinations of PBH variables, by considering clustering. Although the PBHs have an initial Poisson distribution, at redshift $z \sim 10$ they could have clustered, hence some constraints can fall. This possibility is investigated in chapter 4.

Another prospect would be to consider clustering from the beginning, by applying an initial PBH distribution which is not purely Poissonian. An overview of the possibilities of this subject are discussed in Appendix E.

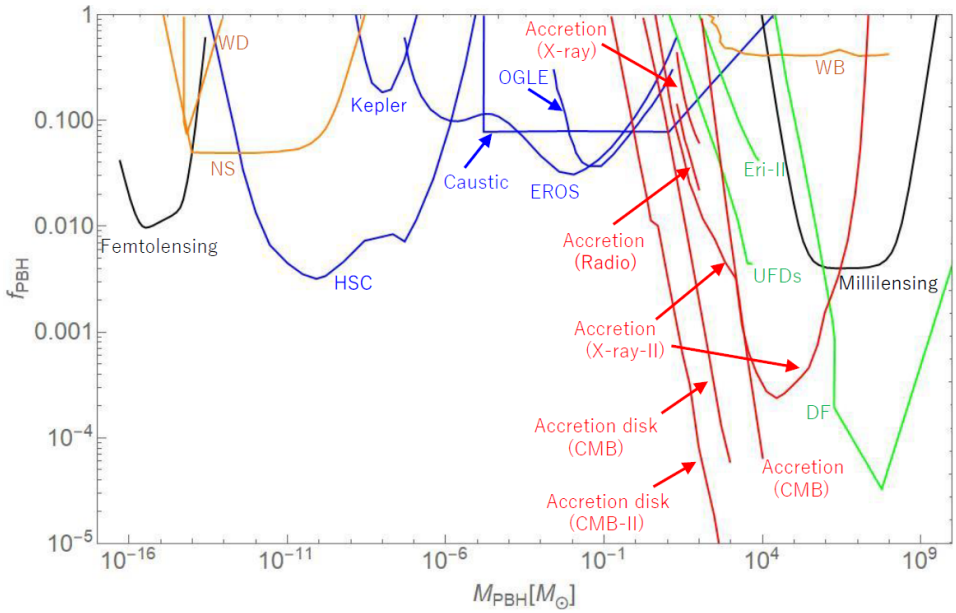

Figure 3.5: Constraints on PBH parameters. The graph is taken directly from article [2], and it show the different constraints from observation and method of derivation. The results shown come from a set of studies, whose references can be checked in [2]. The constraints of interest for this report are the ones for $m_{PBH} \gtrsim 10^5 M_\odot$. Therefore the ones due to PBH accretion, observed through X-rays, come from [31] and [32] (red line), while the ones from dynamical friction of PBHs within galaxies is studied in [33] (green line). Going even further, to high f_{PBH}, the millilensing constraint is analysed in [35] (black line) and the limit on PBH parameters due to wide halo binaries disruption from PBHs encounter is taken from [36] (orange line).

4 PBH clustering

From the results of the previous chapter the possibility that PBHs exist in our universe, leading to an early formation of galaxies, seems feeble. From both [9] and chapter 3, the combinations of PBH masses that could explain JWST observation are quite extreme. However, there is an important element that was not considered in these studies, the PBH clustering. Firstly, the validity of chapter 3 analysis (hence [9]) should be checked, by understanding whether or not clustering effects should have been considered. Secondly, the scenario for which Poisson distributed PBHs [37] [38] evolve into clusters cannot be neglected and is thus studied, together with some possible implications.

Although the inside structures and dynamics of clusters are very complex and difficult to analyse, their formation process and conditions are more accessible. For this reason, in this chapter, the scenarios and the PBH variables that lead clusters to form and play a relevant role are investigated. In order to achieve this goal, many approaches are analysed, taking inspiration and combining the ideas of different references: [14], [39], [40] and [41].

In the first part, in section 4.1, a direct numerical approach, that considers PBHs as discrete particles is analysed. In the following segments a completely different strategy is used, starting from the initial randomly distributed PBH perturbations. In section 4.2 PBH clusters formation is analysed by finding the conditions for their evolution from the initial Poisson noise to halos and their sizes. By the end of the section, the validity of the study performed in chapter 3 is discussed. After an introduction to *excursion set theory*, in section 4.3, in section 4.4 an analysis of clusters accretion and survival times is performed. A discussion of the results in comparison with the current PBH constraints is proposed in section 4.5 to close the chapter.

4.1 Discrete particle PBHs

The first possibility to study cluster formation of PBH and their effect is given in [14], where PBHs are treated as discrete particles that could cluster. Starting with initial Poisson distributed particles, the total number of halos N_{halo} containing N PBHs is recovered from [42] and [43].

$$N_{halo}(N) = \frac{N_{PBH}}{N} \frac{\delta_*}{1+\delta_*} \left(\frac{N}{1+\delta_*}\right)^{N-1} \frac{e^{-\frac{N}{1+\delta_*}}}{(N+1)!} \tag{4.1}$$

In this formula N_{PBH} represents the total number of PBHs, while δ_* is given by $f_{PBH}\delta_* = \delta_i$, which can be rewritten by recalling (2.53).

$$\delta_*(z_{obs}) = \frac{\delta_i(z_{obs})}{f_{PBH}} = \frac{\delta_c(z_{obs})}{D_{iso}(z_{obs}) f_{PBH}} \tag{4.2}$$

This means that $\delta_*(z_{obs})$ is the overdensity required so that the initial density contrast $\delta_i(z_{obs})$ is reached by the only presence of PBHs.

Since the total number of both halos and PBHs cannot be computed, using the number density instead can solve this problem. Therefore (4.1) must be modified from total number of PBHs to average number density $\overline{n}_{PBH}$. This process can be seen as if (4.1) would be divided by the volume of the whole universe, giving the number density. For monochromatic PBHs this can be achieved in the following way.

$$\overline{n}_{PBH} = \frac{\overline{\rho}_{PBH}}{m_{PBH}} = \frac{\Omega_{PBH}\rho_{cr}}{m_{PBH}} = \frac{f_{PBH}\Omega_c\rho_{cr}}{m_{PBH}} = \frac{3H_0^2}{8\pi G}\frac{f_{PBH}}{m_{PBH}}(\Omega_m - \Omega_b) \tag{4.3}$$

where ρ_{cr} is the critical density used to calculate abundances (C.31) and Ω_c is the clustering matter abundance (2.24).

$$n_{halo}(N) = \frac{3H_0^2}{8\pi G}\frac{f_{PBH}}{m_{PBH}}\frac{\Omega_m - \Omega_b}{N}\frac{\delta_*}{1+\delta_*}\left(\frac{N}{1+\delta_*}\right)^{N-1}\frac{e^{-\frac{N}{1+\delta_*}}}{(N+1)!} \tag{4.4}$$

As a first rough approximation, the mass of the halo can be considered to be made by PBHs only $M^0_{halo} = Nm_{PBH}$[1], therefore having HMF

$$\begin{aligned}\rho^0_{halo}(N) &= n_{halo}(N) N m_{PBH} \\ &= \frac{3H_0^2}{8\pi G} f_{PBH}(\Omega_m - \Omega_b)\frac{\delta_*}{1+\delta_*}\left(\frac{N}{1+\delta_*}\right)^{N-1}\frac{e^{-\frac{N}{1+\delta_*}}}{(N+1)!}\end{aligned} \tag{4.5}$$

With this solution, it is possible to calculate the cumulative stellar mass density as in (3.59).

$$\boxed{\rho^0_*(>M_*) = \varepsilon f_b \rho^0(>M_{halo}) = \varepsilon f_b \int_{\frac{M_{halo}}{m_{PBH}}}^{\infty} \rho^0_{halo}(N) dN} \tag{4.6}$$

The results for the same variables as in chapter 3 are shown in Figure 4.1, as well as the relative differences with the pure PS model, displayed in Figure 4.2.

[1]The superscript ^{0} on mass represents the fact that a bare PBH cluster is considered.

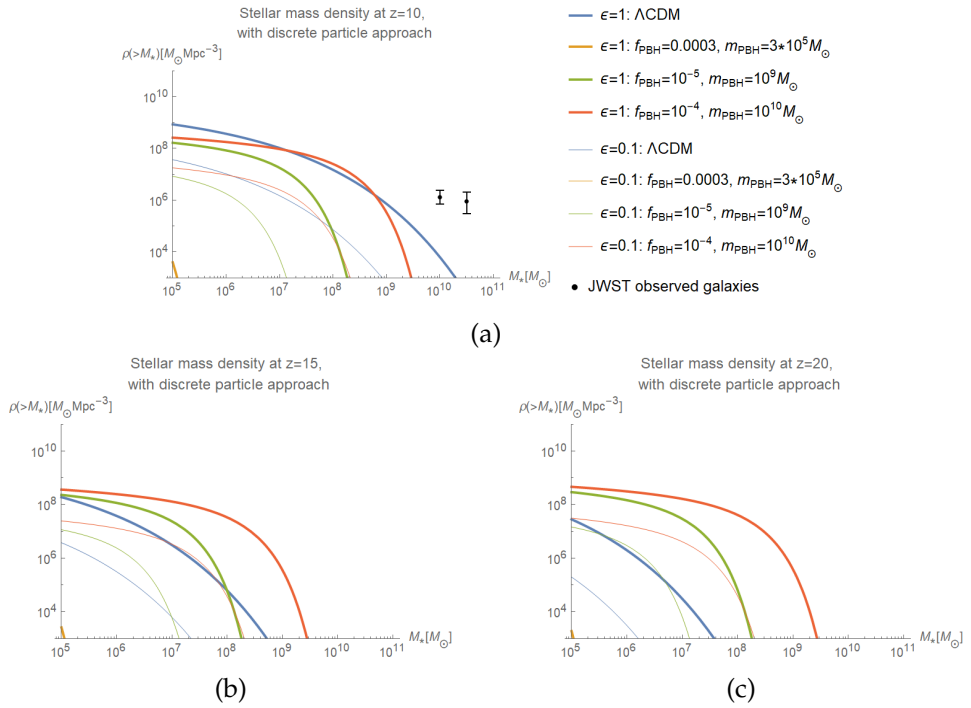

Figure 4.1: Comoving cumulative stellar mass density at different redshifts using the formula for stellar mass from (4.6). The ΛCDM model is reported from the previous chapter as well, using PS.

In addition to that, it is also possible to compute the PBH fraction of DM required for the Poisson effect to not be dominant anymore. This can be achieved by knowing that when PBH will be mostly clustered (therefore in a halo with at least one counterpart), and the number of halos with only 1 PBH will be less than half the total number of PBHs.

$$\frac{N_{halo}(1)}{N_{PBH}} = \frac{\delta_*}{1+\delta_*} e^{-\frac{1}{1+\delta_*}} = \frac{1}{2} \tag{4.7}$$

Inserting $z = 10$, which is the redshift of main interest, leads to

$$f_{PBH} \approx 0.0032 \tag{4.8}$$

This result gives the fraction of PBH DM below which no clustering effect is expected. For this reason, for the variables plotted in Figure 4.1, no major differences due to clusters are expected. Thus using this discrete particle approach for such low f_{PBH} is impractical. An increase in f_{PBH} would be required for PBH halos to form and to justify the usage of this approach. On the other hand, (4.8) confirms the correctness of the previous analysis in chapter 3 and [9] to not consider any clustering effect.

Figure 4.3 shows different combinations of f_{PBH} and m_{PBH}, where clustering is expected as the PBH fraction of DM is higher than (4.8), for the three different $f_{PBH}m_{PBH}$ of Table 3.1 at the redshift of interest $z \sim 10$. It can be noticed that the

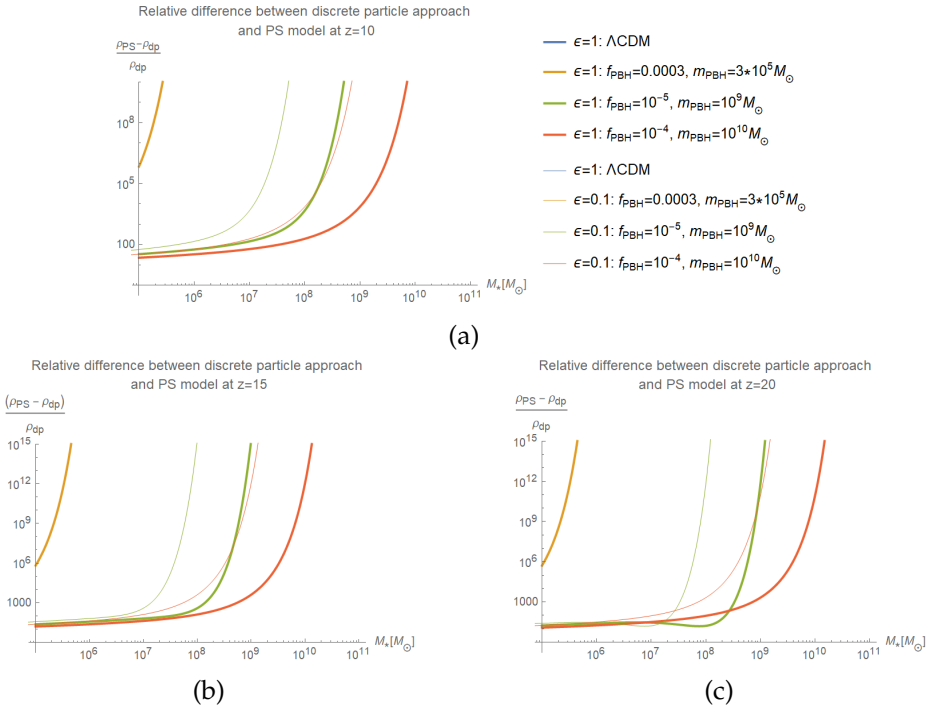

Figure 4.2: Relative differences between comoving cumulative stellar mass density calculated using the formula (4.6) and the PS model of chapter 3, at different redshifts.

curves with the discrete particle approach get lower as f_{PBH} gets larger, moving away from their counterparts of the PS model. This means that despite the higher fraction of DM occupied by PBH, which should enhance clustering and consequently galaxy formation, their lower mass plays a more important role, making the HMF drop.

4.1.1 Mass correction for particle dark matter

One of the reasons behind the very low curves found in Figure 4.3 is due to the lack of PDM. In fact, (4.5) only includes the masses of PBHs, while also the other components of DM should be taken into account. This adjustment can be performed directly on the mass of the halo.

$$M_{halo} \approx N m_{PBH} \left(1 + f_{halo} \frac{1 - f_{PBH}}{f_{PBH}}\right) \tag{4.9}$$

where $f_{halo} = \frac{N_{PDM \in halo}}{N_{PDM}}$ is the proportion of PDM particles that are present in clusters. This is an additional free parameter, that can vary between 0 and 1. Therefore the bare PBH halo mass $M^0_{halo} = N m_{PBH}$ only represents a portion of the whole ensemble. The HMF (4.5) becomes

$$\rho_{halo}(N) = n_{halo}(N) M_{halo} = \rho^0_{halo}(N) \left(1 + f_{halo} \frac{1 - f_{PBH}}{f_{PBH}}\right) \tag{4.10}$$

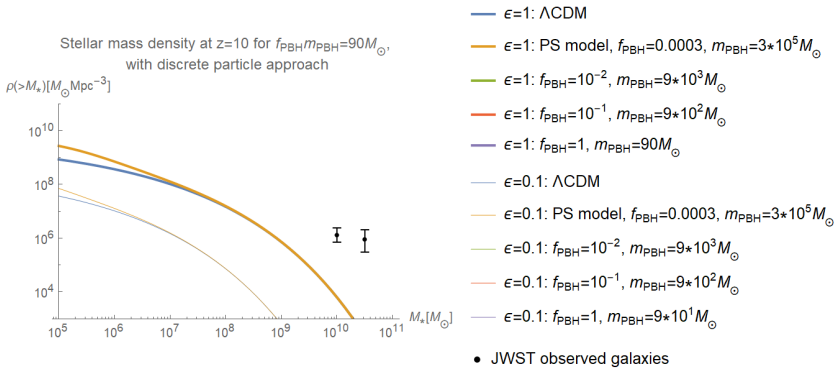

(a)

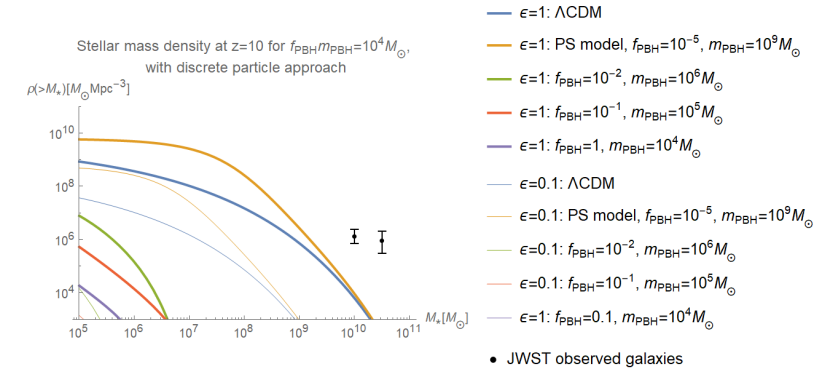

(b)

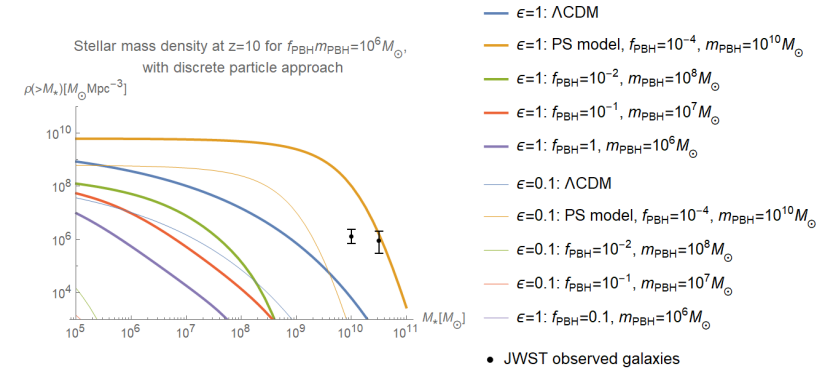

(c)

Figure 4.3: Comoving cumulative stellar mass density at $z = 10$ using the formula for stellar mass from (4.6), for different combination of f_{PBH} and m_{PBH}, but with constant $f_{PBH}m_{PBH}$ from Table 3.1. The ΛCDM model as well as the results from the pure PS model are recalled from chapter 3.

Consequently, the stellar mass (4.6) is

$$\rho_*(>M_*) = \varepsilon f_b \rho(>M_{halo}) = \varepsilon f_b \int_{\frac{M_{halo}}{m_{PBH}}}^{\infty} \rho_{halo}(N) dN \tag{4.11}$$
$$= \left(1 + f_{halo}\frac{1-f_{PBH}}{f_{PBH}}\right)\rho_*^0(>M_*)$$

This means that the stellar mass found considering only the bare PBH halos must be multiplied by a constant. The only possibility to have the curve found in Figure 4.1 and 4.3 increased significantly in value, is to consider small f_{PBH} and not negligible f_{HL}. Nevertheless, from Figure 4.2 the differences between PS and the discrete particle model on the masses of interest ($10^9 - 10^{11} M_\odot$) gets enormous, and could get compensated only with tiny f_{PBH}, which however do not lead to clustering. Therefore it is not expected that the discrete particles approach leads to better results than the PS model considering the clustering effect.

This method clearly fails to describe the formation of galaxies at high redshifts observed by JWST. However, it does not mean that clustering fails too. In fact, the discrete particle approach has as its main flaw that does not consider gravitation. It is expected that accretion plays a fundamental role in the growth of galaxies around $z \sim 10$. For this reason, gravity cannot be neglected and this approach results to be flawed. Other methods need to be considered to study the possibility of clusters as a boost for galaxy formation.

4.2 Clustering evolution

Clusters are ensembles of objects, and in the case of PBHs, they could form modifying greatly the dynamics and evolution of the halo around them. In addition to that, the different kinds of signals emitted from a lonely PBH and a cluster, hence their observations, can result fundamentally different. Therefore it is important to understand whether PBH clusters can form, and their presence must be taken into account, or not, leading to conclude that the results of chapter 3 cannot be extended.

The size and requirements for PBH clusters to form are studied here. Starting from the initial spatial distribution of PBHs, cluster evolution is analysed in various regimes. Despite two components being highlighted for the initial PBH overdensities: shot noise and initial PBH clustering, the evolution of PBH clusters is calculated for initially Poisson distributed objects. These results are then used to understand the conditions for cluster formation and their sizes.

4.2.1 Spatial clustering

The spatial overdensity of discrete monochromatic PBHs can be written in terms of number densities instead of standard energy densities [39].

$$\delta_{PBH}(\mathbf{x}) = \frac{n_{PBH}(\mathbf{x}) - \overline{n}_{PBH}}{\overline{n}_{PBH}} = \frac{1}{\overline{n}_{PBH}} \sum_i \delta^3(\mathbf{x} - \mathbf{x}_i) - 1 \tag{4.12}$$

where $n_{PBH}(\mathbf{x})$ is the PBHs number density per comoving volume in $\mathbf{x}$, which is discrete, while $\overline{n}_{PBH}$ is its average density (3.31), and $\mathbf{x}_i$ are the positions of the discrete PBHs.

$$\overline{n}_{PBH} = f_{PBH} \frac{\Omega_{DM}}{m_{PBH}} \rho_{cr} = f_{PBH} \frac{\Omega_m - \Omega_b}{m_{PBH}} \rho_{cr} \tag{4.13}$$

where once again ρ_{cr} is the critical density (C.31).

In order to find the power spectrum, the two-points correlation function can be calculated first. The passages to find it are shown in their extensive form here below [39].

$$\langle \delta_{PBH}(\mathbf{x}) \delta_{PBH}(\mathbf{0}) \rangle = \frac{1}{V} \int_V d^3\mathbf{x}' \delta_{PBH}(\mathbf{x}') \delta_{PBH}(\mathbf{x}' - \mathbf{x}) \tag{4.14}$$

$$= \frac{1}{V} \int_V d^3\mathbf{x}' \left(\frac{1}{\overline{n}_{PBH}} \sum_i \delta^3(\mathbf{x}' - \mathbf{x}_i) - 1 \right) \left(\frac{1}{\overline{n}_{PBH}} \sum_j \delta^3(\mathbf{x}' - \mathbf{x} - \mathbf{x}_j) - 1 \right) \tag{4.15}$$

$$= \frac{1}{V} \int_V d^3\mathbf{x}' + \frac{1}{\overline{n}_{PBH}^2} \frac{1}{V} \int_V d^3\mathbf{x}' \sum_{ij} \delta^3(\mathbf{x}' - \mathbf{x}_i) \delta^3(\mathbf{x}' - \mathbf{x} - \mathbf{x}_j) - \frac{1}{\overline{n}_{PBH}} \frac{1}{V} \int_V d^3\mathbf{x}' \sum_i \delta^3(\mathbf{x}' - \mathbf{x}_i) - \frac{1}{\overline{n}_{PBH}} \frac{1}{V} \int_{V''} d^3\mathbf{x}'' \sum_j \delta^3(\mathbf{x}'' - \mathbf{x}_j) \tag{4.16}$$

$$=1+\frac{1}{\overline{n}_{PBH}^2}\frac{1}{V}\int_V d^3\mathbf{x}'\sum_i \delta^3(\mathbf{x}'-\mathbf{x}_i)\delta^3(\mathbf{x}'-\mathbf{x}-\mathbf{x}_i) \tag{4.17}$$
$$+\frac{1}{\overline{n}_{PBH}^2}\frac{1}{V}\int_V d^3\mathbf{x}'\sum_{i\neq j} \delta^3(\mathbf{x}'-\mathbf{x}_i)\delta^3(\mathbf{x}'-\mathbf{x}-\mathbf{x}_j)-2$$
$$=\frac{\delta^3(\mathbf{x})}{\overline{n}_{PBH}^2}\frac{1}{V}\int_V d^3\mathbf{x}'\sum_i \delta^3(\mathbf{x}'-\mathbf{x}_i) \tag{4.18}$$
$$+\left\langle \frac{1}{\overline{n}_{PBH}^2}\sum_{i\neq j}\delta^3(\mathbf{x}-\mathbf{x}_i)\delta^3(\mathbf{x}_j)\right\rangle -1$$

$$\boxed{\langle \delta_{PBH}(\mathbf{x})\delta_{PBH}(\mathbf{0})\rangle = \frac{\delta^3(\mathbf{x})}{\overline{n}_{PBH}}+\xi_{PBH}(x)} \tag{4.19}$$

where the first passage comes from the correlation function definition (D.1), in the third one the substitution $\mathbf{x}'' = \mathbf{x}' - \mathbf{x}$ ($V = V''$) was applied, while in the fourth and last passages the definition of average PBH number density was used $\overline{n}_{PBH} = \int_V d^3\mathbf{x}\sum_i \delta^3(\mathbf{x}-\mathbf{x}_i)$. The term $\xi_{PBH}(x)$ is called *reduced PBH correlation function* and it defines the spatial distribution correlation between PBHs. Having its value not null would mean that a clustering effect is present from the PBH formation epoch. Therefore its effect is expected to be on small rather than large scales. Mathematically it is defined as follows.

$$\xi_{PBH}(x) = \left\langle \frac{1}{\overline{n}_{PBH}^2}\sum_{i\neq j}\delta^3(\mathbf{x}-\mathbf{x}_i)\delta^3(\mathbf{x}_j)\right\rangle -1 \tag{4.20}$$

The reduced PBH correlation function clearly has no vectorial dependence as the typical correlation function (D.1). If ξ_{PBH} is small, at small scales the shot noise will dominate, while if it is the opposite, there could be an ensemble of PBHs at one point.

The first part of the above solution (4.19) is the Poisson noise given by the discreteness of PBHs. It represents the same component used in chapter 3, where no clustering effect was considered. It follows that the dimensionless PBH power spectrum has the following form.

$$\Delta^2_{PBH}(k,z) = \frac{k^3}{2\pi^2}\int d\mathbf{x}^3 e^{i\mathbf{k}\mathbf{x}}\,\langle \delta_{PBH}(\mathbf{x},z)\delta_{PBH}(\mathbf{0},z)\rangle \tag{4.21}$$

Two PBHs cannot be found arbitrarily close to each other, due to their formation conditions. The spatial exclusion x_{esc} is the minimum comoving distance at which two PBHs can be found.

$$\xi_{PBH}(x)\approx -1, \qquad \text{for} \qquad x\lesssim x_{esc} \tag{4.22}$$

PBHs are anti-correlated at these distances.

Article [40] gives an introduction to PBHs clustering evolution, and suggests using a different normalization of the overdensities for the study of PBH perturbations. PBH overdensity is therefore defined over the whole DM instead of PBH only.

$$\delta_{PBH}(\mathbf{x},z) = \frac{\delta\rho_{PBH}(\mathbf{x},z)}{\overline{\rho}_{PBH}} = \frac{\delta\rho_{PBH}(\mathbf{x},z)}{f_{PBH}\overline{\rho}_{DM}} \tag{4.23}$$

This leads to finding a new equation for the correlation function.

$$\frac{\delta\rho_{PBH}(\mathbf{x},z)}{\overline{\rho}_{DM}} = f_{PBH}\left[\frac{1}{\overline{n}_{PBH}}\sum_i \delta^3(\mathbf{x}-\mathbf{x}_i) - 1\right] \tag{4.24}$$

$$\left\langle \frac{\delta\rho_{PBH}(\mathbf{x},z)}{\overline{\rho}_{DM}} \frac{\delta\rho_{PBH}(\mathbf{0},z)}{\overline{\rho}_{DM}} \right\rangle = \frac{f_{PBH}^2}{\overline{n}_{PBH}}\delta^3(\mathbf{x},z) + \xi(x,z) \tag{4.25}$$

where the reduced PBH correlation function is also redefined with a new notation $\xi(x,z) = f_{PBH}^2 \xi_{PBH}(x,z)$.

As a consequence, the PBH power spectrum over the whole DM can be written as follows.

$$\Delta^{DM\,2}_{PBH}(k,z) = \frac{k^3}{2\pi^2}\int d\mathbf{x}^3 e^{i\mathbf{kx}} \left\langle \frac{\delta\rho_{PBH}(\mathbf{x},z)}{\overline{\rho}_{DM}} \frac{\delta\rho_{PBH}(\mathbf{0},z)}{\overline{\rho}_{DM}} \right\rangle \tag{4.26}$$

This new power spectrum differs from (4.21) only by the constant f_{PBH} squared and represents the purely PBH power spectrum in the bigger picture where all DM components are included.

4.2.2 Evolution regimes

As clusters represent small scale perturbations, but with large amplitude, linear theory cannot be used for their fluctuations description. Starting from Poisson distributed PBHs, as suggested by [37] [38], and having PBH power spectrum over DM (4.26) found above, the evolution of PBH clusters perturbations towards their non-linearities is studied following article [40]. Thus only PBH perturbations in the universe are taken into account in this section.

In the scenario assumed, at the time of PBH formation z_*, at Hubble horizon reentry, the clustering component is irrelevant and the initial PBH power spectrum is given by the only Poisson distribution. In fact, the characteristic PBH clustering length is smaller than the mean comoving separation between PBHs. From (4.19) and (4.26) the initial power spectrum can be rewritten [40].

$$\Delta^2_*(k) = \Delta^{DM\,2}_{PBH}(k,z_*) \approx f^2_{PBH}\left(\frac{k}{k_*}\right)^3 \tag{4.27}$$

where k_* is the characteristic wavenumber. The numerical value of this wavenumber can be written explicitly using (4.13)

$$k_* = (2\pi^2\overline{n}_{PBH})^{\frac{1}{3}} = \left(2\pi^2 f_{PBH}\frac{\Omega_m - \Omega_b}{m_{PBH}}\rho_{cr}\right)^{\frac{1}{3}} \tag{4.28}$$

It can be noticed that this is the dimensionless initial power spectrum of PBHs, given by the shot noise (3.30), with the addition of f^2_{PBH} already, as only PBHs in the whole DM are considered.

In order to better put this into context (3.35) can be recalled, to write the dimensionless power spectrum of PBHs.

$$\Delta^2_{PBH}(k,a) = D^{2\,0}_{ad}(a)\Delta^{0\,2}_{ad}(k) + \left[1 + (D_{iso}(a) - 1)f_{PBH}\right]^2 \Delta^{0\,2}_{iso}(k) + D^{mix\,2}_{PBH}(a)\Delta^{0\,2}_{iso}(k) \tag{4.29}$$

In this section, only PBH perturbations and their own interactions are of interest, because clusters only made of PBHs are analysed. Since the initial PBH perturbations can be assumed to be only of the isocurvature type $\delta^0_{iso} \approx \delta^0_{PBH}$, as in subsection 3.1.2, only that component is taken into account.

$$\Delta^2_{PBH}(k,a) \approx [1 + (D_{iso}(a) - 1) f_{PBH}]^2 \, \Delta^{0\,2}_{iso}(k) \tag{4.30}$$

where for $0.5 \leq \gamma \leq 1$, which is the case in the assumed scenario, the linear evolution term is the same as (2.31) [14].

$$D_{iso}(s) \approx \left(1 + \frac{3\gamma}{2a_-} s\right)^{a_-} \tag{4.31}$$

where once again

$$s = \frac{a}{a_{eq}}, \qquad \gamma = \frac{\Omega_m - \Omega_b}{\Omega_m}, \qquad a_- = \frac{1}{4}\left(\sqrt{1 + 24\gamma} - 1\right) \tag{4.32}$$

Clearly, for the initial condition $s \to 0$ the evolution factor becomes $D_{iso}(s) \to 1$, and considering the power spectrum over all DM, the following substitution is valid.

$$\Delta^2_*(k) \to \Delta^{0\,2}_{iso}(k) \tag{4.33}$$

Consequently, the linear evolution of the power spectrum of interest, which is the isocurvature one, is the following.

$$\Delta^2_{PBH}(k,a) \approx \left[1 + \left(\left(1 + \frac{3\gamma}{2a_-}\frac{a}{a_{eq}}\right)^{a_-} - 1\right) f_{PBH}\right]^2 \Delta^2_*(k) \tag{4.34}$$

From the initial conditions, linear (L), quasi-linear (QL) and non-linear (NL) situations can be studied.

4.2.2.1 Linear regime

The linear evolution of isocurvature perturbations of PBHs in the early universe can be expected to be frozen (see subsection 2.1.2), while it will evolve only after radiation-matter equivalence z_{eq}. With the approximation of DM dominating the matter abundance $\gamma \approx 1$, the evolution equation (4.31) can be used to obtain the isocurvature component of the linear power spectrum.

$$\boxed{\Delta^2_L(k,z) \approx \left(1 + \frac{3}{2} f_{PBH} \frac{1+z_{eq}}{1+z}\right)^2 \Delta^2_*(k) \approx \left(1 + \frac{3}{2} f_{PBH} \frac{1+z_{eq}}{1+z}\right)^2 f^2_{PBH} \left(\frac{k}{k_*}\right)^3} \tag{4.35}$$

where Δ^2_* comes from (4.27).

4.2.2.2 Quasi-linear regime

The quasi-linear regime represents the transition between linear and non-linear situations. This transition can be identified when the dimensionless power spectrum reaches unity [40].

$$\Delta^2_L(k = k_{L-QL}(z), z) \sim 1 \tag{4.36}$$

The explicit value of this wavenumber that satisfies the QL condition can be calculated.

$$k_{L-QL}(z) \approx \frac{k_*}{f_{PBH}^{\frac{2}{3}}} \left(1 + \frac{3}{2} f_{PBH} \frac{1+z_{eq}}{1+z}\right)^{-\frac{2}{3}} \tag{4.37}$$

$$= \left(2\pi^2 \frac{\Omega_m - \Omega_b}{f_{PBH} m_{PBH}} \rho_{cr}\right)^{\frac{1}{3}} \left(1 + \frac{3}{2} f_{PBH} \frac{1+z_{eq}}{1+z}\right)^{-\frac{2}{3}} \tag{4.38}$$

In fact, the QL validity range is identified to be the following [40].

$$1 \lesssim \Delta^2_{QL}(k,z) \lesssim 200 \tag{4.39}$$

A useful value for this regime is the characteristic squared overdensity, which is defined as follows [40].

$$\overline{\xi}(R,z) = \frac{3}{4\pi R^3} \int_0^R dx 4\pi x^2 \xi(x,z) \qquad \text{with} \qquad \xi(x,z) \approx \int \frac{dk}{k} e^{i\mathbf{kx}} \Delta^2(k,z) \tag{4.40}$$

The second part follows from (4.25) and (4.26), where the Poisson noise is neglected as it plays a subdominant role in the QL situation, hence the approximation[2]. Another important relation follows.

$$\Delta^{DM2}_{PBH}(k,z) \approx \overline{\xi}\left(\frac{1}{k}, z\right) \tag{4.41}$$

where the equivalence $x = \frac{1}{k}$ is valid.

To connect the linear and quasi-linear regimes, the conservation of particle pairs (PBHs pairs) can be used in terms of mass conservation relation [44].

$$x^3(1 + \overline{\xi}(x,z)) = R^3 \tag{4.42}$$

where R is the initial shell radius of the perturbation. When the perturbation is still linear, therefore $\overline{\xi}_L \ll 1$, $x \sim R$ is valid. However, as soon as clusters develop, meaning there is a shift to a quasi-linear regime, $\overline{\xi}$ grows. This leads to a relation $x^3 \overline{\xi}_{QL} \sim R^3$ in the quasi-linear regime.

A dependence analysis can be done starting from mass conservation. A density peak which clusters, is surrounded by a larger region of radius R', which can be described with linear theory, and is expected to cluster too at a later stage. This profile can therefore be described in the linear regime as a initial shell of comoving radius R', and the average linear correlation function is $\overline{\xi}_L(R')$. The proper maximum radius of the perturbation, also called turnaround radius, is proportional to $\frac{R'}{\sqrt{\overline{\xi}_L(R')}}$[3]. This must be proportional to the effective radius of the

[2]The correlation function (4.19) can be used at any time. Initially, the reduced PBH correlation function should be null in the scenario considered, however as clusters grow it would get more and more relevant, becoming larger than the Poisson noise, as in QL regime.

[3]This can be checked putting together (2.2) and (2.19), where in this case $R \sim R'$, $\zeta_{ta} = const$, $\Phi = \delta(x) \approx \sqrt{\overline{\xi}_L(R)}$, and consequently $a_{ta} = s_{ta} a_{eq} \propto \frac{1}{\sqrt{\overline{\xi}_L(R)}}$.

halo of mass M, hence the comoving radius x, where the quasi-linear regime is valid.

$$\overline{\xi}_{QL} \sim \delta_{QL}(x)^2 \sim \left(\frac{M}{x^3}\right)^2 \propto \left(\frac{M}{r_{ta}^3}\right)^2 \sim \frac{R'^6}{\left(\frac{R'}{\sqrt{\overline{\xi}_L(R')}}\right)^6} = \overline{\xi}_L^3(R') \tag{4.43}$$

$$\Rightarrow R'^3 \sim x^3 \overline{\xi}_{QL}(x) \sim x^3 \overline{\xi}_L^3(R') \tag{4.44}$$

where the fact that overdensities are proportional to the excess energy density was used [23].

Using the fact that $\overline{\xi}_L(R') \approx \Delta_L^2(1/R', z) \propto \Delta_*^2(1/R') \propto \left(\frac{1}{R'}\right)^3$ coming from a combination of (4.35) and (4.41), it is possible to find a relation between x and R'.

$$R'^3 \sim x^3 \overline{\xi}_L^3(R') \sim \frac{x^3}{R'^9} \qquad \Rightarrow \qquad R' \sim x^{\frac{1}{4}} \tag{4.45}$$

Consequently, the x dependence of the volume-averaged quasi-linear correlation function can be calculated.

$$\overline{\xi}_{QL}(x) \sim \frac{R'^3}{x^3} \sim \frac{x^{\frac{3}{4}}}{x^3} = x^{-\frac{9}{4}} \tag{4.46}$$

In addition to that, the solution must match the behaviour of the linear regime at small perturbations $\Delta_{QL}^2(k, z) \sim 1$. For this reason and property (4.41), the power spectrum of the quasi-linear situation can be approximated as follows.

$$\boxed{\Delta_{QL}^2(k, z) \approx \left(\frac{k}{k_{L-QL}(z)}\right)^{\frac{9}{4}}} \tag{4.47}$$

where the formula for k_{L-QL} can be found in (4.37).

4.2.2.3 Non-linear regime

In the NL situation, the perturbation is the largest of the regimes studied, however the stable clustering hypothesis can be assumed, which says that their internal structure does not change with the universe's expansion [44]. The QL-NL limit is defined by the overdensity within a virialized object, which happens at $\Delta^2(k, z) \sim 200$ as in (4.39).

$$\Delta_{QL}^2(k = k_{QL-NL}(z), z) \sim 200 \tag{4.48}$$

$$\Rightarrow \qquad k_{QL-NL}(z) = k_{L-QL}(z)\,(200)^{\frac{4}{9}} = \frac{(200)^{\frac{4}{9}}\, k_*}{f_{PBH}^{\frac{2}{3}}} \left(1 + \frac{3}{2} f_{PBH} \frac{1 + z_{eq}}{1 + z}\right)^{-\frac{2}{3}} \tag{4.49}$$

where k_{L-QL} represents the limit of the linear regime (4.37) and k_* the characteristic wavenumber (4.28).

The study of this regime can be done through the particle pairs conservation [45][4]. The mean number of PBH neighbours is

$$N(x, z) = \overline{n}_{PBH} \int_0^x dx' 4\pi x'^2 \left[1 + \xi(x', z)\right] \tag{4.50}$$

[4] In particular chapter 5 of the book [45].

The flux of neighbours leaving the volume of interest is given by $4\pi\tilde{x}^2\tilde{n}_{PBH}[1+\xi(x,z)]\tilde{v}(x,t)$ [45], where $\tilde{v}(x,t)$ is the mean relative velocity of pairs at separation x and time t. As this last value represents a velocity, it must be written in proper coordinates, as well as all other coordinates $\tilde{x} = ax$ and $\tilde{\tilde{n}}_{PBH} = \frac{\overline{n}_{PBH}}{a^3}$. For the conservation of particle pairs, the following equality must be valid.

$$\frac{\partial N(\tilde{x},t)}{\partial t} = -4\pi\tilde{x}^2\tilde{\tilde{n}}_{PBH}[1+\xi(x,t)]\tilde{v}(x,t) = -4\pi x^2\frac{\overline{n}_{PBH}}{a}[1+\xi(x,t)]\tilde{v}(x,t) \quad (4.51)$$

Deriving over x leads to the next relation.

$$\frac{\partial\xi(x,t)}{\partial t} + \frac{1}{ax^2}\frac{\partial}{\partial x}\left[x^2\left(1+\xi(x,t)\right)\tilde{v}(x,t)\right] = 0 \quad (4.52)$$

The non-linear regime is expected to dominate at small scales, where the approximation $\tilde{v}(x,t) \approx -\dot{a}x$ is valid [45], as it is expected that the Hubble expansion is cancelled to keep the structure bounds.

$$\frac{\partial}{\partial t}\left(1+\xi(x,z)\right) = \frac{H}{x^2}\frac{\partial}{\partial x}\left[x^3\left(1+\xi(x,z)\right)\right] \quad (4.53)$$

In this regime the perturbation are very large $\xi_{NL} \gg 1$, hence $(1+\xi_{NL}(x,z)) \approx \xi_{NL}(x,z)$. Consequently, this equation can be approximated.

$$\left[a\frac{\partial}{\partial a} - x\frac{\partial}{\partial x} - 3\right]\xi_{NL}(x,a) \approx 0 \quad (4.54)$$

where $\frac{\partial}{\partial t} = \dot{a}\frac{\partial}{\partial a}$ was used. It follows that this equation admits a power law solution.

$$\xi_{NL}(x,a) \sim a^{3-m}x^{-m} \qquad \text{or} \qquad \xi_{NL}(x,z) \sim (1+z)^{m-3}x^{-m} \quad (4.55)$$

where m is a rational number to be defined.

In order to find the solution to this equation, a step back needs to be taken, in particular to the collisionless Boltzmann equation. In [46] [47] this equation, together with PBH self-gravitation, is used to find a relation between the correlation function and its time and space dependence.

$$\xi(x,t) = f\left(\frac{x}{t^\alpha}\right) \quad (4.56)$$

where f is a function to be defined. Since this relation must be valid and equal for all scenarios, the linear one sets the stricter constraints as it can be expected to be the most accurate, having fewer approximations. Recalling (4.35), the proportionality of PBH correlation function to the time dependence can be found, given by redshift, or scale factor, as follows.

$$\xi_L\left(\frac{1}{k},z\right) \approx \Delta_L^2(k,z) \propto \frac{k^3}{(1+z)^2} \qquad \text{or} \qquad \xi_L\left(x,a\right) \propto \frac{a^2}{x^3} \quad (4.57)$$

In the MD universe $\frac{1}{1+z} \propto a \propto t^{\frac{2}{3}}$ from (C.14).

$$\xi_L\left(x,t\right) \propto \frac{t^{\frac{4}{3}}}{x^3} = \left(\frac{x}{t^{\frac{4}{9}}}\right)^{-3} \quad (4.58)$$

which leads to $\alpha = \frac{4}{9}$. It can be checked that this is consistent with the quasi-linear regime.

$$\overline{\xi}_{QL}\left(\frac{1}{k}, z\right) \propto \left(\frac{k}{(1+z)^{\frac{2}{3}}}\right)^{\frac{9}{4}} \qquad \Rightarrow \qquad \overline{\xi}_{QL}\left(x, a\right) = \left(\frac{a^{\frac{2}{3}}}{x}\right)^{\frac{9}{4}} \tag{4.59}$$

$$\overline{\xi}_{QL}\left(x, t\right) \propto \left(\frac{t^{\frac{4}{9}}}{x}\right)^{\frac{9}{4}} \tag{4.60}$$

coming from (4.37) and (4.47) combined. It turns out that the function f changes, but the factor $\alpha = \frac{4}{9}$ is the same.

For the non-linear regime, both (4.55) and (4.56) must be respected for $\alpha = \frac{4}{9}$. Therefore the power law solution of the non-linear PBH correlation function in a MD universe with $\frac{1}{1+z} \propto a \propto t^{\frac{2}{3}}$ must respect the following proportionality.

$$\xi_{NL}(x,t) = f\left(\frac{x}{t^{\frac{4}{9}}}\right) \propto \left(\frac{x}{t^{\frac{4}{9}}}\right)^{n} \qquad \text{and} \qquad \xi_{NL}(x,t) \sim \frac{t^{2-\frac{2}{3}m}}{x^m} \tag{4.61}$$

$$\Rightarrow \qquad \xi_{NL}(x,t) \propto \frac{x^n}{t^{\frac{4}{9}n}} = \frac{t^{2-\frac{2}{3}m}}{x^m} \tag{4.62}$$

where n is also a rational factor to be defined as m. This leads to a system of equations that has a single solution.

$$\begin{cases} m = -n \\ \frac{4}{9}n = -2 + \frac{2}{3}m \end{cases} \qquad \Rightarrow \qquad m = \frac{9}{5} \tag{4.63}$$

The final solution can be found with the same steps used for the quasi-linear regime in (4.47), therefore making NL and QL scenarios match at $\Delta^2 \sim 200$

$$\boxed{\Delta^2_{NL}(k,z) \approx 200 \left(\frac{k}{k_{QL-NL}(z)}\right)^{\frac{9}{5}}} \tag{4.64}$$

where k_{QL-NL} comes from (4.49). As k_{QL-NL} scales with $(1+z)^{\frac{2}{3}}$, hence $\Delta^2_{NL}(k,z) \propto \left(\frac{1}{1+z}\right)^{\frac{6}{5}}$, it can be checked that its time dependence in the MD universe is in fact $\propto t^{\frac{4}{5}}$, in agreement with both approaches (4.55) and (4.56).

4.2.2.4 Number density

In order to find the number density of the halos, the whole power spectrum (3.36) must be recalled and then PS formalism can be applied as in section 3.2. However this time the number density of the pure PBH clusters is searched. Therefore only the linear isocurvature component of the power spectrum is required.

$$\Delta^2_{iso}(k,a) \approx \frac{k^3}{2\pi^2} \frac{\left[f_{PBH} D_{iso}(a)\right]^2}{\overline{n}_{PBH}} \tag{4.65}$$

where $\overline{n}_{PBH}$ and $D_{iso}(a)$ were mentioned again just above in (4.13) and (4.31). As first step, the variance (3.49) can be computed, using again a Gaussian window (3.47).

$$\sigma^2(R) = \langle \delta^2(\mathbf{x}, R) \rangle = \int d\ln(k) \Delta^2_{iso}(k,a) |W(k,R)|^2 = \frac{f^2_{PBH} D^2_{iso}(a) m_{PBH}}{2^{\frac{3}{2}} M} \tag{4.66}$$

where the monochromatic case with PBH mass m_{PBH} is studied, while the PBH average number density $\overline{n}_{PBH}$ has been expanded. M is the mass of the PBH cluster, hence only given by PBH (3.52): $M = f_{PBH} \gamma V_W \overline{\rho}_m$. In addition to that, the second ingredient to this procedure is the critical density δ_c, which once again can be found to be 1.686 (2.32). This also represents the cutoff of the integral (3.53) in the PS formalism, under which the linear scenario is expected to be valid.

Plugging all components together in (3.55) the number density of PBH halos with mass between M and $M + dM$ can be found accordingly to [40].

$$\frac{dn}{dM} dM = \frac{\overline{\rho}_{PBH}}{\sqrt{\pi}} \left(\frac{M}{M_*(z)} \right)^{\frac{1}{2}} \frac{e^{-\frac{M}{M_*(z)}}}{M^2} dM \tag{4.67}$$

where $M_*(z)$ is the typical mass of PBH halos that collapse at redshift z [48].

$$\boxed{M_*(z) = \frac{1}{\sqrt{2}\delta_c^2} f^2_{PBH} D^2_{iso}(z) m_{PBH}} \tag{4.68}$$

4.2.3 Clustering conditions

Once equipped with the PBH clusters evolution formulas, it is possible to study their sizes and PBH parameters required for formation. In particular, it is interesting to understand if the previous analysis, done in chapter 3, was right to not include any kind of clustering. In order to do that, the limits of the linear and quasi-linear regimes are studied: (4.37) and (4.49). In fact, these wavelengths determine the border of the perturbed scenarios and are inversely proportional to their radius: $k = \frac{1}{R}$. Consequently, it is possible to find the halos masses by choosing the preferred window, and its volume. A Gaussian window volume from (3.47), accordingly to the analysis in chapter 3, is chosen, leading to the mass of the quasi-linear and non-linear clusters.

$$M_{QL} = V_W(k_{L-QL}) \overline{\rho}_m = \frac{(2\pi)^{\frac{3}{2}}}{k^3_{L-QL}} \overline{\rho}_m = \frac{(2\pi)^{\frac{3}{2}}}{k^3_*} f^2_{PBH} \left(1 + \frac{3}{2} f_{PBH} \frac{1+z_{eq}}{1+z} \right)^2 \overline{\rho}_m \tag{4.69}$$

$$M_{NL} = V_W(k_{QL-NL}) \overline{\rho}_m = \frac{(2\pi)^{\frac{3}{2}}}{k^3_{QL-NL}} \overline{\rho}_m = \frac{(2\pi)^{\frac{3}{2}}}{(200)^{\frac{4}{3}} k^3_*} f^2_{PBH} \left(1 + \frac{3}{2} f_{PBH} \frac{1+z_{eq}}{1+z} \right)^2 \overline{\rho}_m \tag{4.70}$$

where $k_* = (2\pi^2 \overline{n}_{PBH})^{\frac{1}{3}}$ as in (4.28). The first mass in particular can be considered the mass of a cluster since it delimits the boundary between the background linear regime and the perturbed quasi-linear one. It must be noted that these results give the volume of the QL and NL perturbations, where the approximation $\gamma \approx 1$

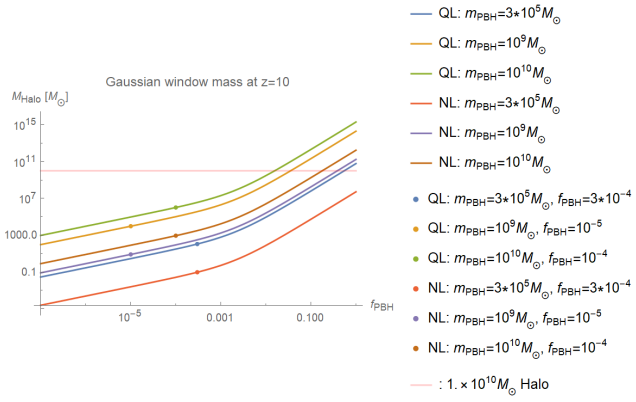

(a)

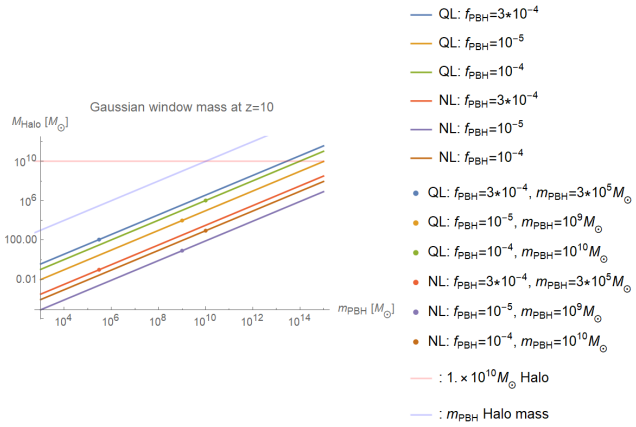

(b)

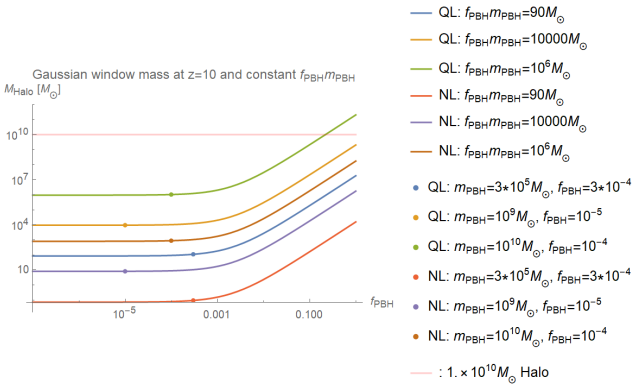

(c)

Figure 4.4: These figures show the masses of the halos with varying f_{PBH}, m_{PBH} and both f_{PBH} and m_{PBH} keeping $f_{PBH}m_{PBH}$ constant, for the same three specific combinations of Table 3.1 from chapter 3. In addition to that, the $10^{10}M_\odot$ halo mass is highlighted, underlining the scale of interest in this report.

was applied, as in the previous section. Therefore the resulting mass is a rough approximation.

Masses (4.69) and (4.70) have two variables which are the PBHs mass m_{PBH} and fraction of DM f_{PBH}. These results are plotted in Figure 4.4 for the cases studied in chapter 3 and compared with the scale of interest.

It is clear from these plots that the specific situations of [9], studied in chapter 3 (see Table 3.1) do not form any relevant cluster for the analysis performed. In particular, Figure 4.4b shows the mass of the halos compared to the mass of PBHs. The clusters' masses always stay below this threshold for the chosen variable, which is a contradiction since at least one PBH has to be in it. Clearly, this means that PBHs do not cluster significantly in the scenarios described in chapter 3, hence the previous study was correct in not considering this phenomenon.

Despite the clustering can be avoided for the previous choice of parameters, it is useful to study the combinations that actually make PBHs cluster relevant. In order to find these scenarios, Figure 4.5 shows a 3D graph of the QL and NL halo masses depending on PBH monochromatic mass and its DM fraction.

These latter graphs help to understand which PBH properties should be required for the clustering evolution to play an important role at $z \sim 10$: $f_{PBH} \gtrsim 0.001$ from Figure 4.5b. In addition to that, the halos of interest with mass $M_{halo} \gtrsim 10^{10} M_\odot$ are expected only for large PBH masses $m_{PBH} \gtrsim 10^4 M_\odot$. A combination of these two results leads to being interesting for large PBH masses with a significant PBH fraction of DM. These results are however very rough and only indicative. Their study thus continues further in the next sections.

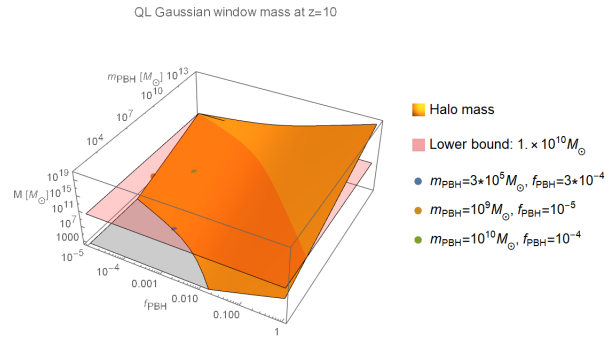

(a)

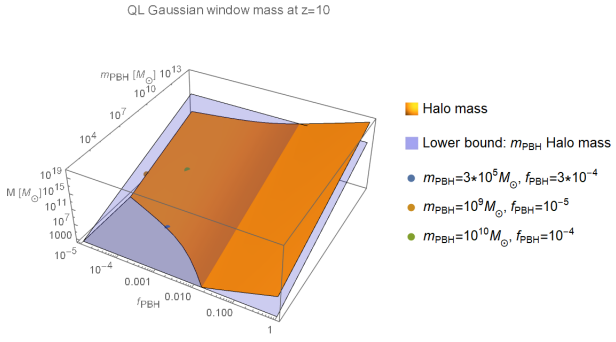

(b)

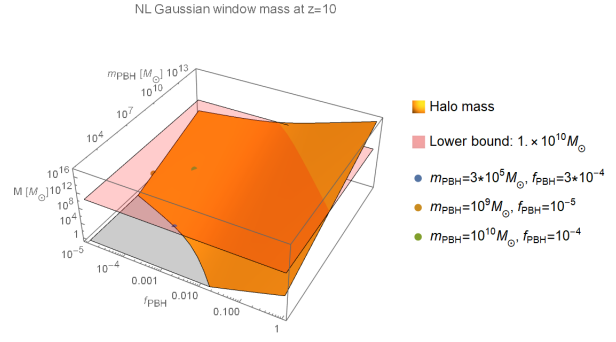

(c)

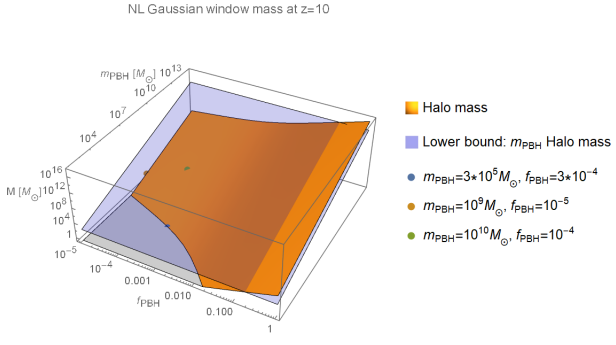

(d)

Figure 4.5: These figures show the masses within the quasi-linear and non-linear scenarios respectively, depending on f_{PBH} and m_{PBH}. In addition to that, the red surface delimits the $10^{10} M_\odot$ halo mass, while the blue one highlights m_{PBH}.

4.3 Excursion set theory

For the next part of this study on clusters, excursion set theory [49] requires an introduction. This model has an analogue objective to PS formalism of calculating the number of virialized objects in the universe, however with a different approach. The qualitative difference of this model is that it solves the problem of the missing factor 2 required with PS (3.54), by studying random walks of overdensities. It is in fact also called *random walks* formalism. The process for its derivation is discussed below following references [28] and [41].

This analysis can start by recalling the fact that initial perturbations are expected to be randomly distributed, hence they are described by an initial Gaussian distribution (3.50).

$$Q_0(S,\delta)d\delta = \frac{1}{\sqrt{2\pi S(M)}} e^{-\frac{\delta^2}{2S(M)}} d\delta \tag{4.71}$$

where dependence on the smoothing scale (R or M) is expressed with the variance (3.49), which is redefined to match the references' notation [28] [41].

$$S(M) = \sigma^2(M) = \langle |\delta(\mathbf{x}, M)|^2 \rangle = \int d\ln(k) \Delta^2(k,a) |W(k,M)|^2 \tag{4.72}$$

where, for consistency, a Gaussian window is used (3.47), and (3.52) provides the transition from R to M dependence.

Fluctuations δ have a dependence on the mass scale, described by S (if S increases so does δ). However as they are randomly distributed, so are their evolution and trajectories, meaning that they can be described by a Brownian motion. It follows that the perturbation distribution can be related to S by a simple diffusion equation [28] [41]. This is possible by substituting the time t dependence with mass scale S, and its location x with δ.

$$\frac{\partial Q}{\partial S} = \frac{1}{2} \frac{\partial^2 Q}{\partial \delta^2} \tag{4.73}$$

This equation describes the diffusion of overdensities with a Brownian motion [28] [41]. However, fluctuations collapse for density contrasts larger than the critical overdensity δ_c (see section 2.3), which leads to break this scenario, since it makes the evolution of perturbations depended on gravity, thus not random anymore. For this reason, a barrier ω is defined from the linear evolution of the critical overdensity (2.48) to highlight this threshold, and be consistent with the references [28] [41].

$$\omega(z_{coll}) = \delta_L(z_{coll}) = \frac{3}{20}(12\pi)^{\frac{2}{3}} \left(\frac{1+z_{coll}}{1+z_{obs}} \right) \tag{4.74}$$

It represents the overdensity barrier observed at z_{obs} that made a perturbation collapse at z_{coll}. Analogously to the critical density contrast, it represents the overdensity barrier, over which the gravitational collapse starts, hence the formation of clusters.

The influence of this barrier over the overdensities random walks is shown in Figure 4.6. It follows that the diffusion equation (4.73) can be used to distinguish the number density of perturbation above and below this threshold (4.74). In fact,

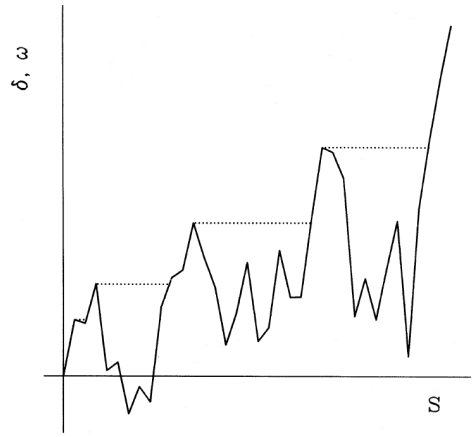

Figure 4.6: The temporal evolution can be followed from the top right corner towards left and downwards, as the overdensities tend to decrease, while the halo mass grows (hence S also decreases). A random trajectory of an overdensity δ together with the evolution of the barrier ω (dotted line) are plotted with their perturbation mass development $S(M)$. The actual mass evolution of the halo follows the barrier as it determines the collapse. The depressions in the random overdensity walk, for which it does not match with the barrier, represents the moment before a merger. This image is taken directly from the article [41].

while trajectories over the barrier threshold do not follow a random evolution, perturbations below the critical overdensity can be still considered to do that.

This value can be found by supposing that for a small mass interval S to $S + dS$ the overdensity places itself at a barrier ω. A Brownian motion dictates that the following fluctuation evolution could randomly go either way, above or below this threshold. The perturbations number density which stays below the barrier is therefore defined as the difference between the initial perturbation distribution, around 0, and the number density at an opposite distance from the critical overdensity[5], hence 2ω.

$$Q(S,\delta,\omega)d\delta = \frac{1}{\sqrt{2\pi S(M)}}\left(e^{-\frac{\delta^2}{2S(M)}} - e^{-\frac{(\delta-2\omega)^2}{2S(M)}}\right)d\delta \tag{4.75}$$

Now, in order to find the total halo mass function, it is required to find the equation describing the probability of an overdensity to be found above the threshold, hence collapsing into a halo. The first step consists in finding a formula which describes the decrease of the number density of perturbations below the chosen barrier, due to collapse, in the interval S to $S + dS$.

$$f_S(S,\omega) = \left[-\frac{\partial}{\partial S}\int_{-\infty}^{\omega} Q d\delta\right] = -\left[\frac{1}{2}\frac{\partial Q}{\partial \delta}\right]_{-\infty}^{\omega} \tag{4.76}$$

[5]This distance is intended as fluctuation magnitude gap, as for the diffusion equation (4.73).

where in the second passage (4.73) was used. This result is the transition rate through a barrier ω in a mass range S to $S + dS$.

$$\boxed{f_S(S,\omega)dS = \frac{\omega}{\sqrt{2\pi S(M)^3}} e^{-\frac{\omega^2}{2S(M)}} dS} \tag{4.77}$$

But it also represents the fraction of halos with clustered mass M, associated to S. This formula is one of the main results of the excursion set theory, which is recalled in the next section to study accretion and survival times. In addition to that, it can be used to find the number density of halos with mass M similarly to (3.55).

$$\begin{aligned}
\frac{dn}{dM}(M,t)dM &= \frac{\overline{\rho}_m}{M} f_S\left(S(M), \omega(t)\right) \left|\frac{dS(M)}{dM}\right| dM \\
&= \frac{1}{\sqrt{2\pi}} \frac{\overline{\rho}_m}{M} \frac{\omega(t)}{\sigma(M)^3} \left|\frac{d\sigma(M)^2}{dM}\right| e^{-\frac{\omega(t)^2}{2\sigma(M)^2}} dM \\
&= \sqrt{\frac{2}{\pi}} \frac{\overline{\rho}_m}{M^2} \frac{\omega(t)}{\sigma(M)} \left|\frac{d\ln(\sigma(M))}{d\ln(M)}\right| e^{-\frac{\omega(t)^2}{2\sigma(M)^2}} dM
\end{aligned} \tag{4.78}$$

where in the second passage the substitution $S(M) = \sigma(M)^2$ of (4.72) was applied. This solution is exactly the same halo mass function obtain with the PS method (3.55), once the barrier $\omega(t)$ is substituted with δ_c [6]. In addition, it must be noted that this approach directly leads to the correct HMF, without encountering the problematic of the missing factor 2 (3.54), as claimed at the beginning.

Other than the clean result of obtaining a precise HMF, no conclusion is drawn from excursion set formalism directly, as its usefulness becomes important in the next section where (4.77) will be at the centre of attention.

[6] As δ_c has no mass dependence, the derivative of (3.55) becomes

$$\frac{d\ln(\nu)}{d\ln(M)} = \frac{d\ln\left(\frac{\delta_c}{\sigma(M)}\right)}{d\ln(M)} = \frac{d\ln(\delta_c)}{d\ln(M)} - \frac{d\ln\left(\frac{1}{\sigma(M)}\right)}{d\ln(M)} = \frac{d\ln(\sigma(M))}{d\ln(M)}$$

4.4 Clusters accretion and survival times

The study of clusters cannot be done alone without considering side effects. In particular the halo accretion, clusters merger and their survival time. In this section clusters that could lead to an explanation of JWST observation are studied [5], hence the PBH ensembles that could lead to halos mass of approximately $10^{10} M_\odot$ by $z \sim 10$. The objective is to understand to which extent PBH clusters are relevant to lead to early galaxy formation. In order to study this topic, the previous excursion set formalism is recalled and the articles [40] and [41] are followed.

The first step to be taken is to find an approximate formation redshift of an halo. In order to achieve this goal, (4.68) is recalled. In fact, this formula represents the typical mass of halos collapsed at redshift z, hence it can be inverted to find the collapsing time based on its mass, but also on the PBH characteristics f_{PBH} and m_{PBH} [48]. This time $\gamma \approx 1$ approximation is dropped, hence (4.68) together with (4.31) leads to a more accurate typical PBH cluster mass.

$$M_*(a) = \frac{1}{\sqrt{2}\delta_c^2} f_{PBH}^2 D_{iso}^2(z) m_{PBH} \approx \frac{1}{\sqrt{2}\delta_c^2} f_{PBH}^2 \left(1 + \frac{3\gamma}{2a_-}\frac{a}{a_{eq}}\right)^{a_-} m_{PBH} \tag{4.79}$$

$$= \frac{1}{\sqrt{2}\delta_c^2} f_{PBH}^2 \left(1 + \frac{3\gamma}{2a_-}\frac{1+z_{eq}}{1+z}\right)^{a_-} m_{PBH} \tag{4.80}$$

where one more time

$$s = \frac{a}{a_{eq}}, \qquad \gamma = \frac{\Omega_m - \Omega_b}{\Omega_m}, \qquad a_- = \frac{1}{4}\left(\sqrt{1+24\gamma} - 1\right) \tag{4.81}$$

Reversing this formula gives the formation redshift.

$$\boxed{z_{form} = \frac{3\gamma(1+z_{eq})}{2a_-} \frac{1}{\left(\frac{\delta_c}{f_{PBH}}\sqrt{\frac{\sqrt{2}M_*}{m_{PBH}}}\right)^{\frac{1}{a_-}} - 1} - 1} \tag{4.82}$$

It is clear that the main variables of this formula are two: f_{PBH} and the relation between m_{PBH} and M_* which can also be interpreted as the halo mass M_{halo}. The formation time for different variables is shown in Figure 4.7. This graph shows that if PBHs would make up a small portion of DM, no clustering would form. The threshold value of f_{PBH} for clustering at present time $z_{form} = 0$ and redshift of interest $z_{form} = 10$ can be calculated directly from (4.82) for a minimal halo, of a single PBH $\frac{M_{halo}}{m_{PBH}} = 1$, since it maximise the formation redshift. The results can be computed numerically.

$$0 = \frac{3\gamma(1+z_{eq})}{2a_-} \frac{1}{\left(\frac{2^{\frac{1}{4}}\delta_c}{f^0_{PBH}}\right)^{\frac{1}{a_-}} - 1} - 1 \tag{4.83}$$

$$\Rightarrow f^0_{PBH} = 2^{\frac{1}{4}}\delta_c \left(\frac{3\gamma(1+z_{eq})}{2a_-} + 1\right)^{-a_-} \approx 0.00096$$

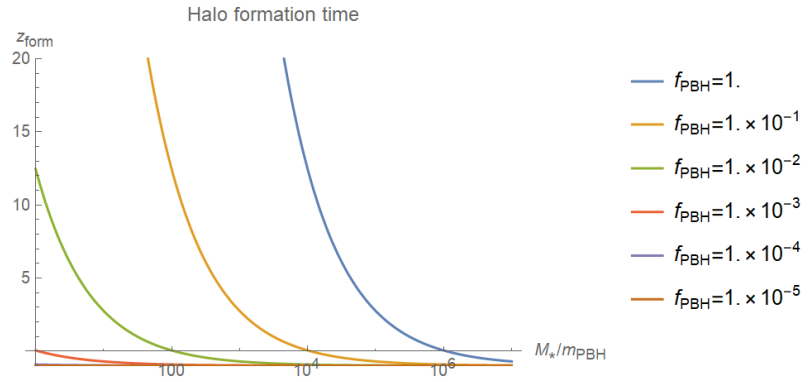

Figure 4.7: Formation redshift of PBH clusters (4.82) for different PBHs portions of DM f_{PBH} and depending on the ration between the halo of interest and PBH monochromatic mass $\frac{M_*}{m_{PBH}}$ or $\frac{M_{halo}}{m_{PBH}}$.

$$10 = \frac{3\gamma(1+z_{eq})}{2a_-}\frac{1}{\left(\frac{2^{\frac{1}{4}}\delta_c}{f_{PBH}^{10}}\right)^{\frac{1}{a_-}}-1} - 1 \tag{4.84}$$

$$\Rightarrow f_{PBH}^{10} = 2^{\frac{1}{4}}\delta_c\left(\frac{3\gamma(1+z_{eq})}{22a_-}+1\right)^{-a_-} \approx 0.0083$$

where the second result is similar to the clustering limit of $f_{PBH} \gtrsim 0.001$ at $z = 10$ from subsection 4.2.3. It is however more interesting for the purpose of this report to do the same process for a relevant cluster at $z \sim 10$, made of at least 10 PBHs, hence $\frac{M_{halo}}{m_{PBH}} = 10$.

$$10 = \frac{3\gamma(1+z_{eq})}{2a_-}\frac{1}{\left(\frac{2^{\frac{1}{4}}\delta_c}{f_{PBH}^{10}}\right)^{\frac{1}{a_-}}-1} - 1 \qquad \Rightarrow \qquad f_{PBH} \approx 0.026 \tag{4.85}$$

This result clearly strengthens the constraint of the PBH fraction of DM to approximately $f_{PBH} \gtrsim 0.01$.

On the other hand, the fraction of DM made as PBH has an upper limit $f_{PBH} \leq 1$, which can be used to determine the largest number of PBHs in a halo, that can be generated by a certain redshift. This is achieved by repeating the process above, but for $f_{PBH} = 1$ and $\frac{M_{halo}}{m_{PBH}}$ as variable

$$0 = \frac{3\gamma(1+z_{eq})}{2a_-}\frac{1}{\left(\delta_c^2\frac{\sqrt{2}M_{halo}^0}{m_{PBH}}\right)^{\frac{1}{2a_-}}-1} - 1 \tag{4.86}$$

$$\Rightarrow \frac{M_{halo}^0}{m_{PBH}} = \frac{1}{\sqrt{2}\delta_c^2}\left(\frac{3\gamma(1+z_{eq})}{2a_-}+1\right)^{2a_-} \approx 1.1\cdot 10^6$$

$$10 = \frac{3\gamma(1+z_{eq})}{2a_-}\frac{1}{\left(\delta_c^2\frac{\sqrt{2}M_{halo}^{10}}{m_{PBH}}\right)^{\frac{1}{2a_-}}-1}-1 \tag{4.87}$$

$$\Rightarrow \frac{M_{halo}^0}{m_{PBH}} = \frac{1}{\sqrt{2}\delta_c^2}\left(\frac{3\gamma(1+z_{eq})}{22a_-}+1\right)^{2a_-} \approx 1.4\cdot 10^4$$

These results indicate the largest cluster that PBHs can generate by themselves, by respective redshift $z = 0$ and $z = 10$.

4.4.1 Accretion rate

The main phenomenon that allows the PBH clusters to grow is accretion, which effect is now analysed. The accretion rate is studied through excursion set theory, therefore formulas from section 4.3 are often be recalled. In particular the barrier (4.74) for a collapse to have happened by the time of interest $z_{obs} \sim 10$.

$$\omega_{10}(z_{coll}) = \frac{3}{220}(12\pi)^{\frac{2}{3}}(1+z_{coll}) \tag{4.88}$$

In fact, it is investigated whether or not a peak in accretion, leading to galaxy formation, could be found around $z \sim 10$.

Before being able to calculate the accretion rate, additionally useful formulas can be found by applying the excursion set theory to different situations, as it is done in [28] and [41]. The first element to be computed is the conditional probability that a halo which reaches the barrier ω_2 with a specific mass M_2 (hence $S_2 = S(M_2)$) crossed a barrier $\omega_1 > \omega_2$ within a mass interval $M_1 < M_2$ to $M_1 + dM_1$ (hence $S_1 = S(M_1) > S_2$ to $S_1 + dS_1$), in a previous stage of its evolution. This is achieved by simply setting the starting barrier and mass to ω_2 and S_2 instead of the origin as in (4.77) [41].

$$\begin{aligned} f_{S_1}(S_1,\omega_1|S_2,\omega_2)dS_1 &= f_S(S_1-S_2,\omega_1-\omega_2)dS_1 \\ &= \frac{\omega_1-\omega_2}{\sqrt{2\pi(S_1-S_2)^3}}e^{-\frac{(\omega_1-\omega_2)^2}{2(S_1-S_2)}}dS_1 \end{aligned} \tag{4.89}$$

where $S_1 > S_2$ and $\omega_1 > \omega_2$ is required[7]. The opposite way can also be computed, therefore the conditional probability that given a halo of mass M_1 at barrier ω_1, this will evolve into a cluster with mass range S_2 to $S_2 + dS_2$ at a barrier ω_2.

$$\begin{aligned} f_{S_2}(S_1,\omega_1|S_2,\omega_2)dS_2 &= \frac{f_{S_1}(S_1,\omega_1|S_2,\omega_2)dS_1 f_{S_2}(S_2,\omega_2)dS_2}{f_{S_1}(S_1,\omega_1)dS_1} \\ &= \frac{1}{\sqrt{2\pi}}\frac{\omega_2(\omega_1-\omega_2)}{\omega_1}\left(\frac{S_1}{S_2(S_1-S_2)}\right)^{\frac{3}{2}}e^{-\frac{(\omega_2 S_1-\omega_1 S_2)^2}{2S_1S_2(S_1-S_2)}}dS_2 \end{aligned} \tag{4.90}$$

where once again $S_1 > S_2$ and $\omega_1 > \omega_2$ is required.

[7] The barrier decreases with time (4.74), while a halo is expected to grow through accretion or merger, hence S also decreases (4.72).

With these equations the transition rate from a halo S_1 to an halo S_2 in an infinitesimal time can be calculated by applying $\omega_1 \to \omega_2 = \omega$, hence $\omega_1 - \omega_2 = d\omega \to 0$.

$$\boxed{\frac{d^2p}{dS_2 d\omega}(S_1 \to S_2|\omega)dS_2 d\omega = \frac{1}{\sqrt{2\pi}}\left(\frac{S_1}{S_2(S_1-S_2)}\right)^{\frac{3}{2}} e^{-\frac{\omega^2(S_1-S_2)}{2S_1S_2}} dS_2 d\omega} \tag{4.91}$$

Since this formula expresses the halo mass variation in an infinitesimal time, it can be expected that this mass increase is due to only one event, hence a merger[8]. It is sometimes useful to rewrite this equation in terms of mass variation $\Delta M = M_2 - M_1$.

$$\begin{aligned}\frac{d^2p}{d\ln(\Delta M)d\ln(a)}(M_1 \to M_2|a) &= \left|\frac{dS_2}{d\ln(\Delta M)}\right|\left|\frac{d\omega}{d\ln(a)}\right|\frac{d^2p}{dS_2 d\omega}(S_1 \to S_2|\omega) \\ &= \frac{1}{\sqrt{2\pi}}\Delta M a\left|\frac{dS_2}{dM_2}\right|\left|\frac{d\omega}{da}\right|\left(\frac{S_1}{S_2(S_1-S_2)}\right)^{\frac{3}{2}} e^{-\frac{\omega^2(S_1-S_2)}{2S_1S_2}} \qquad (4.92) \\ &= \sqrt{\frac{2}{\pi}}\left|\frac{d\sigma(M_2)}{dM_2}\right|\left|\frac{d\omega(a)}{da}\right|\frac{\Delta M a}{\sigma(M_2)^2}\frac{e^{-\frac{\omega(a)^2}{2}\left(\frac{1}{\sigma(M_2)^2}-\frac{1}{\sigma(M_1)^2}\right)}}{\left(1-\frac{\sigma(M_2)}{\sigma(M_1)}\right)^{\frac{3}{2}}} \qquad (4.93)\end{aligned}$$

While these two formulas give the probability of accretion from a M_1 halo to a higher mass M_2, another quantity that gives useful insight on accretions is the fractional mass accretion rate, given by the same equations multiplied by $\frac{\Delta M}{M_1}$.

4.4.1.1 ΛCDM standard model

The first use of the formulas found above is to replicate prior studies. This is achieved by imitating [28], where a power law solution of the variance in the standard ΛCDM model is used.

$$S(M) \approx \delta_c^2\left(\frac{M}{M'}\right)^{0.35} \approx \frac{115818}{M^{0.35}} \tag{4.94}$$

where $M' = 10^{13}h_0 M_\odot$ is a normalization mass used in the article. This leads to finding the accretion rates, as well as the fractional mass accretion rates at z=0, for different initial conditions, as shown in Figure 4.8. The shape of the plot has a strong resemblance to [28], despite the obtained values are not exactly the same. This divergence must be due to differences in the constants used, such as h_0, δ_c or even the barrier ω in (4.93), thus the replication can be considered successful.

A similar analysis can be performed by starting from the adiabatic power spectrum (3.19), which alone represents the standard model power spectrum. As for subsection 3.3.1, a power law fit for the adiabatic variance is required in order to plot the results. The range chosen for this fit clearly determines the resulting variance, hence the accretion rate. For a range $M_W = 10^{10} - 10^{20} M_\odot$, similar to the initial halo masses of Figure 4.8, the fitted variance is the following.

$$S(M) \approx \frac{250615}{M^{0.37455}} \tag{4.95}$$

[8] Although only mergers can produce discrete mass increases, these mass gains can be many and due to very small particles, generating the phenomenon of accretion.

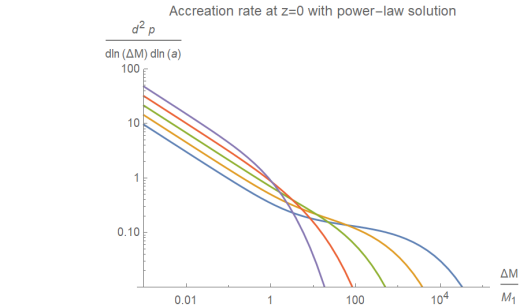

(a)

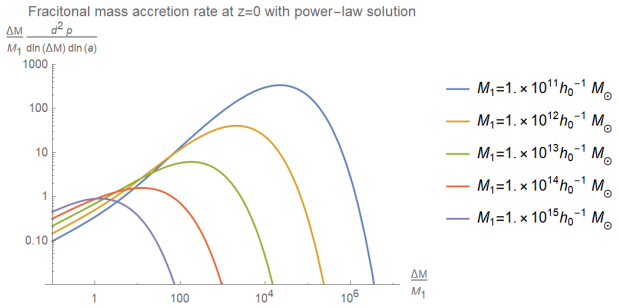

(b)

Figure 4.8: Growth rate for different halo masses at $z = 0$ analogously to [28]. While 4.8a shows accretion rate, 4.8b describe the fractional mass accretion rate. Both these results try to replicate the graphs in [28].

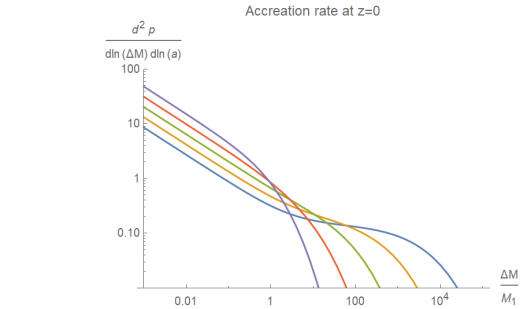

(a)

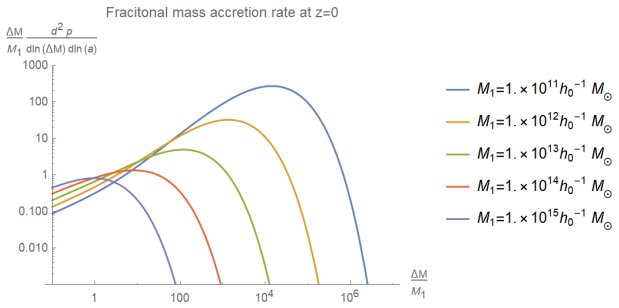

(b)

Figure 4.9: Growth rate for different halo masses at $z = 0$ starting from the adiabatic power spectrum (3.19). The accretion rate and the fractional mass accretion rate are displayed.

which is very similar to (4.94) in terms of mass dependence, but not quite the same. This result leads to similar accretion rates to the replication of [28], shown in Figure 4.9. It must however be noted that the fit of the adiabatic power spectrum variance could drastically change these curves. It is therefore important to evaluate the best fit on the halo masses of interest.

4.4.1.2 Poissonian distributed PBHs

The main topic of interest in this chapter is now treated. The possibility that that PBH cluster evolution leads to halos that quickly grow with the accretion rate around $z \sim 10$, from initially randomly distributed PBH, is investigated. This rapid accretion could explain the early formation of very massive halos and consequently boost the generation of galaxies, such as the ones observed by JWST. In order to do that, accretion rates that peak, or at least exceed the standard model scenario, around $z \sim 10$, forming $10^{10} M_\odot$ halos, are looked for.

Firstly, the total variance required for the calculation of (4.93) must be determined. This is achieved once again by applying (4.72) to both adiabatic (3.19) and isocurvature power spectrum from Poissonian distributed PBHs (3.36).

$$S_{10}(M) = \sigma^2_{ad}(M, z = 10) + \sigma^2_{iso}(M, f_{PBH}, m_{PBH}, z = 10) \tag{4.96}$$

$$= \sigma^2_{ad,10}(M) + \sigma^2_{iso,10}(M, f_{PBH}, m_{PBH}) \tag{4.97}$$

By taking a deeper look at the formulas composing this total variance, one thing can be noted, which has been already mentioned in chapter 3. From (3.36-3.39), f_{PBH} and m_{PBH} dependence of the isocurvature component always come in pair, leading to the simplification

$$\sigma^2_{iso,10}(M, f_{PBH}, m_{PBH}) = \sigma^2_{iso,10}(M, f_{PBH} m_{PBH}) \tag{4.98}$$

Hereafter, the accretion rate is calculated numerically using *Mathematica*, by applying the same process described in subsection 3.3.1 for the variance, and then inserting all the parameters in (4.93). Once more, PBHs are considered to be Poisson distributed at the beginning, hence having initial power spectrum equal to the shot noise (3.30).

However, before moving to the numerical computation, some considerations on the possible values of $f_{PBH} m_{PBH}$ must be discussed. Firstly, f_{PBH} cannot be larger than 1, it follows that $m_{PBH} \geq f_{PBH} m_{PBH}$. Secondly, the objective is to minimise the possible PBH mass m_{PBH}, thus the smallest halo, after accretion, that could generate a $10^{10} M_\odot$ stellar mass galaxy is searched. To respect this focused analysis, $f_{PBH} m_{PBH} \lesssim 10^8 M_\odot$. This comes from the fact that if the starting cluster has a significant mass increase, up to $10^{10} M_\odot$, its growth is expected to be of at least an order of 10, hence must have a maximum initial mass of $10^9 M_\odot$. At the same time, the scenario discussed here is the clustering of PBHs, therefore the cluster before accretion is expected to be composed of at least 10 PBHs. Nevertheless, both PBHs mass and starting cluster could be larger, as long as the SFE is smaller.

$$10^{10} M_\odot \gtrsim M_1 \gtrsim 10 m_{PBH} \gtrsim 10 f_{PBH} m_{PBH} \;\Rightarrow\; \begin{cases} M_1 \lesssim 10^9 M_\odot \\ f_{PBH} m_{PBH} \lesssim m_{PBH} \lesssim 10^8 M_\odot \end{cases} \tag{4.99}$$

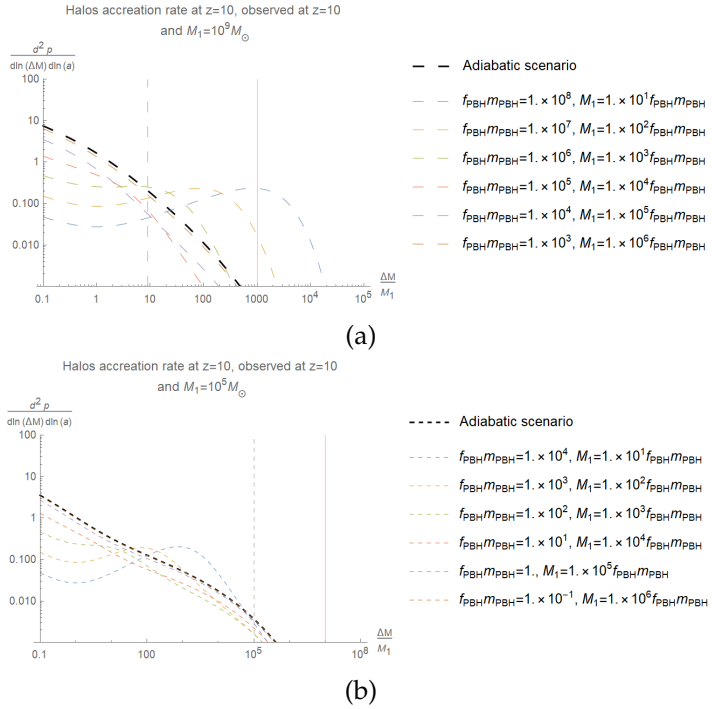

Figure 4.10: Comparison between the accretion rates of halos in the standard model scenario and with the inclusion of PBH at $z = 10$. The two graphs are evaluated for starting clusters of mass $10^9 M_\odot$ and $10^5 M_\odot$ respectively. The vertical lines indicate a final halo mass of $10^{10} M_\odot$ (dashed black line), and the limit mass used for the fitting range (red).

In addition to that, it must be recalled that the PBH fraction of DM is also constrained from (4.85) $f_{PBH} \gtrsim 0.01$. In order to understand which value of $f_{PBH} m_{PBH}$ and M_1 could be considered to explain an increase in $10^{10} M_\odot$ halos, many different combinations were tested through their accretion rates. Some of these results are shown in Figure 4.10, and highlight the fact that only combinations of $M_1 > 10^5 M_\odot$ lead to relevant accretion rates (see Figure 4.10b), higher than the standard model's adiabatic case. Since PBHs contribution to accretion clearly decreases with $f_{PBH} m_{PBH}$, Figure 4.10a can be used to determine that M_1 can be composed of a maximum number of approximately 10^4 PBHs, for their presence to boost the halos accretion. This limit is in accordance with the constraint given by (4.87).

Further analysis of this kind lead to finding the possible combinations of PBH variables $f_{PBH} m_{PBH}$ and initial halo mass M_1 that are likely to grow into a $10^{10} M_\odot$ halo at $z \sim 10$. The main results are shown in Figure 4.11 in terms of accretion rate, and in Figure 4.12 in terms of fractional mass accretion.

In conclusion, PBH presence associated with their clusters' evolution, could lead to an increase of $10^{10} M_\odot$ halos number, hence galaxies, with PBH parameters of approximately $f_{PBH} m_{PBH} \approx 10^5 - 10^6 M_\odot$. Before accretion to a mass of $10^{10} M_\odot$, those halos are expected be composted of $10 - 1000$ PBHs, depending on the situation. Consequently the mass of PBHs can be expected to be in the range

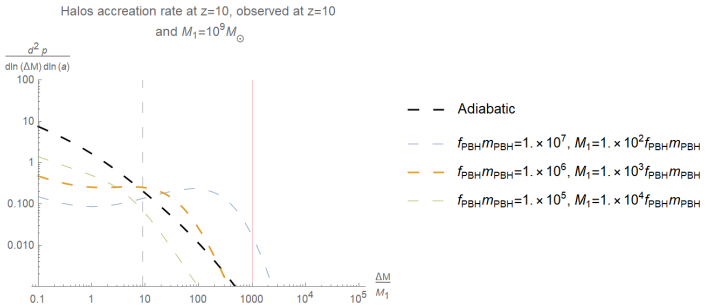

(a)

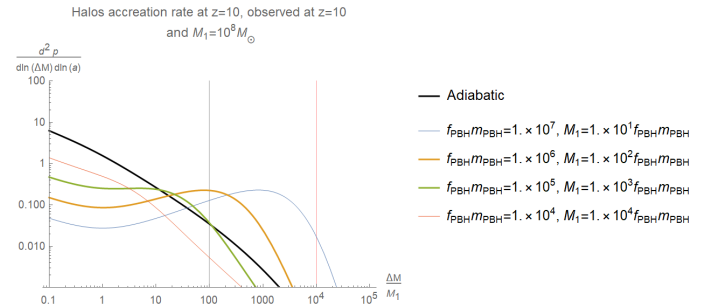

(b)

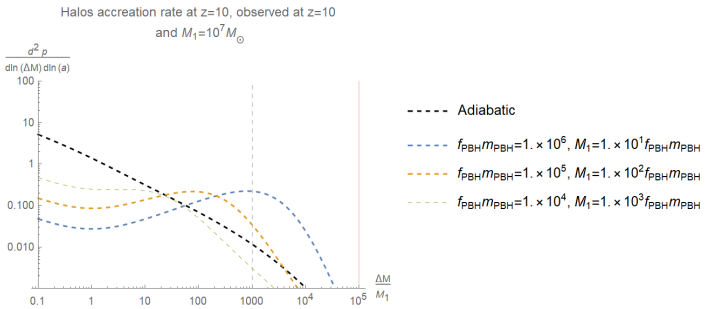

(c)

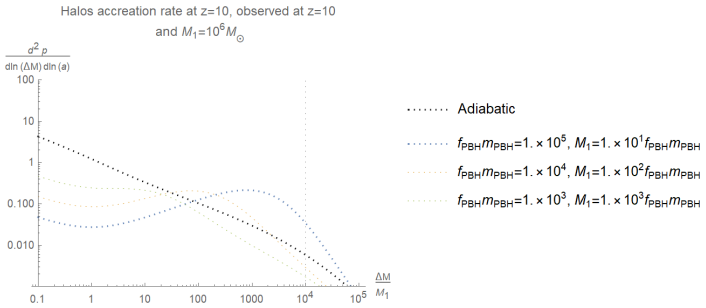

(d)

Figure 4.11: Accretion rates of halos at $z = 10$, in the standard model scenario and with the inclusion of PBH, for clusters with masses 10^9, 10^8, 10^7 and $10^6 M_\odot$. The thicker lines represent the most likely variables combinations that could lead to an accretion to a $10^{10} M_\odot$ halo. This latter threshold is also highlighted by the vertical black line. The vertical red line indicates the higher limit of the fitting mass range for the adiabatic variance.

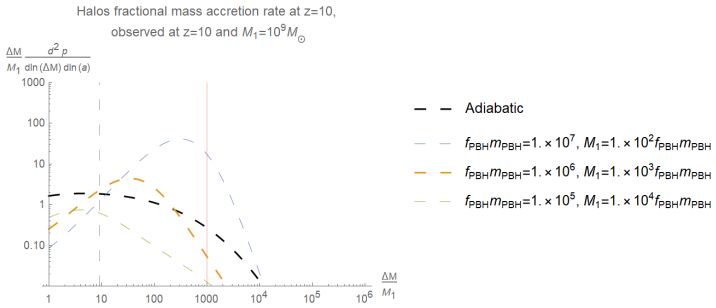

(a)

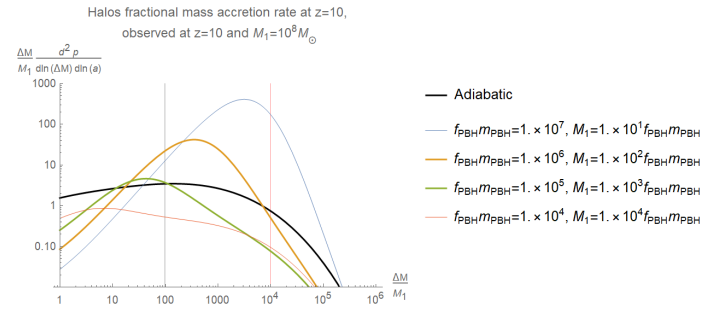

(b)

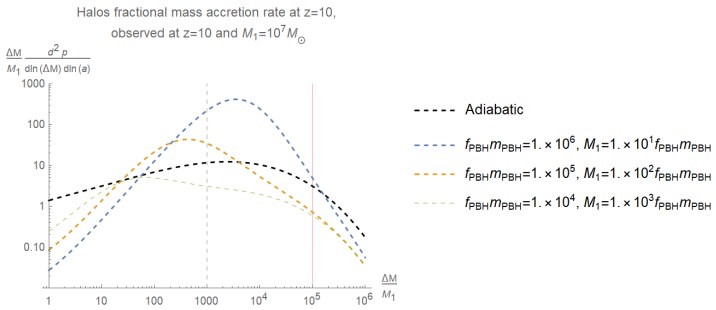

(c)

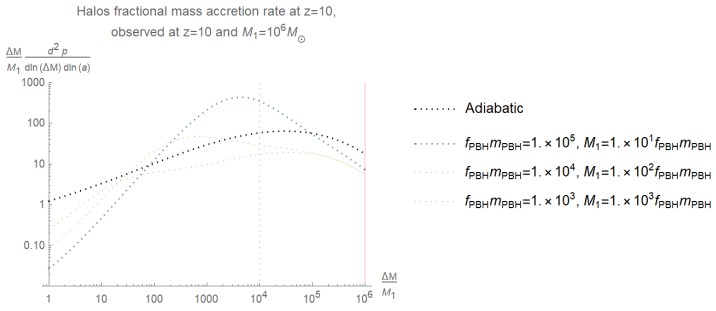

(d)

Figure 4.12: Fractional mass accretion rates of halos at $z = 10$, in the standard model scenario and with the inclusion of PBH, for halos with masses 10^9, 10^8, 10^7 and $10^6 M_\odot$. The thicker lines represent the most likely variables combinations that could lead to an accretion to a $10^{10} M_\odot$ halo. This latter threshold is also highlighted by the vertical black line. The vertical red line indicates the higher limit of the fitting mass range for the adiabatic variance.

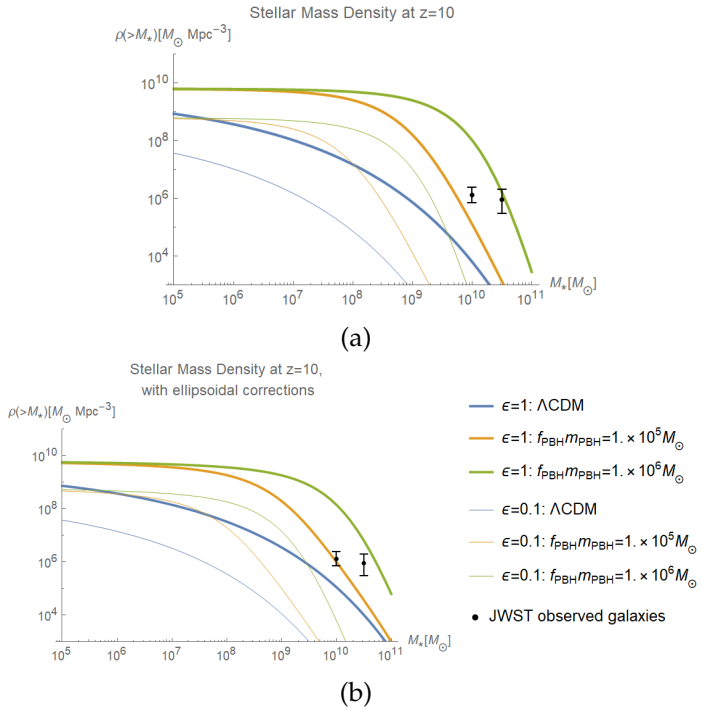

Figure 4.13: Stellar mass density at $z = 10$ for the possible PBH variables combinations highlighted in (4.100).

$10^5 M_\odot \lesssim m_{PBH} \lesssim 10^8 M_\odot$.

In summary:

$$\begin{aligned} f_{PBH} m_{PBH} &\approx 10^5 - 10^6 M_\odot \\ 10^5 M_\odot \lesssim m_{PBH} &\lesssim 10^8 M_\odot \\ f_{PBH} &\gtrsim 0.01 \\ 10^6 M_\odot \lesssim M_1 &\lesssim 10^9 M_\odot \end{aligned} \tag{4.100}$$

where the different possible combinations must be checked with Figure 4.11 and 4.12.

The stellar mass density of the possible combinations (4.100) can be found with the same analysis on Poisson distributed PBHs of section 3.3. These results are shown in Figure 4.13, with and without ellipsoidal correction (subsection 3.2.4), depending on $f_{PBH} m_{PBH}$ as these variables always come together in the cumulative stellar mass density formula (3.59).

4.4.2 Survival time

Another question that could arise after having found PBH parameters for which accretion peaks around $z \sim 10$, is whether or not the PBH clusters evaporation should be taken into account or not. Following [40], [41] and [50], it is possible to study this phenomenon. On one hand, [50] provides a formula to compute an approximate evaporation time of a halo composed of N discrete objects, due to

gravitational forces.

$$\boxed{t_{ev} \approx \frac{14}{N^2 \ln(N)} \frac{v^9}{n^2 G^5 m^5}} \tag{4.101}$$

where $v = \sqrt{\frac{GNm}{R_{cl}}}$ is the mean particles velocity, R_{cl} is the radius of the clusters, n is the number density and m the particles mass. This formula can be applied to PBH clusters, by approximating the scenario to the monochromatic PBHs case and neglecting the adiabatic matter. In order to do this, the number density can be called $n = n_{PBH}$[9], while PBH monochromatic mass $m = m_{PBH}$ is used and N is the number of PBH in the halos. The typical clusters radius is defined as the scale of virialized objects that include N PBHs. For this reason, the same approximation used to define the overdensity of a collapsed, hence non-linear, perturbation can be used (4.48) [40].

$$n_{PBH} \approx 200 \overline{n}_{PBH} \approx \frac{3N}{4\pi R_{cl}^3} \;\Rightarrow\; R_{cl} \approx \left(\frac{3N}{4\pi 200 \overline{n}_{PBH}} \right)^{\frac{1}{3}} \tag{4.102}$$

With this knowledge, the explicit evaporation time can be found.

$$t_{ev} \approx \frac{224\pi^2 N}{9 \ln(N)} \sqrt{\frac{R_{cl}^3}{GNm_{PBH}}} \approx \frac{224\pi^2 N}{9 \ln(N)} \sqrt{\frac{3}{4\pi 200 G \overline{n}_{PBH} m_{PBH}}} \tag{4.103}$$

The evaporation must take place after the formation of a halo and is expected to happen in the MD universe. It is therefore possible to compute the evaporation redshift by applying (C.14).

$$z_{ev} + 1 \approx \left(\frac{t_0}{t_{ev} + t_{form}} \right)^{\frac{2}{3}} = \left(\frac{t_0}{t_{ev} + \frac{t_0}{(z_{form}+1)^{\frac{3}{2}}}} \right)^{\frac{2}{3}} = \frac{z_{form} + 1}{\left(\frac{t_{ev}(z_{form}+1)^{\frac{3}{2}}}{t_0} + 1 \right)^{\frac{2}{3}}} \tag{4.104}$$

where t_0 is the present time of the universe and its value is listed in Appendix A.

On the other hand, the time required for a halo to undergo accretion or merger with other halos, and grow in mass and size, contrasts the evaporation process. With the excursion set theory, it is possible to find the survival time of halos, before they get included in larger ones, either by accretion or merger. This can be then compared to the evaporation time to understand whether growth or evaporation takes place sooner. The survival time can be found by firstly computing the total probability, that a cluster present at time ω_1 with mass S_1 is included in a halo of a larger mass $S_2 < S_1$ at time $\omega_2 > \omega_1$ or earlier [41]. This is also equivalent to the probability of a halo to be included in a cluster of mass S_2 or larger, by a precise time ω_2, since finding larger halo masses means that its perturbation has crossed a higher barrier beforehand. This probability can be calculated by integrating (4.90).

$$P(S_1, \omega_1 | S < S_2, \omega_2) = P(S_1, \omega_1 | S_2, \omega > \omega_2) = \int_0^{S_2} f_{S_2'}(S_1, \omega_1 | S_2', \omega_2) dS_2' \tag{4.105}$$

$$= \frac{1}{2} \frac{\omega_1 - 2\omega_2}{\omega_1} e^{\frac{2\omega_2(\omega_1 - \omega_2)}{S_1}} [1 - \mathrm{erf}(X)] + \frac{1}{2} [1 - \mathrm{erf}(Y)] \tag{4.106}$$

[9] Notice that this is not the average number density, but the local one.

where

$$X = \frac{S_2(\omega_1 - 2\omega_2) + S_1\omega_2}{\sqrt{2S_1S_2(S_1 - S_1)}}, \qquad Y = \frac{S_1\omega_2 - S_2\omega_1}{\sqrt{2S_1S_2(S_1 - S_1)}} \tag{4.107}$$

The infinitesimal probability of a halo being included in a larger one can also be very useful, in order to understand the process dynamics. This in fact gives the probability that a cluster S_1 is incorporated into a larger S_2 halo in an interval between ω_2 and $\omega_2 + d\omega_2$.

$$g_{\omega_2}(S_1,\omega_1|S_2,\omega_2)d\omega_2 = -\frac{\delta}{\delta\omega_2}P(S_1,\omega_1|S_2,\omega > \omega_2)d\omega_2 \tag{4.108}$$

$$\begin{aligned} =&\sqrt{\frac{2}{\pi}}\frac{1}{\omega_1}\sqrt{\frac{S_1}{S_2(S_1 - S_2)}}e^{\frac{2\omega_2(\omega_1-\omega_2)}{S_1}}\left[\frac{S_1(\omega_1 - \omega_2) - S_2(\omega_1 - 2\omega_2)}{S_1}e^{-X^2}\right. \\ &\left.+\sqrt{\frac{\pi}{2}}\sqrt{\frac{S_2(S_1 - S_2)}{S_1}}\left(1 - \frac{(\omega_1 - 2\omega_2)^2}{S_1}\right)[1 - \mathrm{erf}(X)]\right] \end{aligned} \tag{4.109}$$

With all these formulas it is possible to study how PBH clusters would behave in terms of survival and evaporation times. Plots with the different possible PBH variables (4.100) can be extracted from the above formulas for both infinitesimal (4.109) and total (4.106) survival times probabilities. Their results are shown in Figure 4.14 and 4.15.

It is clear that for most situations, evaporation does not play an important role, as the halos get incorporated by larger ones before they have time to evaporate. In many cases, the evaporation times' lines are not shown, since it would be later than $z \sim 10$. The only case where evaporation is relevant is shown in Figure 4.14c and 4.15c for $f_{PBH} = 0.1$ and a cluster of 10 PBHs. In this scenario, it can be expected that some such halos evaporate since the evaporation time sets when $\sim 40\%$ still has not been incorporated.

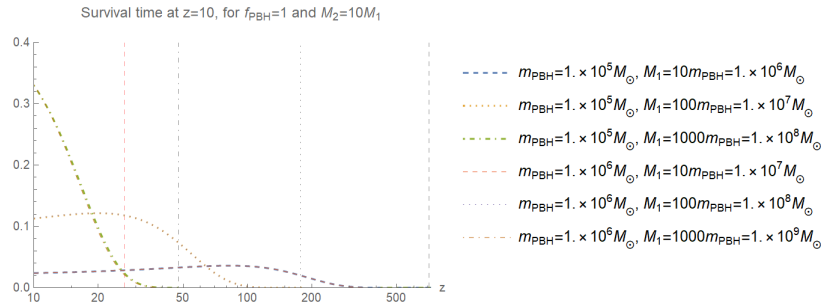

(a)

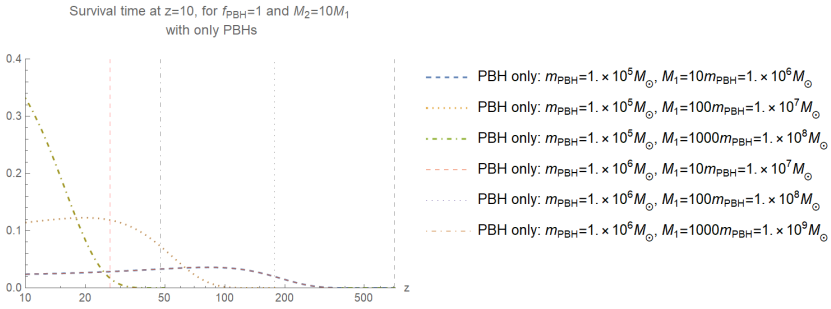

(b)

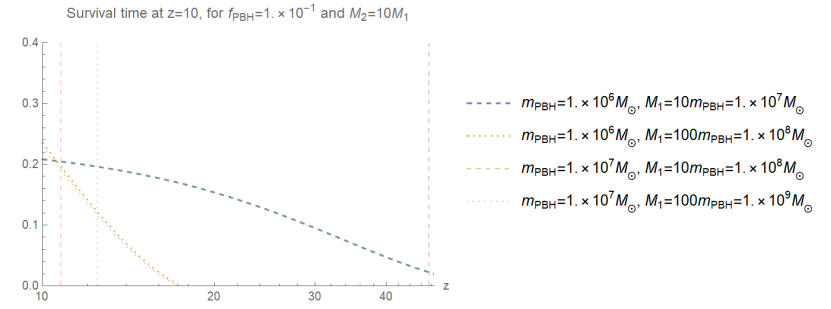

(c)

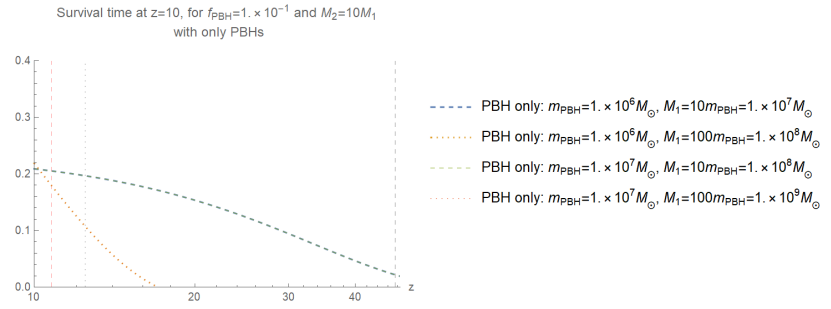

(d)

Figure 4.14: Incorporation probability into a 10 times larger halo over different redshifts, for initial PBH clusters. The plots show the cases with (first and third) and without (second and fourth) adiabatic component of the power spectrum. The vertical black lines indicates the formation time of the PBH halos, calculated with (4.82), while the red ones indicate the evaporation time, for their respective scenario, indicated by the shape of the curves.

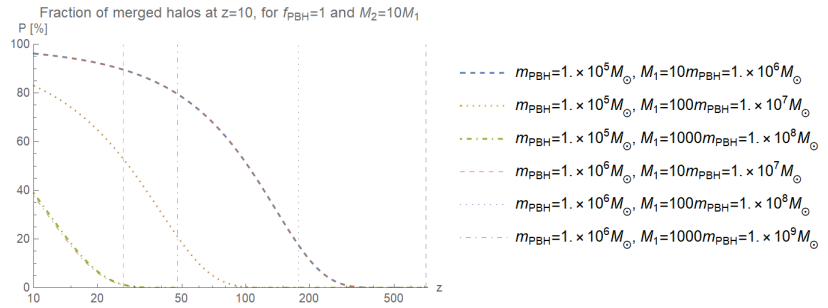

(a)

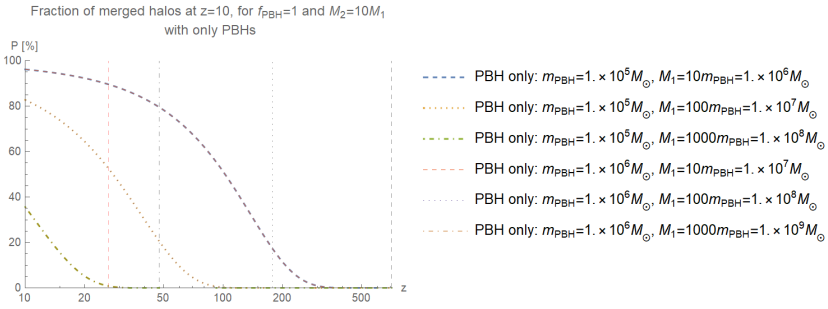

(b)

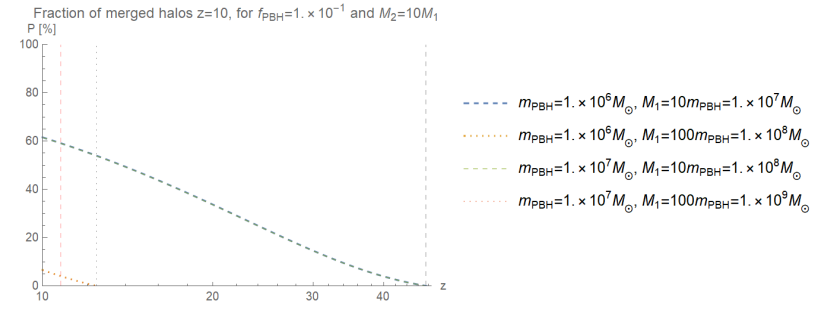

(c)

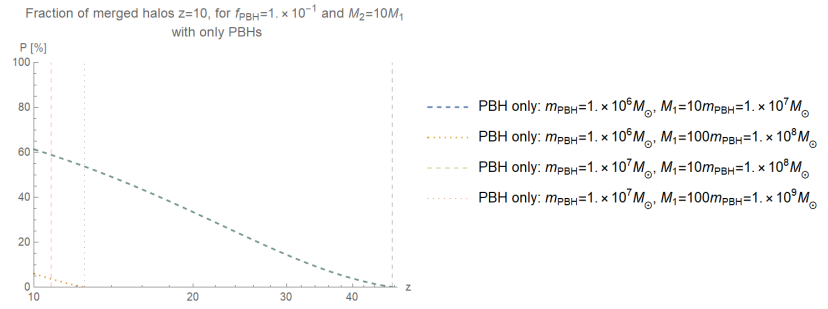

(d)

Figure 4.15: Percentage inclusion in a 10 times larger halo one, for initial PBH clusters. The plots show the cases with (first and third) and without (second and fourth) adiabatic component of the power spectrum. The vertical black lines indicate the formation time of the PBH halos, calculated with (4.82), while the red ones indicate the evaporation time, for their respective scenario indicated by the shape of the curves.

4.5 Discussion and constraints for PBH clusters evolution

The objective of this chapter is to better comprehend the type and effects of PBH clustering on galaxy formation. From section 4.1, it was understood that the discrete particle approach for PBH distribution is not a good model for this task. The results were in fact far from the ones in chapter 3 for similar scenarios, and are unsatisfactory for situations where clustering is expected.

In section 4.2, the size of clusters was studied considering only the presence of PBHs, leading to the conclusion that this effect becomes relevant only for a large PBH portion of DM $f_{PBH} \gtrsim 0.001$, from Figure 4.5, which is out of the values considered before. Although including other components, such as PDM and baryons could modify the results slightly, this constraint could become even stricter considering a relevant cluster of at least 10 PBHs (4.85), which leads to $f_{PBH} \gtrsim 0.01$. Therefore the validity of not considering the clustering effect in chapter 3 is confirmed.

The most interesting results come from section 4.4. With the formula of the formation time of cluster (4.82) it is already possible to draw some conclusions on the PBH portion of DM and the monochromatic mass required for clustering effects. In fact with (4.85) and (4.87) it is possible to compute the limits on PBH variables to obtain clusters of the mass of interest $\sim 10^{10} M_\odot$. The first equation tells that $f_{PBH} \gtrsim 0.01$ is the lower limit for a PBH halo to have formed by $z \sim 10$. The second outcome leads to the finding that PBHs can have masses as low as $m_{PBH} \gtrsim 10^6 M_\odot$, in the case PBHs take a large fraction of DM $f_{PBH} \sim 1$. However, these constraints do not take into consideration any accretion or evaporation effects, which could lead the halos to become too massive or fade away. For this reason, in the following part of the section, these phenomena were taken into account, and a more detailed analysis was performed to find the PBH variables that lead to the halo mass of interest. These results are taken from (4.100).

$$\begin{aligned} f_{PBH} m_{PBH} &\gtrsim 10^5 M_\odot \\ m_{PBH} &\gtrsim 10^5 M_\odot \\ f_{PBH} &\gtrsim 0.01 \\ M_1 &\gtrsim 10^6 M_\odot \end{aligned} \tag{4.110}$$

where M_1 is the starting bare PBH cluster mass that grows to the mass of interest around $z \sim 10$ with accretion. It must be noted that only the lower constraints are reported here from (4.100). This is due to the fact that if SFE is small, the mass of the formed halo should be much larger than the mass of interest used above $\sim 10^{10} M_\odot$. Clearly, larger PBH mass would increase both $f_{PBH} m_{PBH}$ and M_1, leading to larger halos as $z \sim 10$. However, as SFE is not defined, the most stringent constraint from above still comes from the limited observations of super massive BHs $\gtrsim 10^{11} M_\odot$ [34].

To conclude the section, survival times by incorporation and evaporation where covered. It was found that all halos tend to grow or be incorporated in larger clusters long before evaporation for $f_{PBH} = 1$. However, the smaller the PBH fraction of DM, the more relevant evaporation becomes. In fact, Figure 4.15 shows that

already for some PBH clusters (made of 100 PBHs) with $f_{PBH} = 0.1$ the evaporation effects are relevant before $z \sim 10$ when not all halos have grown significantly yet. This means that although accretion and merger appear to still be prevailing on evaporation, this last phenomenon becomes more relevant as f_{PBH} gets smaller, and should therefore be taken into account.

The new limits found, do however conflict with the constraints coming from observation [2], shown in Figure 3.5. From reference [2], it is clear that for a PBH range of masses $m_{PBH} \approx 10^5 - 10^9 M_\odot$ there are strict constraints on f_{PBH} coming from X-rays observation of accretion onto PBHs [16] [17], dynamical friction of PBHs into galaxies [33] and PBHs millilensing [35]. In fact, the highest PBH fraction of DM allowed would be $f_{PBH} \lesssim 0.001$. Although these constraints seem to rule out the newly found combinations of PBH variables, many of these limits are dependent on the models used to calculate them. In general, PBHs are considered to be randomly distributed, even at the time of the observation. The addition of clusters could drastically modify these constraints. By considering clustering, on one hand, less lonely PBHs than the ones formed would be found in the universe, while on the other, PBH clusters would have very different effects of accretion, dynamical friction and gravitational lensing than the single ones, modifying their signals. For this reason, constraints coming from observations should be reevaluated for the case of PBH clusters, to better understand if large PBH fractions of DM $f_{PBH} \gtrsim 0.01$ could be allowed for the mass range $m_{PBH} \approx 10^5 - 10^{10} M_\odot$. While these constraints are expected to drop drastically, only a focused study on the matter could clarify it.

5 Conclusions

With this work, different possibilities on how the presence of initially Poisson distributed PBHs could have led to accelerating galaxy formation and explain JWST observation of a population of these massive star systems $M_* \sim 10^{10} M_\odot$ in the early universe $z \sim 10$ were investigated [5]. While chapter 3 studied the stellar mass density depending on PBH fraction of DM f_{PBH} and monochromatic mass m_{PBH}, in chapter 4 the focus was on how these galaxies could have formed through PBH clustering.

The result that arises from both analyses is a lower constraint for the combination of PBH variables $f_{PBH} m_{PBH} \gtrsim 10^5 M_\odot$, which however should be moved up if lower SFE values are considered. Other than that, the two chapters lead to very different conclusions.

In chapter 3, lonely PBHs were considered for the results obtained. The replication of the outcomes of article [9] were quite accurate, moreover, the correctness of the analysis of not considering clustering was confirmed. The limits of this study are dictated by the measured constraints on PBHs [2], which are quite stringent for randomly distributed PBHs of mass $m_{PBH} \gtrsim 10^5 M_\odot$ (see Figure 3.5). In this scenario, the smallest PBH mass admitted is $m \gtrsim 10^9 M_\odot$, which is already very large and should increase as soon as SFE falls. Despite this possibility is not to discard, it has strong limitations. In fact, BHs masses in general are confined from above because of the very poor number of observations of super massive BH $\gtrsim 10^{11} M_\odot$ [34]. Thus considering PBH constraints [2], the possibilities to explain JWST measurements with this model have strict boundaries.

$$\boxed{f_{PBH} m_{PBH} \gtrsim 10^5 M_\odot} \tag{5.1}$$

$$\begin{aligned} m_{PBH} &\approx 10^9 - 10^{10} M_\odot \\ f_{PBH} &\lesssim 10^{-3} \\ \varepsilon &\gtrsim 0.1 \end{aligned} \tag{5.2}$$

The unknown SFE represents an additional aspect that limits the precision of the results and could even lead to ruling out this possibility if too small $\varepsilon \lesssim 0.01$.

In chapter 4, the constraints on PBH variables applied in chapter 3 [2] were not taken into account, as calculated considering lonely PBHs. It is in fact expected that these constraints drop drastically with the clustering effect. Large fractions of DM composed of PBH were studied, for which the PBH clustering should play an important role in the halo formation.

$$f_{PBH} \gtrsim 0.01 \tag{5.3}$$

Particular attention was paid to PBH clusters that increase their accretion rate drastically around $z \sim 10$, to form $\gtrsim 10^{10} M_\odot$ halos. This led to finding a much

lower constraint for PBH masses $m_{PBH} \gtrsim 10^5 M_\odot$ that could explain the formation of JWST observed galaxies. This means that if PBHs cluster, their possible mass has a wider range, hence SFE is much less confined from below, increasing the probability of this model being successful.

$$\boxed{m_{PBH} \approx 10^5 - 10^{10} M_\odot} \tag{5.4}$$

Consequently, PBH clusters growing into the halos of interest should have a minimum mass of $M_1 \approx 10^6 M_\odot$. It must however be mentioned that the smaller the PBH fraction of DM, the stronger the effect of the evaporation on PBH clusters, which cannot be neglected for $f_{PBH} \lesssim 0.1$.

On a general note, very loose approximations were used throughout the project. Thus important information about the results is their order of magnitude. Additionally, PBH mass distribution was considered monochromatic. An extended PBH mass function could be used to have better results.

The main conclusion from these analyses is that PBH clustering has more probabilities to explain JWST observation than the randomly distributed PBHs, whose results are quite extreme. This is due to the fact that, for the clustering case, PBH masses are much less restricted and consequently also SFE. Therefore if PBHs are discovered to have a mass smaller than $10^9 M_\odot$, or SFE are found to be lower than 0.1[1], only the clustering model would remain a plausible theory. On the other hand, f_{PBH} can be capped from above if other DM constituents are proven to exist, restricting the PBH clustering possibility.

This outcome has a strong limit though, which is represented by the constraints coming from observations. In fact, the possibility of clustering is based on the fall of these constraints at large f_{PBH}. However, this cannot be given for granted. Although these limits are expected to weaken with the clustering effect, their new values could not be high enough to allow PBH clustering to take place. Thus a new study to reevaluate the constraints on the PBH fraction of DM in the mass range $m_{PBH} \approx 10^5 - 10^{10} M_\odot$ is required to support or rule out PBH clustering possibility. Nevertheless, a similar study could be very complex as the dynamics inside of a cluster are difficult to predict.

Furthermore, other possibilities that could explain JWST measurements through PBHs existence could be considered. For example, the addition of a cluster component in the initial PBH distribution could drastically boost galaxy formation (see Appendix E) and it is worth exploring this scenario further.

[1] Although SFE is still unknown, values of unity are not expected to be reached as considered extremely high.

References

[1] Bernard Carr and Florian Kühnel. Primordial Black Holes as Dark Matter: Recent Developments. *Annual Review of Nuclear and Particle Science*, 70(1):355–394, 2020.

[2] Misao Sasaki, Teruaki Suyama, Takahiro Tanaka, and Shuichiro Yokoyama. Primordial black holes—perspectives in gravitational wave astronomy. *Classical and Quantum Gravity*, 35(6):063001, feb 2018.

[3] Hakim Atek, Marko Shuntov, Lukas J Furtak, Johan Richard, Jean-Paul Kneib, Guillaume Mahler, Adi Zitrin, H J McCracken, Sté phane Charlot, Jacopo Chevallard, and Iryna Chemerynska. Revealing galaxy candidates out to $z \sim 16$ with JWST observations of the lensing cluster SMACS0723. *Monthly Notices of the Royal Astronomical Society*, 519(1):1201–1220, dec 2022.

[4] Yuichi Harikane, Masami Ouchi, Masamune Oguri, Yoshiaki Ono, Kimihiko Nakajima, Yuki Isobe, Hiroya Umeda, Ken Mawatari, and Yechi Zhang. A Comprehensive Study of Galaxies at z $\sim$ 9–16 Found in the Early JWST Data: Ultraviolet Luminosity Functions and Cosmic Star Formation History at the Pre-reionization Epoch. *The Astrophysical Journal Supplement Series*, 265(1):5, feb 2023.

[5] Ivo Labbé, Pieter van Dokkum, Erica Nelson, Rachel Bezanson, Katherine A Suess, Joel Leja, Gabriel Brammer, Katherine Whitaker, Elijah Mathews, Mauro Stefanon, and Bingjie Wang. A population of red candidate massive galaxies 600 Myr after the Big Bang. *Nature*, February 2023.

[6] Michael Boylan-Kolchin. Stress Testing ΛCDM with High-redshift Galaxy Candidates, 2022.

[7] Kohei Inayoshi, Yuichi Harikane, Akio K. Inoue, Wenxiu Li, and Luis C. Ho. A Lower Bound of Star Formation Activity in Ultra-high-redshift Galaxies Detected with JWST: Implications for Stellar Populations and Radiation Sources. *The Astrophysical Journal Letters*, 938(2):L10, oct 2022.

[8] Christopher C Lovell, Ian Harrison, Yuichi Harikane, Sandro Tacchella, and Stephen M Wilkins. Extreme value statistics of the halo and stellar mass distributions at high redshift: are *JWST* results in tension with ΛCDM? 518(2):2511–2520, nov 2022.

[9] Boyuan Liu and Volker Bromm. Accelerating Early Massive Galaxy Formation with Primordial Black Holes. *The Astrophysical Journal Letters*, 937(2):L30, sep 2022.

[10] Bernard Carr and Joseph Silk. Primordial black holes as generators of cosmic structures. *Monthly Notices of the Royal Astronomical Society*, 478(3):3756–3775, 05 2018.

[11] Edward W. Kolb and Igor I. Tkachev. Large-amplitude isothermal fluctuations and high-density dark-matter clumps. *Physical Review D*, 50(2):769–773, jul 1994.

[12] J. A. Peacock. *Cosmological Physics*. Cambridge University Press, 1998.

[13] V Sahni. Approximation methods for non-linear gravitational clustering. *Physics Reports*, 262(1-2):1–135, nov 1995.

[14] Derek Inman and Yacine Ali-Haïmoud. Early structure formation in primordial black hole cosmologies. *Phys. Rev. D*, 100:083528, Oct 2019.

[15] Luc Voruz, Julien Lesgourgues, and Thomas Tram. The effective gravitational decoupling between dark matter and the CMB. *Journal of Cosmology and Astroparticle Physics*, 2014(03):004–004, mar 2014.

[16] Martin Bucher, Kavilan Moodley, and Neil Turok. General primordial cosmic perturbation. *Phys. Rev. D*, 62:083508, Sep 2000.

[17] J. Chluba and D. Grin. CMB spectral distortions from small-scale isocurvature fluctuations. *Monthly Notices of the Royal Astronomical Society*, 434(2):1619–1635, 07 2013.

[18] S. Naoz and R. Barkana. The formation and gas content of high-redshift galaxies and minihaloes. *Monthly Notices of the Royal Astronomical Society*, 377(2):667–676, 04 2007.

[19] Antonio Riotto. Lecture Notes on Cosmology, 2022.

[20] Scott Dodelson and Fabian Schmidt. In Scott Dodelson and Fabian Schmidt, editors, *Modern Cosmology (Second Edition)*, pages 195–229. Academic Press, second edition edition, 2021.

[21] Michele Maggiore. *Gravitational Waves: Volume 2: Astrophysics and Cosmology*. Oxford University Press, 03 2018.

[22] Planck Collaboration, Aghanim, N., and Akrami, Y. et al. Planck 2018 results - VI. Cosmological parameters. *A&A*, 641:A6, 2020.

[23] James M. Bardeen, J. R. Bond, Nick Kaiser, and A. S. Szalay. The Statistics of Peaks of Gaussian Random Fields. *Astrophys. J.*, 304:15–61, 1986.

[24] A. J. S. Hamilton. Formulae for growth factors in expanding universes containing matter and a cosmological constant. *Monthly Notices of the Royal Astronomical Society*, 322(2):419–425, apr 2001.

[25] Boyuan Liu, Saiyang Zhang, and Volker Bromm. Effects of stellar-mass primordial black holes on first star formation. *Monthly Notices of the Royal Astronomical Society*, 514(2):2376–2396, August 2022.

[26] N. Afshordi, P. McDonald, and D. N. Spergel. Primordial black holes as dark matter: The power spectrum and evaporation of early structures. *The Astrophysical Journal*, 594(2):L71–L74, aug 2003.

[27] William H. Press and Paul Schechter. Formation of Galaxies and Clusters of Galaxies by Self-Similar Gravitational Condensation. *The Astrophysical Journal*, 187:425–438, February 1974.

[28] Andrew R. Zentner. The Excursion Set Theory of Halo Mass Functions, Halo Clustering, and Halo Growth. *International Journal of Modern Physics D*, 16(05):763–815, may 2007.

[29] R. K. Sheth, H. J. Mo, and G. Tormen. Ellipsoidal collapse and an improved model for the number and spatial distribution of dark matter haloes. *Monthly Notices of the Royal Astronomical Society*, 323(1):1–12, may 2001.

[30] Ravi K. Sheth and Giuseppe Tormen. Large-scale bias and the peak background split. *Monthly Notices of the Royal Astronomical Society*, 308(1):119–126, sep 1999.

[31] Daniele Gaggero, Gianfranco Bertone, Francesca Calore, Riley M. T. Connors, Mark Lovell, Sera Markoff, and Emma Storm. Searching for Primordial Black Holes in the Radio and X-Ray Sky. *Physical Review Letters*, 118(24), jun 2017.

[32] Yoshiyuki Inoue and Alexander Kusenko. New X-ray bound on density of primordial black holes. *Journal of Cosmology and Astroparticle Physics*, 2017(10):034, October 2017.

[33] B. J. Carr and M. Sakellariadou. Dynamical Constraints on Dark Matter in Compact Objects. *The Astrophysical Journal*, 516(1):195, may 1999.

[34] Brockamp, M., Baumgardt, H., Britzen, S., and Zensus, A. Unveiling Gargantua: A new search strategy for the most massive central cluster black holes. *A&A*, 585:A153, 2016.

[35] P. N. Wilkinson, D. R. Henstock, I. W. A. Browne, A. G. Polatidis, P. Augusto, A. C. S. Readhead, T. J. Pearson, W. Xu, G. B. Taylor, and R. C. Vermeulen. Limits on the Cosmological Abundance of Supermassive Compact Objects from a Search for Multiple Imaging in Compact Radio Sources. *Physical Review Letters*, 86(4):584–587, jan 2001.

[36] D. P. Quinn, M. I. Wilkinson, M. J. Irwin, J. Marshall, A. Koch, and V. Belokurov. On the reported death of the MACHO era. *Monthly Notices of the Royal Astronomical Society: Letters*, 396(1):L11–L15, jun 2009.

[37] Yacine Ali-Haïmoud. Correlation Function of High-Threshold Regions and Application to the Initial Small-Scale Clustering of Primordial Black Holes. *Physical Review Letters*, 121(8), aug 2018.

[38] Azadeh Moradinezhad Dizgah, Gabriele Franciolini, and Antonio Riotto. Primordial black holes from broad spectra: abundance and clustering. *Journal of Cosmology and Astroparticle Physics*, 2019(11):001–001, nov 2019.

[39] Vincent Desjacques and A. Riotto. Spatial clustering of primordial black holes. *Physical Review D*, 98(12), dec 2018.

[40] V. De Luca, V. Desjacques, G. Franciolini, and A. Riotto. The clustering evolution of primordial black holes. *Journal of Cosmology and Astroparticle Physics*, 2020(11):028–028, nov 2020.

[41] Cedric Lacey and Shaun Cole. Merger rates in hierarchical models of galaxy formation. *Monthly Notices of the Royal Astronomical Society*, 262(3):627–649, June 1993.

[42] Richard I. Epstein. Proto-galactic perturbations. *Monthly Notices of the Royal Astronomical Society*, 205(1):207–229, 11 1983.

[43] W. C. Saslaw and A. J. S. Hamilton. Thermodynamics and galaxy clustering - Nonlinear theory of high order correlations. *The Astrophysical Journal*, 276:13–25, January 1984.

[44] P. J. E. Peebles. *Principles of Physical Cosmology*. 1993.

[45] T. Padmanabhan. *Structure Formation in the Universe*. 1993.

[46] M. Davis and P. J. E. Peebles. On the integration of the BBGKY equations for the development of strongly nonlinear clustering in an expanding universe. *The Astrophysical Journal*, 34:425–450, August 1977.

[47] F. Bernardeau, S. Colombi, E. Gaztañaga, and R. Scoccimarro. Large-scale structure of the Universe and cosmological perturbation theory. *Physics Reports*, 367(1-3):1–248, sep 2002.

[48] Gert Hütsi, Martti Raidal, and Hardi Veermäe. Small-scale structure of primordial black hole dark matter and its implications for accretion. *Physical Review D*, 100(8), oct 2019.

[49] J. R. Bond, S. Cole, G. Efstathiou, and N. Kaiser. Excursion Set Mass Functions for Hierarchical Gaussian Fluctuations. *Astrophys. J.*, 379:440, October 1991.

[50] James Binney and Scott Tremaine. *Galactic Dynamics: Second Edition*. 2008.

[51] Valerio De Luca, Gabriele Franciolini, Antonio Riotto, and Hardi Veermäe. Ruling Out Initially Clustered Primordial Black Holes as Dark Matter. *Physical Review Letters*, 129(19), nov 2022.

A Constants and formulae

Parameter	Symbol	Formula
Density parameter	Ω	$\frac{\rho}{\rho_c} = \frac{8\pi G\rho}{3H_0^2} = \Omega_m + \Omega_r + \Omega_\Lambda$
Dimensionless Hubble parameter	h	$\frac{H_0}{100}\,\frac{\mathrm{s}}{\mathrm{km}}\mathrm{Mpc}$
Inverse comoving horizon at equality	k_{eq}	$a_{eq}H_{eq}$
Scale factor	a	$\frac{a}{a_0} = \frac{1}{1+z}$

Table A.1: Table of formulae

Constant	Symbol	Value	Reference
Speed of light	c	$2.99792458 \cdot 10^8\ \frac{\mathrm{m}}{\mathrm{s}}$	
Gravitational constant	G	$6.6743015 \cdot 10^{-11}\ \frac{\mathrm{Nm}^2}{\mathrm{kg}^2}$	
Solar mass	$M_\odot$	$1.98847 \cdot 10^{30}\,\mathrm{kg}$	
Hubble constant at present time	H_0	$67.37 \pm 0.54\ \frac{\mathrm{km}}{\mathrm{s}}\mathrm{Mpc}^{-1}$	[22][1]
Dimensionless Hubble parameter	h	0.6736 ± 0.0054	Table A.1
Matter abundance at present time	Ω_m^0	0.3153 ± 0.0073	[22][1]
Baryon abundance at present time	Ω_b^0	0.0493 ± 0.0009	[22][1]
Cosmological abundance at present time	Ω_Λ^0	0.6847 ± 0.0073	[22][1]
Curvature abundance at present time	Ω_K^0	$-0.011^{+0.013}_{-0.012}$	[22][1]
Inverse comoving horizon at RD-MD equality	k_{eq}	$0.010398 \pm 0.000094\,\mathrm{Mpc}^{-1}$	[22][1]
Redshift at RD-MD equality	z_{eq}	3402 ± 26	[22][1]
Scale factor at RD-MD equality	a_{eq}	$(2.94 \pm 0.02)10^{-4}$	Table A.1
Pivot scale	k_p	$0.05\,\mathrm{Mpc}^{-1}$	[20] [21]
Primordial power spectrum amplitude	$\mathcal{A}_\mathcal{R}$	$(2.100 \pm 0.030)10^{-9}$	[22][1]
Scalar spectral index	n_s	0.9649 ± 0.0042	[22][1]
Age of the universe	t_0	$13.8 \cdot 10^9\,\mathrm{yr}$	[22]

Table A.2: Table of constants.

[1]Quantities measured for ΛCDM model, from Planck CMB power spectrum, considering TT,TE,EE+lowE+lensing observation. The values come from Table 2 of [22].

B Acronyms

Acronym	Meaning
BH	Black Holes
CDM	Cold Dark Matter
CMB	Cosmic Microwave Background
DE	Dark Energy
DM	Dark Matter
HMF	Halo Mass Function
JWST	James Webb Space Telescope
L	Linear
ΛCDM	Lambda-CDM
MD	Matter-Dominated
NL	Non-Linear
PBH	Primordial Black Holes
PDM	Weakly interacting massive Particle Dark Matter
PS	Press-Schechter
QL	Quasi-Linear
RD	Radiation-Dominated
SFE	Star Formation Efficiency

Table B.1: Table of Acronyms

C Cosmological properties

In this appendix, the fundamental properties of cosmology are recalled, but also their main implications useful for this report, as well as some important notation. In addition to that, it must be mentioned that throughout the whole report, natural units apply.

C.1 Coordinates formalism

As formalism in cosmology can sometimes become a little bit confusing and contradictory throughout different sources, here is a brief summary of the notation used in this report.

C.1.1 Comoving coordinates

Physical, observable, or also called *proper distances* can be split into a scale factor $a(t)$, which represents the expansion of the universe, and an epoch independent component called *comoving distance*. This report makes use predominantly of the comoving coordinates, however proper distances can occasionally be used. Whenever the latter ones come into play, and their distinction is relevant, they will be addressed with a tilde: $\tilde{\mathbf{x}}$ are the proper vectors and $\mathbf{x}$ the comoving ones. The difference in coordinates can also be applied to other variables, such as wavenumber or energy density, as shown below.

$$\mathbf{x} = \frac{\tilde{\mathbf{x}}}{a(t)} \qquad \mathbf{k} = a(t)\tilde{\mathbf{k}} \qquad \rho = a(t)^3\tilde{\rho} \tag{C.1}$$

It must be noted that for matter overdensity, comoving and proper values are the same

$$\delta = \frac{\delta\tilde{\rho}_m}{\bar{\tilde{\rho}}_m} = \frac{\delta\rho_m}{\bar{\rho}_m} \tag{C.2}$$

since $\delta\tilde{\rho}_m$ behave exactly the same as $\tilde{\rho}_m$ under coordinates transformation.

C.1.2 Conformal time

In addition to that, another important variable in the study of cosmology is the *conformal time* η, which can substitute the *proper time* t. This new coordinate is represented through the comoving *particle horizon* l_p. This horizon is defined as the maximum distance between two objects so that they have been in causal contact within the age of the universe, hence it represents the observable universe. On the other hand, conformal time is the amount of time a photon would take to travel from a specific location to the furthest visible point in space, or in other words to the particle horizon. Since the speed of light is c, the conformal time and particle horizon can be linked with it.

$$l_p = c\eta \tag{C.3}$$

This means that in natural units, the two variables match, and can be written as follows.

$$\eta = \int_0^t \frac{dt'}{a(t)} \qquad \text{or} \qquad d\eta = \frac{dt}{a(t)} \tag{C.4}$$

C.1.3 Scale factor

A main element of cosmology is the *scale factor* $a(t)$. Its importance comes as a consequence of the wide use of comoving coordinates and conformal time in cosmology, making its appearance in both (C.1) and (C.4). It must therefore be noted that the scale factor $a(t)$ is unit-less and only time dependent. In fact, it is sometimes used as time reference instead of the time $a = a(t)$. In general, although most variables have a time dependence, this is often not explicitly written, as thought to be implicit (e.g. $a(t) = a$, $\tilde{\mathbf{x}}(t) = \tilde{\mathbf{x}}$, ...). It may happen that this dependence is shown only when relevant for calculations. It also relates to the redshift.

$$\frac{a}{a_0} = \frac{1+z_0}{1+z} \tag{C.5}$$

On a side note, the scale factor at present time is $a(t_0) = 1$ and the redshift $z_0 = 0$.

C.1.4 Coordinates derivation

Another element useful for the report, that sometimes can not be as straightforward as it seems at first look is the change between different derivation coordinates, or even the derivation itself. This subsection has the objective to provide a brief summary of the properties required for the report, their formalism and some small reminder to not fall into foolish mistakes.

While derivatives over time and space can be rewritten following the traditional properties,

$$\frac{d}{d\mathbf{x}} = \frac{d\tilde{\mathbf{x}}}{d\mathbf{x}}\frac{d}{d\tilde{\mathbf{x}}} = a\frac{d}{d\tilde{\mathbf{x}}} \qquad \frac{d}{d\eta} = \frac{dt}{d\eta}\frac{d}{dt} = a\frac{d}{dt} \tag{C.6}$$

the derivation over proper and comoving time is written differently.

$$\frac{d}{d\eta}a(\eta) = a'(\eta) \qquad \frac{d}{dt}a(t) = \dot{a}(t) \tag{C.7}$$

The Hubble parameter is defined with the proper time coordinates.

$$H = \frac{\dot{a}}{a} \neq \frac{a'}{a} \tag{C.8}$$

As derivation is the argument of interest in this subsection, it is worth mentioning the velocities. The definitions of proper and comoving velocities, together with other useful properties are shown below.

$$\mathbf{v} = \frac{d\mathbf{x}}{d\eta} = \tilde{\mathbf{v}} - H\tilde{\mathbf{x}} \qquad \tilde{\mathbf{v}} = \frac{d\tilde{\mathbf{x}}}{dt} = \mathbf{v} + \frac{a'}{a}\mathbf{x} \tag{C.9}$$

$$\frac{d\mathbf{x}}{dt} = \frac{\tilde{\mathbf{v}}}{a} - \frac{H}{a}\tilde{\mathbf{x}} = \frac{\mathbf{v}}{a} \qquad \frac{d}{d\mathbf{v}} = \frac{d\tilde{\mathbf{v}}}{d\mathbf{v}}\frac{d}{d\tilde{\mathbf{v}}} = \frac{d}{d\tilde{\mathbf{v}}} \tag{C.10}$$

C.2 Friedmann equations

As they represent the main element for the description of the dynamics of the universe in the standard model, *Friedmann equations* need a brief introduction and discussion in the context of this report. Without going into details on their derivation, the *Einstein equations*, together with the fundamental assumptions that the universe is homogeneous and isotropic, lead to a set of two equations.

$$\frac{\dot{a}^2}{a^2} + \frac{K}{a^2} - \frac{\Lambda}{3} = \frac{8\pi G}{3}\tilde{\rho} \qquad \text{and} \qquad 2\frac{\ddot{a}}{a} + \frac{\dot{a}^2}{a^2} + \frac{K}{a^2} - \Lambda = -8\pi G\tilde{p} \tag{C.11}$$

where the three unknowns are the scale factor a, pressure $\tilde{p}$ and energy density $\tilde{\rho}$. In addition to that, K (-1 open, 0 flat, $+1$ closed) is the curvature and Λ is the cosmological constant.

The *equation of state* complements Friedmann equations, by providing the third equation to the three unknown variables.

$$\tilde{p} = \sum w\tilde{\rho}, \qquad \begin{cases} w = 0, & \text{non-relativistic matter} \\ w = \frac{1}{3}, & \text{relativistic matter} \\ w = -1, & \text{dark energy} \end{cases} \tag{C.12}$$

These three equations can often come in different forms, however, they provide a complete description of the expansion of the universe in the ΛCDM model, and can be used to detect many useful properties. Two scenarios that are of main importance in this report, but also in cosmology in general, are the radiation and matter dominated epochs. In the next subsections, these two situations are discussed and their properties relevant to this report are calculated.

C.2.1 Matter dominated universe

In a flat MD universe: $K = 0$, $\Lambda = 0$, $\tilde{\rho} = \tilde{\bar{\rho}}_m$ and with the equation of state (C.12) $\tilde{p}_m = 0$. Consequently Friedmann equations (C.11) lead to

$$\tilde{\bar{\rho}}_m = \frac{3H^2}{8\pi G}, \qquad 2\frac{\ddot{a}}{a} + H^2 = 0 \tag{C.13}$$

where the Hubble factor is $H = \frac{\dot{a}}{a}$. The second equation can be solved to show the time dependence of the scale factor in this flat MD universe.

$$a = a_0\left(\frac{t}{t_0}\right)^{\frac{2}{3}} \qquad \Rightarrow \qquad H(t) = \frac{2}{3t} \tag{C.14}$$

From this result, the first equation of (C.13) can be used to compute the background matter energy density explicitly, but also to find its dependence on the scale factor.

$$\tilde{\bar{\rho}}_m = \frac{1}{6\pi G}\frac{1}{t^2} \qquad \text{and} \qquad \tilde{\bar{\rho}}_m \propto \frac{1}{a^3} \tag{C.15}$$

Following these results the important relation between overdensity and scale factor can be found. In a MD universe, the first Friedmann equation (C.11) must be

valid for the background density, but also for the small locally overdense regions, for which the curvature is non-null ($K \neq 0$). This property can be used to find the energy density difference between the perturbed and unperturbed scenarios.

$$H^2 - \frac{8\pi G}{3}\tilde{\bar{\rho}}_m = 0 \tag{C.16}$$

$$H^2 - \frac{8\pi G}{3}\rho_m(\mathbf{x}) = -\frac{K}{a^2} \tag{C.17}$$

$$\Rightarrow \delta\tilde{\rho}_m = \tilde{\rho}_m(\mathbf{x}) - \tilde{\bar{\rho}}_m = \frac{3K}{8\pi G a^2} \propto \frac{1}{a^2} \tag{C.18}$$

Using the background densities dependence on the scale factor (C.15), it is possible to find the relation between overdensity and scale factor in a MD universe.

$$\delta_m(\mathbf{x}) = \frac{\tilde{\rho}_m(\mathbf{x}) - \tilde{\bar{\rho}}_m}{\tilde{\bar{\rho}}_m} \propto a \tag{C.19}$$

Another important property for this report comes from the linear perturbation theory. Without going into details on its origin, the general evolution equation of a linear overdensity can be recalled from [12].

$$\ddot{\delta}_L + 2H\dot{\delta}_L = \delta_L\left(4\pi G\tilde{\rho} - \frac{c_s^2 k^2}{a^2}\right) \tag{C.20}$$

where $c_s^2 = \frac{\partial\tilde{p}}{\partial\tilde{\rho}}$ is the so called speed of sound, while k is the comoving wavevector of the perturbation. In the case of MD universe, the action of pressure is neglected $p = 0$, meaning that also $c_s = 0$. Consequently the overdensity evolution equation gets simplified.

$$\ddot{\delta}_L + 2H\dot{\delta}_L - 4\pi G\tilde{\bar{\rho}}_m\delta_L = 0 \tag{C.21}$$

Using the power law to solve this equation $\delta_L \propto a^n$, and the properties found above (C.14) and (C.15), the result for the linear overdensity is the following.

$$\delta_L \propto a \propto t^{\frac{2}{3}} \tag{C.22}$$

It must be noted that this result is in accordance with (C.19).

C.2.2 Radiation dominated universe

Similarly to the MD case, a flat RD universe has $K = 0$, $\Lambda = 0$, $\tilde{\rho} = \tilde{\bar{\rho}}_r$ and with the equation of state (C.12) $\tilde{p}_r = \frac{\tilde{\bar{\rho}}_r}{3}$. Once again Friedmann equations (C.11) lead to

$$\tilde{\bar{\rho}}_r = \frac{3H^2}{8\pi G}, \qquad 2\frac{\ddot{a}}{a} + H^2 = -8\pi G p_r = -\frac{8\pi G}{3}\tilde{\bar{\rho}}_r \tag{C.23}$$

The two equations can be subtracted one from the other and solved with a power law $a = t^n$ to find the result

$$(2n-1)n = 0 \tag{C.24}$$

which has solutions $n = 0$ and $n = \frac{1}{2}$. However, the first option can be discarded as it represents a static universe, which is not the case. Consequently, this leads to finding the time dependence of the scale and Hubble factor.

$$a = a_0 \left(\frac{t}{t_0}\right)^{\frac{1}{2}} \qquad \Rightarrow \qquad H(t) = \frac{1}{2t} \tag{C.25}$$

Analogously to the MD case, the first equation of (C.23) can be recalled to compute the background radiation energy density explicitly, but also to find its dependence on the scale factor.

$$\tilde{\bar{\rho}}_m = \frac{3}{32\pi G}\frac{1}{t^2} \qquad \text{and} \qquad \tilde{\bar{\rho}}_m \propto \frac{1}{a^4} \tag{C.26}$$

Since the scenario is similar to the MD universe, the same analysis of the previous subsection on the overdensity can be applied, by recalling the difference in the curvature of perturbed and unperturbed regions in the first Friedmann equation (C.11).

$$H^2 - \frac{8\pi G}{3}\tilde{\bar{\rho}}_r = 0 \tag{C.27}$$

$$H^2 - \frac{8\pi G}{3}\rho_r(\mathbf{x}) = -\frac{K}{a^2} \tag{C.28}$$

$$\Rightarrow \delta\tilde{\rho}_r = \tilde{\rho}_r(\mathbf{x}) - \tilde{\bar{\rho}}_r = \frac{3K}{8\pi G a^2} \propto \frac{1}{a^2} \tag{C.29}$$

The difference with MD universe comes from the different scale factor dependence on the background densities (C.26). In fact, once this result is applied, it leads to the solution in the RD universe.

$$\delta_r(\mathbf{x}) = \frac{\tilde{\rho}_r(\mathbf{x}) - \tilde{\bar{\rho}}_r}{\tilde{\bar{\rho}}_r} \propto a^2 \tag{C.30}$$

C.3 Abundances

Abundances in cosmology play an important role, as they indicate fractions of each component: relativistic and non-relativistic matter, dark energy and curvature component. They are defined as follows.

$$\tilde{\Omega}_x = \frac{\tilde{\rho}_x}{\rho_{cr}}, \qquad \rho_{cr} = \frac{3H_0^2}{8\pi G} \tag{C.31}$$

where x is a constituent to be defined and ρ_{cr} is the *critical density*. This represents the total energy density if the universe was completely flat at present time (hence H_0 instead of H), and it is used to define the abundances.

It must be noted that since $a(t_0) = 1$ from subsection C.1.3, and the proper energy density scales with it (C.1), the critical density at present time is the same as the comoving critical density. In fact, this is not only the case of critical density, but it is valid for all densities at present time.

Consequently, also the abundances at present time are equal to the comoving abundances.

$$\Omega_x(t_0) = \frac{\rho_x(t_0)}{\rho_{cr}} = \frac{\tilde{\rho}_x(t_0)}{\rho_{cr}} = \tilde{\Omega}_x(t_0) \tag{C.32}$$

In particular, the comoving matter energy density stays constant during the MD universe. The evolution of the proper matter energy density depends on the scale factor (C.15), which is exactly opposed to the change of coordinates from proper to comoving (C.1). In the last phase of the universe the cosmological constant component does not exceed matter excessively, the universe can be approximated to be dominated by matter until present time[1]. Therefore the matter abundance measured today is expected to be the same going back until radiation-matter equality, at redshift z_{eq}. For this reason, throughout this report the comoving matter abundance will be considered constant for the mentioned period, referring to the comoving matter energy density.

$$\Omega_m = \Omega_m^0 = \tilde{\Omega}_m^0 \tag{C.33}$$

Clearly, also the sub-components abundances of the non-relativistic matter, such as DM or baryons, will stay constant.

An additional interesting property of abundances comes from Friedmann equations, which can be combined to give a relation between the Hubble constant H and the one at present time H_0. Without going into details, the equation reads

$$H^2 = H_0^2 \left[\Omega_\Lambda + \Omega_K \left(\frac{a_0}{a} \right)^2 + \Omega_m \left(\frac{a_0}{a} \right)^3 + \Omega_r \left(\frac{a_0}{a} \right)^4 \right] \tag{C.34}$$

where the four abundances are respectively the ones from dark energy, curvature, matter and radiation.

As a side note, non-relativistic matter is often referred to as only "matter", this does not include radiation. Additionally, non-relativistic energy density could be called simply "energy density" since it represents the main focus of the report.

C.4 Hubble horizon

PBHs are expected to generate when a collapsing perturbation re-enters the comoving *Hubble horizon*. This horizon represents the delimiting sphere around an observer, beyond which the particles move away faster than the speed of light. This means that two objects can communicate only if they are one within the Hubble horizon of the other. For this reason, a perturbation is required to enter the Hubble horizon to be able to collapse. If an object is outside the Hubble horizon of an observer, they cannot communicate anymore but could have communicated in the past. For this reason, Hubble horizon is within the particle horizon, mentioned in subsection C.1.2.

The comoving distance of the Hubble horizon is defined as

$$l_H = \frac{1}{aH} \tag{C.35}$$

and the mass within Hubble volume, at the time of PBH formation, is $M_H^{\frac{1}{2}} \propto l_H$. This mass can be computed, knowing that if PBH ever existed, they would

[1]Cosmological constant and matter equality is approximately at $z \sim 0.5$, since the redshift studied in this report are higher, MD universe is always considered.

have formed approximately in RD universe where the properties found in subsection C.2.2 apply.

$$H = \frac{1}{2t} \propto \frac{1}{a^2} \qquad \Rightarrow \qquad l_H \propto a \tag{C.36}$$

Assuming the Hubble horizon to be spherical, the mass included within it, that will form the PBH is calculated below, making use of the comoving coordinates properties (see subsection C.1.1) and the energy density in RD universe (C.26).

$$M_H = \frac{4}{3}\pi\tilde{\rho}_r \tilde{l}_H^3 = \frac{4}{3}\pi\tilde{\rho}_r a^3 l_H^3 \propto a^2 \propto l_H^2 \tag{C.37}$$

D Power spectrum

In this appendix, a brief introduction to the power spectrum as a mathematical element is reported. The material displayed takes inspiration from chapter 16 of [12] and [28].

The correlation function gives the probability of two objects being found at a certain distance. In cosmology, the two-point autocorrelation function between overdensities is used, which describes the probability of finding two galaxies (objects) separated by a certain distance.

$$\xi(|\mathbf{x}_1 - \mathbf{x}_2|) = \langle \delta(\mathbf{x}_1), \delta(\mathbf{x}_2) \rangle = \frac{1}{V} \int d^3\mathbf{x} \delta(\mathbf{x}) \delta(\mathbf{x} - (\mathbf{x}_1 - \mathbf{x}_2)) \tag{D.1}$$

where V is the volume that represents the cutoff of the integration, which is very large, larger than any scale of interest. It is important to recall that the universe is homogeneous and isotropic, therefore the galaxies (or in this case density perturbations) are scattered independently and uniformly, so that the specific location of the two does not play a role, but only their distance.

This autocorrelation probability can also be described using the *power spectrum* $P(k)$.

$$\xi(|\mathbf{x}_1 - \mathbf{x}_2|) = \frac{1}{(2\pi)^3} \int d^3\mathbf{k} e^{-i\mathbf{k}(\mathbf{x}_1 - \mathbf{x}_2)} P(k) \tag{D.2}$$

This mathematically means that the power spectrum is the Fourier transform of the correlation function. Once again, because of the isotropy of the universe, the power spectrum does not depend on the direction but only on the magnitude of $\mathbf{k}$. In addition to that, the power spectrum also has a temporal dependence, usually characterised by the scale factor a: $P(k, a)$. When a is neglected, it is generally considered the power spectrum at the present epoch.

The correlation function could also be written with the Fourier transform of the density perturbations. This is shown below extensively.

$$\xi(|\mathbf{x}_1 - \mathbf{x}_2|) = \frac{1}{(2\pi)^6} \int d^3\mathbf{k} d^3\mathbf{q} e^{-i\mathbf{k}\mathbf{x}_1} e^{-i\mathbf{q}\mathbf{x}_2} \langle \delta(\mathbf{k}), \delta(\mathbf{q}) \rangle \tag{D.3}$$

$$= \frac{1}{V} \frac{1}{(2\pi)^6} \int d^3\mathbf{x} \int d^3\mathbf{k} d^3\mathbf{q} e^{-i\mathbf{k}\mathbf{x}} e^{-i\mathbf{q}(\mathbf{x} - (\mathbf{x}_1 - \mathbf{x}_2))} \delta(\mathbf{k}) \delta(\mathbf{q}) \tag{D.4}$$

$$= \frac{1}{V} \frac{1}{(2\pi)^3} \int d^3\mathbf{k} d^3\mathbf{q} \delta^3(\mathbf{k} + \mathbf{q}) e^{-i\mathbf{k}(\mathbf{x}_1 - \mathbf{x}_2)} \delta(\mathbf{k}) \delta(\mathbf{q}) \tag{D.5}$$

$$= \frac{1}{V} \frac{1}{(2\pi)^3} \int d^3\mathbf{k} e^{-i\mathbf{k}(\mathbf{x}_1 - \mathbf{x}_2)} |\delta(\mathbf{k})|^2 \tag{D.6}$$

$$= \frac{1}{V} \frac{1}{(2\pi)^3} \int d\ln(k) k^3 \frac{\sin(k|\mathbf{x}_1 - \mathbf{x}_2|)}{k|\mathbf{x}_1 - \mathbf{x}_2|} |\delta(\mathbf{k})|^2 \tag{D.7}$$

where in the third passage the properties of the Dirac delta are applied $\delta^3(\mathbf{k}+\mathbf{q}) = \frac{1}{(2\pi)^3}\int d^3\mathbf{x}e^{-i\mathbf{x}(\mathbf{k}+\mathbf{q})}$, while for the forth one the integration over $\mathbf{q}$ is performed using the property $\delta^*(\mathbf{k}) = \delta(-\mathbf{k})$[1]. The last step is a simple change to spherical coordinates together with the fact that $\mathbf{k}$ can be set to have $\theta_\mathbf{k} = 0$ and $\psi_\mathbf{k} = 0$ so that $\mathbf{k}(\mathbf{x}_1 - \mathbf{x}_2) = k|\mathbf{x}_1 - \mathbf{x}_2|\cos(\theta)$ and the integral

$$\int_0^\pi d\theta \sin(\theta) e^{-i\mathbf{k}(\mathbf{x}_1-\mathbf{x}_2)} = \frac{\sin(k|\mathbf{x}_1 - \mathbf{x}_2|)}{k|\mathbf{x}_1 - \mathbf{x}_2|} \tag{D.8}$$

As a consequence, the power spectrum can be defined in different forms comparing (D.3) and (D.6) to (D.2).

$$\langle\delta(\mathbf{k}), \delta(\mathbf{q})\rangle = (2\pi)^3\delta^3(\mathbf{k}+\mathbf{q})P(k) \qquad \text{or} \qquad \boxed{P(k) = \frac{1}{V}\langle|\delta(\mathbf{k})|^2\rangle} \tag{D.9}$$

where in the last formula, the average over the ensemble of the universe is required since the power spectrum needs to be isotropic, therefore it must not have any preferred direction.

The power spectrum has dimension m^3 since both cutoff volume and overdensities[2] in the Fourier space have $[V] = [\delta(\mathbf{k})] = m^3$. Consequently a dimensionless form of the power spectrum which is widely used, and is defined below defined as follows.

$$\Delta^2(k) = \frac{k^3}{2\pi^2}P(k) \tag{D.10}$$

The amplitude of the power spectrum describes the density contrast contribution to the total correlation probability of structures with characteristic length L. k represents the scale factor $k = \frac{1}{L}$ where L is the characteristic length, or the scale of the overdense region[3]. Since the Fourier transform decomposes a function in sinusoidal waves, the power spectrum represents the waveform of the energy density distribution. The correlation function gives the probability of having two overdense regions at a certain distance based on the superposition of all perturbation waves (when the distance is null there is the certainty of finding an overdense region knowing the first one, since it is the same).

[1] This can be found starting from the fact that $\delta(\mathbf{x})$ is real, consequently its Fourier transform $\delta(\mathbf{k}) = \int d^3\mathbf{x}e^{i\mathbf{k}\mathbf{x}}\delta(\mathbf{x})$ has an imaginary component only at the exponential. Conjugating this function would simply lead to the addition of a minus at the exponential.

[2] As the overdensity $\delta(\mathbf{x})$ are dimensionless, their Fourier transform has dimension m^3 due to the integration over a volume $\delta(\mathbf{k}) = \frac{1}{(2\pi)^3}\int d^3\mathbf{x}e^{-i\mathbf{x}\mathbf{k}}\delta(\mathbf{x})$.

[3] It must be noted, that this is just a normalization and can vary, since k is not in the real space. In fact, $k = \frac{2\pi}{L}$ is also often used, which better represent the wavenumber, however, for simplicity in this report the first normalization is chosen.

E Non-Poisson PBH distribution

As last analysis of the formation of galaxies in the early universe, the possibility that PBHs do not have a pure initial Poisson distribution can be considered, despite this scenario is not suggested by [37] [38]. This appendix has the objective of giving insight of how the stellar mass density could vary when a clustering component is taken into account, by having non-null initial reduced PBH correlation function (4.20). This last study however aims to only produce numerical results, following article [51], and does not include specific insights on the results.

The procedure to calculate the stellar mass density for non-Poisson distributed PBHs is the same as chapter 3 and can be achieved by applying PS on the modified power spectrum. Since the goal of this section is to find an estimation due to the addition of the clustering component into the picture, an initially constant reduced PBH correlation function can be used at small scale $r_{cl} \lesssim 1$ kpc [51]. Specifically, the notation of section 4.2 is recalled.

$$\xi_{PBH}(x, z_*) = \xi_{PBH}\Theta\left(r_{cl} - x\right) = \begin{cases} 0, & x \geq r_{cl} \\ \xi_{PBH}, & x < r_{cl} \end{cases} \tag{E.1}$$

where r_{cl} represents the dimension of the clustering, ξ_{PBH} is a constant, while Θ is the Heaviside step function. The initial correlation function (4.19) thus has an additional term.

$$\langle \delta_{PBH}(\mathbf{x})\delta_{PBH}(\mathbf{0})\rangle = \frac{\delta^3(\mathbf{x})}{\overline{n}_{PBH}} + \xi_{PBH}(x)\Theta\left(r_{cl} - x\right) \tag{E.2}$$

Considering perturbations from PBH isocurvature fluctuations, their initial power spectrum (4.21) is the following.

$$\begin{aligned} \Delta^2_{*,cl}(k) &= \frac{k^3}{2\pi^2}\int d\mathbf{x}^3 e^{i\mathbf{k}\mathbf{x}}\left(\frac{1}{\overline{n}_{PBH}}\delta^3(\mathbf{x}, z_*) + \xi_{PBH}(x, z_*)\right) \\ &= \left(\frac{k}{k_*}\right)^3 + \frac{k^3}{2\pi^2}\int d\mathbf{x}^3 e^{i\mathbf{k}\mathbf{x}}\xi_{PBH}\Theta\left(r_{cl} - x\right) \end{aligned} \tag{E.3}$$

Once integrated this leads to the explicit initial dimensionless isocurvature power spectrum.

$$\Delta^2_{*,cl}(k) = \left[\frac{k^3}{2\pi^2\overline{n}_{PBH}} + \xi_{PBH}\frac{2}{\pi}\left(\sin(r_{cl}k) - r_{cl}k\cos(r_{cl}k)\right)\right] \tag{E.4}$$

where the notation with average PBH number density $\overline{n}_{PBH}$ (4.13) was chosen over the characteristic wavelength k_* (4.28).

The Fourier transform in 3 dimension of the Heaviside step function was found as follows.

$$\begin{aligned}\int d\mathbf{x}^3 e^{i\mathbf{k}\mathbf{x}}\Theta\left(r_{cl}-|\mathbf{x}|\right) &= \int_0^{2\pi}\int_0^{\pi}\int_0^{\infty} d\varphi d\theta dx \sin(\theta)x^2 e^{ixk\cos(\theta)}\Theta\left(r_{cl}-x\right)\\ &= 2\pi\int_0^{\pi}\int_0^{r_{cl}} d\theta dx \sin(\theta)x^2 e^{ixk\cos(\theta)}\\ &= 2\pi\int_0^{r_{cl}} dx\frac{e^{ixk}-e^{-ixk}}{ik}x\\ &= \frac{4\pi}{k}\int_0^{r_{cl}} dx\sin(kx)x\\ &= \frac{4\pi}{k^3}\left(\sin(r_{cl}k)-r_{cl}k\cos(r_{cl}k)\right)\end{aligned} \tag{E.5}$$

where in the first passage spherical coordinates are evaluated along $\mathbf{k}$, therefore θ is the angle between the vectors $\mathbf{x}$ and $\mathbf{k}$. In the fourth passage, the exponential formula for the sine function was used $\sin(x)=\frac{e^{iy}-e^{-iy}}{2i}$, while in the last passage the integration by parts.

This resulting power spectrum is included in the bigger DM picture using (3.33).

$$\Delta^2_{DM}(k,a) = D^2_{ad}(a)\Delta^{0\,2}_{ad}(k) + D^2_{iso}(a)f^2_{PBH}\Delta^{0\,2}_{iso}(k) + D^2_{mix}(a)\Delta^{0\,2}_{ad}(k) \tag{E.6}$$

where the isocurvature power spectrum is the one found above $\Delta^{0\,2}_{iso}(k)=\Delta^2_{*,cl}(k)$. Following PS formalism of section 3.2, only the evolution in the linear regime is relevant for the stellar mass calculation. It follows that the perturbation evolution required is given once again by (4.31).

$$\begin{aligned}\Delta^2_{cl}(k,s) &= D_{iso}(s)f^2_{PBH}\Delta^2_{*,cl}(k)\\ &\approx \left(1+\frac{3\gamma}{2a_-}s\right)^{a_-} f^2_{PBH}\left[\frac{k^3}{2\pi^2\overline{n}_{PBH}}+\xi_{PBH}\frac{2}{\pi}\left(\sin(r_{cl}k)-r_{cl}k\cos(r_{cl}k)\right)\right]\end{aligned} \tag{E.7}$$

where $s=\frac{a}{a_{eq}}$. Using the same argument of subsection 3.1.3, and neglecting the mixing term leads to finding the total power spectrum.

$$\Delta^2_{np}(k,a) = \Delta^2_{ad}(k,a)+\Delta^2_{cl}(k,a) \tag{E.8}$$

or

$$P_{np}(k,a) = P_{ad}(k,a)+P_{cl}(k,a) \tag{E.9}$$

where the new power spectrum Δ^2_{np} (P_{np})[1] includes the clustering component and is different from Δ^2 (P) of chapter 3. $P_{ad}(k,a)$ is the adiabatic power spectrum (3.19), while the isocurvature power spectrum Δ^2_{cl} (P_{cl}) is given by PBH presence, hence from the addition of its Poisson noise and clustering component. Without using any approximation, this power spectrum can be used to find the variance (3.49) with a Gaussian window function (3.48).

$$\sigma^2_{np}(R) = \sigma^2(R)+\sigma^2_{cl}(R) = \sigma^2(R)+\int d\ln(k)\Delta^2_{cl}(k,a)|W(k,R)|^2 \tag{E.10}$$

[1]The subscript np stays for non-Poisson initial PBH distribution.

where once again $\sigma^2(R)$ comes from the initially Poisson distribution of PBHs, as in chapter 3. The second component, due to the reduced PBH correlation function, resolves as follows.

$$\begin{aligned}\sigma^2_{cl}(R) &= \int d\ln(k)\Delta^2_{cl}(k,a)|W(k,R)|^2 \\ &= \frac{2}{\pi}\left(1+\frac{3\gamma}{2a_-}s\right)^{a_-} f^2_{PBH}\xi_{PBH}\int d\ln(k)|W(k,R)|^2\left(\sin(r_{cl}k)-r_{cl}k\cos(r_{cl}k)\right) \\ &= \left(1+\frac{3\gamma}{2a_-}s\right)^{a_-} f^2_{PBH}\xi_{PBH}\left(\text{erf}\left(\frac{r_{cl}}{2R}\right)+\frac{r_{cl}}{\sqrt{\pi}R}e^{-\frac{r^2_{cl}}{4R^2}}\right) \end{aligned} \tag{E.11}$$

Plugging this result into the total variance (E.10) the stellar mass density can be calculated numerically using formulas (3.55) and (3.59), as well as the values in Appendix A, similarly to chapter 3. The value of the critical density can be estimated following section 2.3, however for small redshifts $z \lesssim 20$, $\delta_c = 1.686$ (2.32) represents a good approximation.

The results at $z \sim 10$ for different PBH parameters f_{PBH} and m_{PBH}, but also various clustering components are shown in Figure E.1, E.2, E.3 and E.4.

Although many more mixtures of PBH parameters could be studied, it seems that a combination of $\xi_{PBH} \gtrsim 10$ and $f_{PBH} \gtrsim 0.1$ drastically increases the stellar mass density. It would be interesting to further analyse these scenarios. This result is intriguing, as an initial clustering effect would be expected only for large PBH portions of DM. However, it could have been guessed that for large ξ_{PBH} and f_{PBH} the value of the stellar mass density would have grown at large masses. Lastly, it must be mentioned that also the results found here would violate the constraints from section 3.4, but the same justification arising from clusters of section 4.5 could be used.

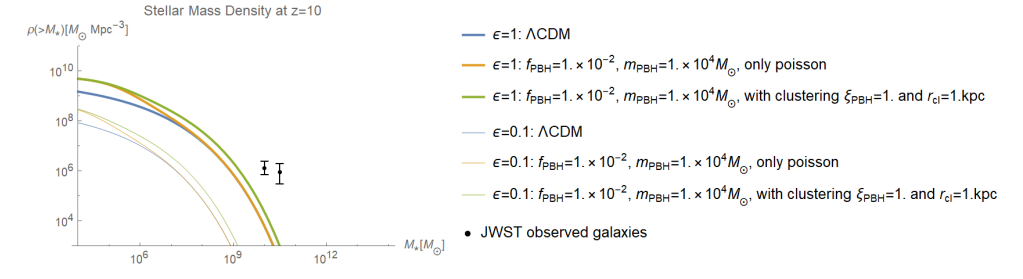

(a)

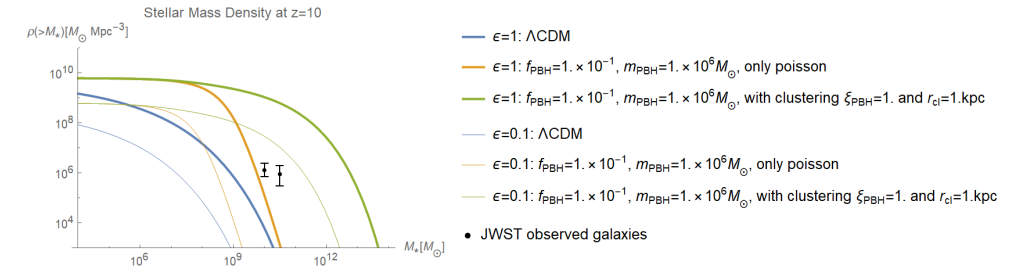

(b)

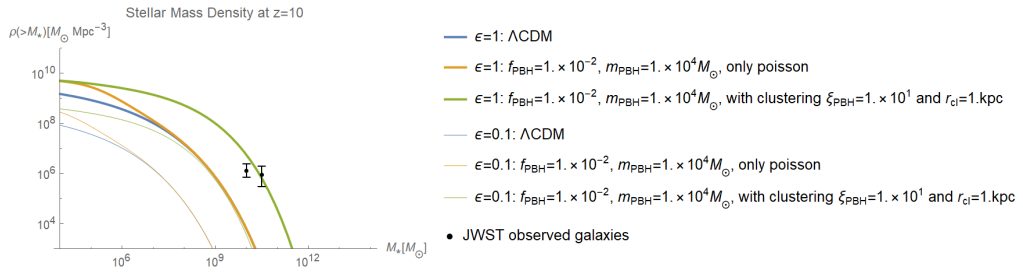

(c)

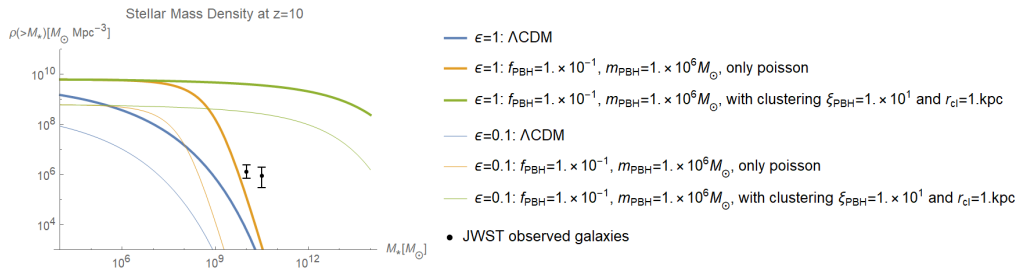

(d)

Figure E.1: These figures show the stellar mass density, depending on the stellar mass of galaxies, for three different scenarios: ΛCDM standard model, PBHs Poisson distributed, and with the clustering effect. These results are plotted for four different combinations of PBH proportions of DM, clustering components, and star formation effect.

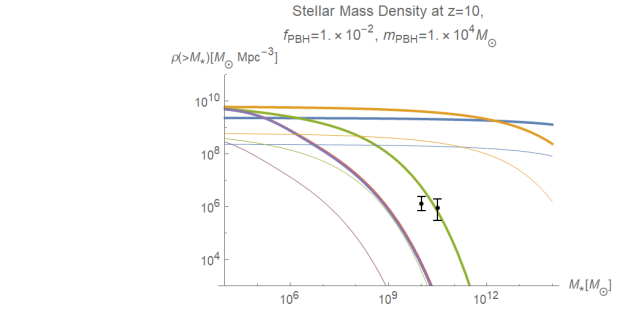

(a)

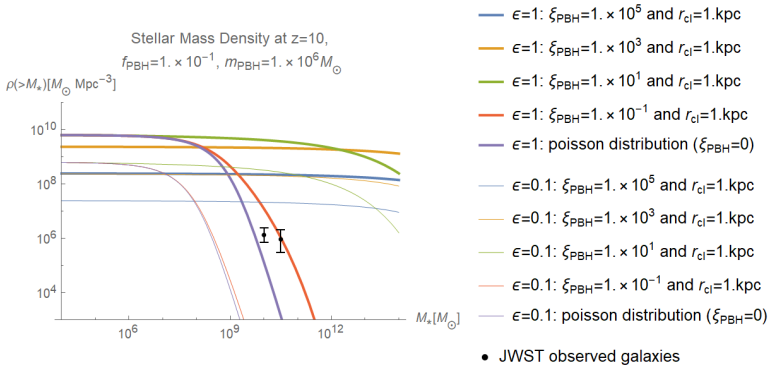

(b)

Figure E.2: Stellar mass density for different ξ_{PBH}.

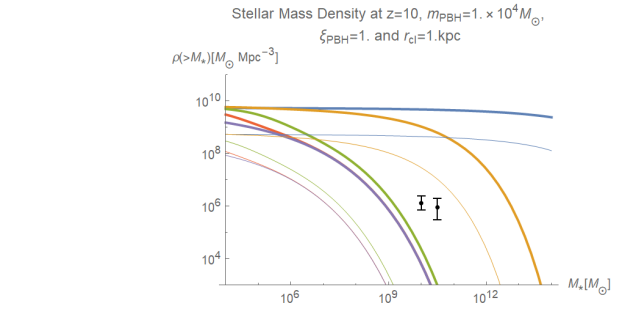

(a)

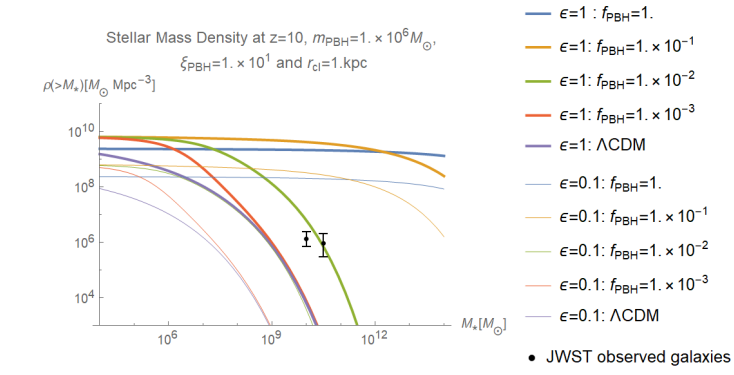

(b)

Figure E.3: Stellar mass density for different f_{PBH}.

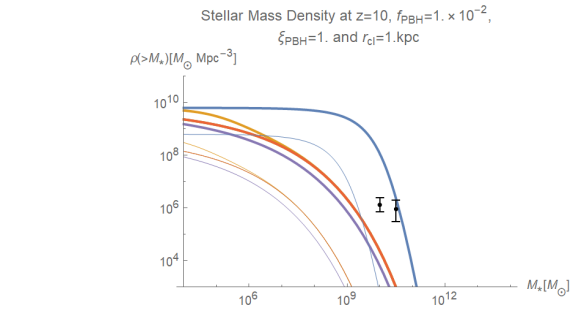

(a)

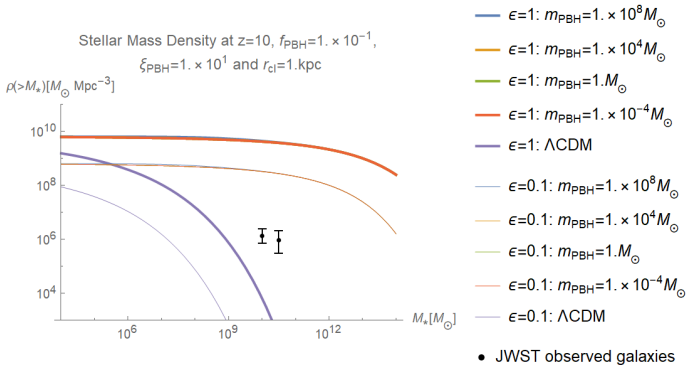

(b)

Figure E.4: Stellar mass density for different m_{PBH}.